



Room 14-0551  
77 Massachusetts Avenue  
Cambridge, MA 02139  
Ph: 617.253.5668 Fax: 617.253.1690  
Email: docs@mit.edu  
<http://libraries.mit.edu/docs>

## **DISCLAIMER OF QUALITY**

Due to the condition of the original material, there are unavoidable flaws in this reproduction. We have made every effort possible to provide you with the best copy available. If you are dissatisfied with this product and find it unusable, please contact Document Services as soon as possible.

Thank you.

**Pages are missing from the original document.**

PAGES 35 AND 102 MISSING FROM ORIGINAL

THE ATTRITIOUS AND FRACTURE  
WEAR OF GRINDING WHEELS

by

STEPHEN MALKIN

S.B., Massachusetts Institute of Technology  
(1963)

S.M., Massachusetts Institute of Technology  
(1965)

SUBMITTED IN PARTIAL FULFILLMENT  
OF THE REQUIREMENTS FOR THE  
DEGREE OF  
DOCTOR OF SCIENCE

at the

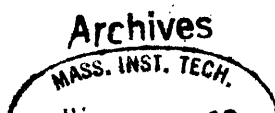
MASSACHUSETTS INSTITUTE OF TECHNOLOGY

February, 1968

Signature of Author . . . . .  
Department of Mechanical Engineering, February 1, 1968

Certified by . . . . .  
Thesis Supervisor

Accepted by . . . . .  
Chairman, Departmental Committee on Graduate Students



ABSTRACT

THE ATTRITIOUS AND FRACTURE

WEAR OF GRINDING WHEELS

by Stephen Malkin

Submitted to the Department of Mechanical Engineering  
February 1968, in partial fulfillment of the requirements for  
the degree of Doctor of Science

A detailed investigation is made of the nature and extent of grinding wheel wear in finish grinding. The wear is broadly classified as either attritious or fracture wear. Attritious wear results in the dulling of the tips of the abrasive grain by rubbing against the workpiece surface. Fracture wear is the removal of abrasive particles from the wheel either by fracturing within the grain (grain fracture) or fracturing at the bond (bond fracture). Most of the wear is found to consist of grain and bond fracture particles. The rate at which fracture wear occurs is directly related to the grinding forces.

The attritious wear, although contributing insignificantly to the total, is the most important form of wear. The dulling of the grains by attrition, measured by the area of the wear flats, uniquely determines the grinding forces for a particular workpiece material and for given grinding conditions. Both the horizontal and vertical grinding force components increase linearly with the wear flat area. (For steel this is true only up to a critical wear flat area where burning occurs.) This linear variation between grinding force and wear flat area is explained by considering the force as the sum of a cutting force due to chip formation and a sliding force due to rubbing between the wear flats and the workpiece.

Related investigations are also made of wheel dressing, surface finish, workpiece burn, and grinding temperatures.

Thesis Supervisor:

Nathan H. Cook  
Professor of Mechanical Engineering

### ACKNOWLEDGEMENTS

The author welcomes this opportunity to express his gratitude to Professor N. H. Cook for his supervision of this thesis and his continual interest and encouragement. He is also indebted to the members of his thesis committee, Professor E. Rabinowicz and Professor R. L. Coble, for their helpful advice and discussions.

The author gratefully acknowledges the financial support of Norton Company. Thanks are due in particular to Dr. G. S. Reichenbach of Norton Company, formerly of M.I.T., who supervised this thesis in its early stages and continued to be helpful for the duration of the work.

A special note of thanks is due to Messrs. S. Marcolongo, R. Bowley, J. Leach, F. Anderson, and R. Whittemore for their practical assistance in the experimental program.

The facilities of the Harvard University Computing Center were used for making numerical calculations. The author's wife, Judith, who is a member of that organization, was especially helpful.

Thanks are also due to Miss Angela Theodore who did the typing.

Finally the author would like to again thank his wife for her support and assistance.

## Table of Contents

Title Page .....	i
Abstract .....	ii
Acknowledgements.....	iii
Table of Contents.....	iv
List of Figures.....	vii
List of Tables .....	xi
List of Symbols.....	xii
I. Introduction.....	1
II. Literature Review of Grinding Wheel Wear.....	4
III. Equipment, Material, Procedures, and Parameters.....	13
3.1. Introduction.....	13
3.2. Equipment.....	13
3.3. Grinding Wheels.....	16
3.4. Workpiece Materials.....	16
3.5. Parameters.....	17
3.5.1. Grinding Forces and Energy.....	17
3.5.2. Per Cent Wear Flat Area.....	18
3.5.3. Active Grains per Unit Area.....	20
3.5.4. Grinding Wheel Wear.....	21
3.5.5. Per Cent Bond Fracture.....	22
IV. Dressing.....	25
4.1. Introduction.....	25
4.2. Results.....	26
4.3. Discussion.....	32

V.	Attritious Wear and Grinding Forces.....	36
	5.1. Introduction.....	36
	5.2. Results.....	36
	5.3. Discussion.....	53
VI.	Grinding Temperatures.....	66
	6.1. Introduction.....	66
	6.2. Geometry of Chip Formation.....	67
	6.3. Energy Partition.....	71
	6.4. Calculated Grinding Temperatures.....	74
VII.	Surface Finish.....	79
	7.1. Introduction.....	79
	7.2. Results and Discussion.....	79
VIII.	Fracture Wear .....	82
	8.1. Introduction.....	82
	8.2. Results.....	82
	8.3. Discussion.....	91
IX.	Conclusions.....	96
X.	Suggestions for Future Work.....	99
	References.....	101
	Appendix A. Calculation of the Maximum Number of Active Grains.....	105
	Appendix B. Calculation of Temperatures due to Cutting.....	106
	Appendix C. Calculation of Temperatures due to Sliding.....	108
	Appendix D. Calculation of the Average Temperature in the Grinding Area.....	110

Tables.....	111
Biographical Note.....	131

## List of Figures

No.	Title	Page
1.	Illustration of the three types of wear.....	3
2.	Photograph of the equipment.....	14
3.	Microphotograph of wear flats.....	19
4.	Number of active grains/inch <sup>2</sup> versus bond per cent for fine and coarse dressing.....	27
5.	Wear flat area versus bond per cent for fine and coarse dressing.....	28
6.	Wear flat area per grain versus bond per cent for fine and coarse dressing.....	29
7.	Particle size distribution for dressing particles and abrasive grain.....	30
8.	Per cent bond fracture versus bond per cent for dressing particles.....	31
9.	Number of active grains per square inch versus 100 minus per cent bond fracture for dressing particles.....	34
10.	Grinding forces and force ratio versus number of passes for 1018 steel workpiece, fine dress, V = 6250 ft./min., v = 8 ft./min., d = .001 in.....	37
11.	Per cent wear flat area and wear flat area per grain versus number of passes for 1018 steel workpiece, fine dress, V = 6250 ft./min., v = 8 ft./min., d = .001 in.....	38



12.	Grinding forces and force ratio versus number of passes for 1018 steel workpiece, coarse dress, $V = 6250$ ft./min., $v = 8$ ft./min., $d = .001$ in.....	39
13.	Per cent wear flat area and wear flat area per grain versus number of passes for 1018 steel workpiece, coarse dress, $V = 6250$ ft./min., $v = 8$ ft./min., $d = .001$ in.....	40
14.	Number of active grains/inch <sup>2</sup> versus bond per cent for 1018 steel workpiece, $V = 6250$ ft./min., $v = 8$ ft./min., $d = .001$ in.....	41
15.	Microphotographs of wear flats after 20, 40, 60, 80, and 100 passes.....	43
16.	Grinding forces versus wear flat area for 1018 steel, fine and coarse dress, $V = 6250$ ft./min., $v = 8$ ft./min., $d = .001$ in.....	45
17.	Grinding forces versus wear flat area for 52100 steel, fine dress, $V = 6250$ ft./min., $v = 8$ ft./min., $d = .001$ in.....	46
18.	Grinding forces versus wear flat area for T1 steel, fine dress, $V = 6250$ ft./min., $v = 8$ ft./min., $d = .001$ in.....	47
19.	Grinding forces versus wear flat area for 130 A titanium, fine dress, $V = 6250$ ft./min., $v = 8$ ft./min., $d = .001$ in.....	48
20.	Grinding forces versus wear flat area for niobium, fine dress, $V = 6250$ ft./min., $v = 8$ ft./min., $d = .001$ in.....	49
21.	Grinding forces versus wear flat area for molybdenum, fine dress $V = 6250$ ft./min., $v = 8$ ft./min., $d = .001$ in.....	50

22.	Grinding forces versus wear flat area, for Stellite No. 6B, fine dress, $V = 6250$ ft./min., $v = 8$ ft./min, $d = .001$ in.....	51
23.	Grinding forces versus wear flat area for 1018 steel, fine dress, $V = 3125$ ft./min., $v = 4$ ft./min., $d = .001$ in....	52
24.	Illustration of chip formation and the cutting and sliding force components.....	54
25.	Illustration of the grinding geometry.....	56
26.	Pressure distribution due to contact between a punch and a semi-infinite elastic solid.....	59
27.	Specific cutting energy versus wear flat pressure.....	62
28.	Specific cutting energy versus melting point of the workpiece..	63
29.	Geometry of undeformed chip.....	68
30.	Geometry of chip formation.....	72
31.	Fraction of grinding energy conducted to the workpiece versus the wear flat area for 1018 steel, fine dress, $V = 6250$ ft./min., $v = 8$ ft./min., $d = .001$ in.....	73
32.	Variation of thermal conductivity and thermal diffusivity with temperature for mild steel.....	75
33.	Distribution of calculated grinding temperatures along workpiece surface.....	77
34.	Surface finish versus the number of passes for fine and coarse dressing for 1018 steel, $V = 6250$ ft./min., $v = 8$ ft./min., $d = .001$ in.....	80

35.	Accumulated wear versus number of passes for 1018 steel, fine dress, $V = 6250$ ft./min., $v = 8$ ft./min., $d = .001$ in.....	83
36.	Accumulated wear versus number of passes for 1018 steel, coarse dress, $V = 6250$ ft./min., $v = 8$ ft./min., $d = .001$ in....	84
37.	Accumulated wear versus number of passes for 52100 steel, fine dress, $V = 6250$ ft./min., $v = 8$ ft./min., $d = .001$ in.....	85
38.	Particle size distribution of wear particles and abrasive grain for 1018 steel, fine dress, $V = 6250$ ft./min., $v = 8$ ft./min., $d = .001$ in.....	87
39.	Particle size distribution of wear particles and abrasive grain for 1018 steel, coarse dress, $V = 6250$ ft./min., $v = 8$ ft./min., $d = .001$ in.....	88
40.	Particle size distribution of wear particles and abrasive grain for 52100 steel, fine dress, $V = 6250$ ft./min., $v = 8$ ft./min., $d = .001$ in.....	89
41.	Per cent bond fracture versus bond per cent for wear particles..	90
42.	Illustration of the force on an active grain.....	92
43.	Correlation between the wear per active grain and the bond stress factor.....	95

## List of Tables

No.	Title	Page
1.	Description of Wheels.....	111
2.	Workpiece Materials.....	112
3.	Wheel Dressing - Experimental Results.....	113
4.	Sieve Number - Screen Opening.....	114
5.	Forces and Wear Flats - 1018 Steel, Fine Dress.....	115
6.	Forces and Wear Flats - 1018 Steel, Coarse Dress.....	116
7.	Forces and Wear Flats - 52100 Steel, Fine Dress.....	117
8.	Forces and Wear Flats - T1 Steel, Fine Dress.....	118
9.	Forces and Wear Flats - 130 A Titanium, Fine Dress.....	119
10.	Forces and Wear Flats - Niobium, Fine Dress.....	120
11.	Forces and Wear Flats - Molybdenum, Fine Dress.....	121
12.	Forces and Wear Flats - Stellite No. 6B, Fine Dress.....	122
13.	Forces and Wear Flats - 1018 Steel, Fine Dress.....	123
14.	Summary of Results From Least Square Analysis.....	124
15.	Energy Partition - 1018 Steel, Fine Dress.....	125
16.	Surface Finish, 1018 Steel.....	126
17.	Wheel Wear - 1018 Steel, Fine Dress.....	127
18.	Wheel Wear - 1018 Steel, Coarse Dress.....	128
19.	Wheel Wear - 52100 Steel, Fine Dress.....	129
B.1.	Calculated Values of $T_c$ .....	130

LIST OF SYMBOLS

<u>Symbol</u>	<u>Description</u>	<u>Dimensions</u>
a	Semi-width of punch	in.
$a_A$	Apparent area of contact between wheel and workpiece	in. <sup>2</sup>
$a_R$	Real area of contact between wear flats and workpiece	in. <sup>2</sup>
A	Wear flat area	per cent
b	Width of cut	in.
B	Per cent of wear due to bond fracture	per cent
c	Correlation coefficient	
$c_1$	Constant	
$c_2$	Constant	
C	Number of cutting points per unit area	in. <sup>-2</sup>
d	Downfeed per pass	in.
D	Wheel diameter	in.
f	Function used for contact pressure distribution	
$f_H$	Horizontal force per grain	lb.
$f_V$	Vertical force per grain	lb.
$F_H$	Horizontal grinding force	lb.
$F_{HC}$	Horizontal force due to cutting	lb.

<u>Symbol</u>	<u>Description</u>	<u>Dimensions</u>
$F_{HS}$	Horizontal force due to sliding	lb.
$F_v$	Vertical force	lb.
$F_{VC}$	Vertical force due to cutting	lb.
$F_{VS}$	Vertical force due to sliding	lb.
H	Workpiece hardness	lb./in. <sup>2</sup>
I	Function used for moving heat source calculation	
k	Thermal conductivity	lb./sec. <sup>o</sup> F
K	Constant	
l	Semi-width of band for moving heat source calculation	in.
$l_c$	Undeformed chip length	
L	Nondimensional variable in moving heat source calculation	
m	Number of grains per unit weight of abrasive	
M	Number of whole grains corresponding to a given weight of abrasive	
n	Number of active grains "instantaneously" in contact with workpiece	
N	Number of contacts which occur between active grains and workpiece	
p	Contact pressure between punch elastic solid or between wear flat and workpiece	lb./in. <sup>2</sup>
$\bar{p}$	Average contact pressure between wear flats and workpiece	lb./in. <sup>2</sup>

<u>Symbol</u>	<u>Description</u>	<u>Dimensions</u>
$P_B$	Probability that a grain will experience a bond fracture for each contact between a grain and the workpiece	
$P$	Force per unit width between punch and semi-finite solid	lb./in.
$q$	Grinding energy flux	in. lb./in. <sup>2</sup> sec.
$q_f$	Energy flux due to sliding between wear flats and workpiece	in. lb./in. <sup>2</sup>
$Q$	Total grinding power	in. lb./sec.
$r$	Ratio of width to thickness of undeformed chip	
$R$	Fraction of grinding energy conducted to workpiece	
$R_1$	Fraction of cutting energy conducted to workpiece	
$R_2$	Fraction of sliding energy conducted to workpiece	
$t_1$	Undeformed chip thickness	in.
$(t_1)_{\max}$	Maximum undeformed chip thickness	in.
$t_2$	Actual chip thickness	in.
$(t_2)_{50}$	Actual chip thickness when the cut is 50% complete	in.
$(t_2)_{\max}$	Maximum value of $t_2$	in.
$T_A$	Calculated temperature rise over the grinding area	<sup>o</sup> F

<u>Symbol</u>	<u>Description</u>	<u>Dimensions</u>
$(T_A)_{ave}$	Average value of $T_A$	$^{\circ}F$
$(T_A)_{max}$	Maximum value of $T_A$	$^{\circ}F$
$T_C$	Calculated temperature rise due to cutting	$^{\circ}F$
$(T_C)_{ave}$	Average value of $T_C$ at shear zone	$^{\circ}F$
$(T_C)_{max}$	Maximum value of $T_C$ at shear zone	$^{\circ}F$
$u$	Specific grinding energy	in. lb./in. <sup>3</sup>
$u_c$	Specific cutting energy	in. lb./in. <sup>3</sup>
$v$	Velocity of workpiece	ft./min.
$V$	Velocity of wheel periphery	ft./min.
	Velocity of moving heat source	ft./min.
$V_b$	Fraction by weight of bonding agent in the wheel	
$w$	Wear per "instantaneous" active grain in 20 passes.	mg.
$W$	Wear in 20 passes	mg.
$x$	Coordinate of punch; wear flat, and moving heat source	in.
$X$	Nondimensional coordinate of moving heat source	
$\alpha$	Thermal diffusivity	in. <sup>2</sup> /sec.
$\beta$	Constant	
$\phi$	Shear angle	degrees



## I. INTRODUCTION

Grinding of metals is similar to other metal cutting operations insofar as metal is removed by a shearing process of chip formation. In most metal cutting operations a tool of known geometry and orientation is used, but grinding is accomplished by numerous tools (abrasive grains) of varied and indeterminate geometry. These hard abrasive grains are held together by a weaker bond to form a grinding wheel. As the wheel rotates, the grains cut chips out of the workpiece.

As a grinding wheel wears, the surface of the wheel becomes uneven. Dulling of the abrasive grains also occurs. This leads to deterioration in the quality of the workpiece surface. For finish grinding where precise surfaces of low surface roughness are required, it is necessary to periodically sharpen or dress the wheel. For abrasive machining, where the objective is bulk metal removal, the quality of the surface is relatively unimportant and the grinding wheel is not periodically dressed. The present investigation is concerned only with finish grinding.

The main difficulty encountered by the grinding engineer is the choice of the grinding wheel best-suited for a given work. It is often found that the best grinding wheel for the job is the one which experiences the least wheel wear. This is not due to the cost of the wheels because in finish grinding that cost is but a small portion of the total expense. The general belief is that if the wheel consumption is low, the unproductive time required for dressing the wheel will be less and the grinding operation will be more efficient.

It is therefore not surprising that grinding wheel wear has been the subject of numerous investigations. Most of these investigations are empirical in nature and the experimental results are usually applicable only to the particular case at hand or a similar one. There has been a pitiful lack of basic research in this area.

Grinding wheel wear can be broadly classified as either attritious wear or fracture wear. Attritious wear results in the flattening or dulling of the abrasive grain by rubbing against the workpiece surface, illustrated by (A) in Figure 1. This accounts for the glazed appearance of a grinding wheel. Fracture wear is the removal of abrasive particles from the wheel by either fracturing within the grain (grain fracture), illustrated by (B) in Figure 1, or fracturing at the bond (bond fracture), illustrated by (C) in Figure 1.

This thesis describes a detailed investigation into the nature and extent of grinding wheel wear. The total wear is measured from the weight of the grinding wheel wear particles. The wear particles are sieved and a statistical analysis is used to determine the relative amounts of grain fracture, bond fracture, and attritious wear. The attritious wear is also measured as the area of the wear flats generated on the grains. The significance of these different types of wear is clearly observed.

Related investigations are also made of grinding forces, wheel dressing, surface finish, grinding temperatures, and workpiece burn.

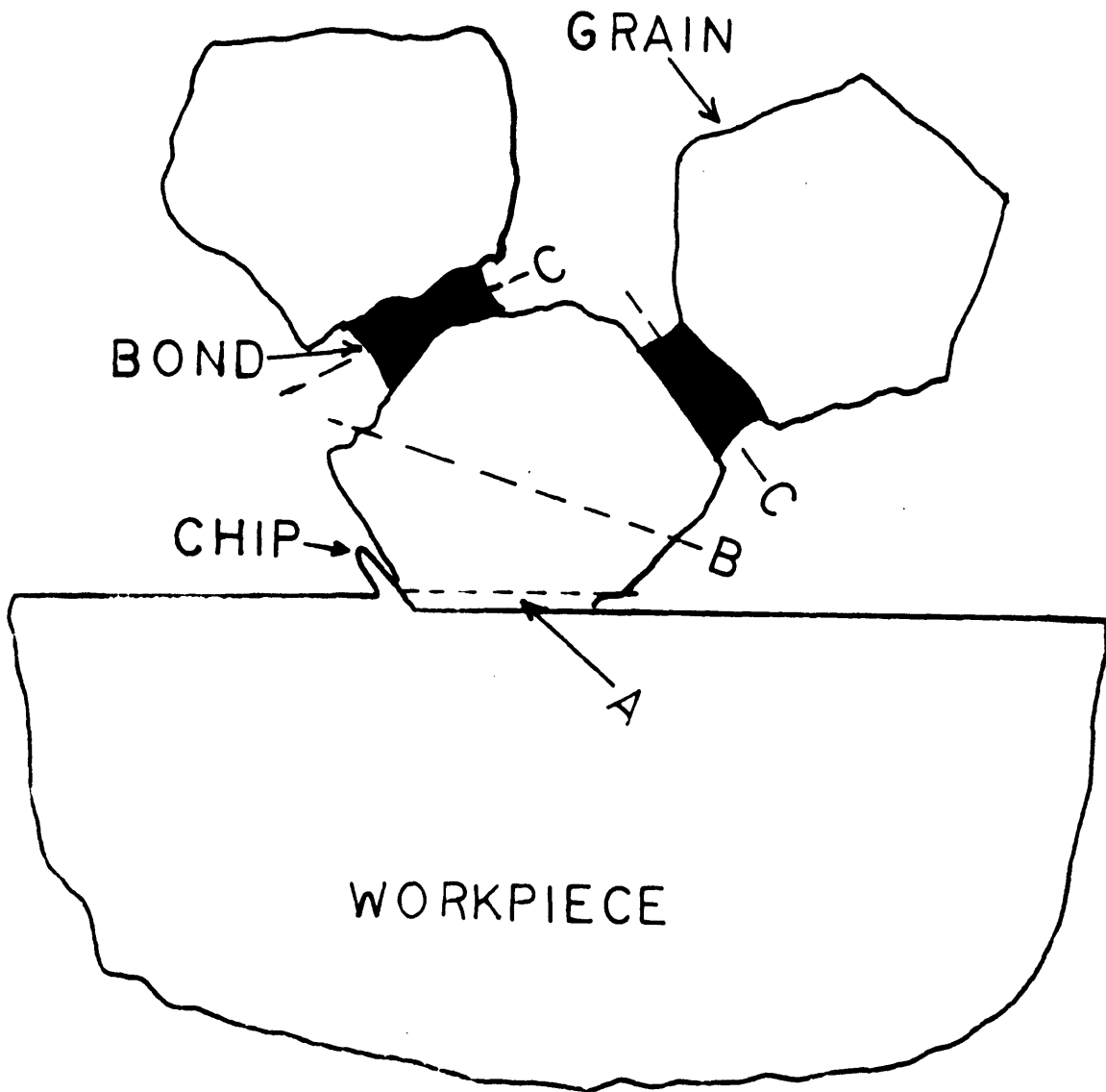


Figure 1. Illustration of the three types of wear.  
A - attritious wear, B - grain fracture,  
C - bond fracture.

## II. LITERATURE REVIEW OF GRINDING WHEEL WEAR

The first significant scientific investigation of the grinding process was performed by G.I. Alden of the Worcester Polytechnic Institute. In his report "Operation of Grinding Wheels in Machine Grinding"<sup>(1)</sup> presented to the A.S.M.E. in 1914, a mathematical relationship was derived for the "grain depth of cut" or chip thickness as a function of the grinding conditions. Alden reasoned that the wear of the grinding wheel "on a given kind of work is almost entirely dependent upon the grain depth of cut", a larger depth of cut causing greater wear.

Almost twenty years later, a Swedish engineer, R. Woxen, working in this country at Norton Company, performed the first extensive and systematic investigation of grinding wheel wear.<sup>(2)</sup> Woxen introduced the wheel wear parameter which he called the specific wear, which is defined as the volume ratio of wheel wear to metal removal. This is equal to the inverse of the grindability index or G-ratio (grinding ratio) which is almost exclusively used today to describe grinding wheel wear. He also originated the notion of a grinding wheel tool life which is arbitrarily judged from the deterioration of the workpiece surface.

The specific wear and the grinding wheel life were related to the grinding variables (wheel speed, table speed, chip thickness, metal removal rate) from which the optimum grinding conditions could be determined. He concluded that the specific wear "is not univocally (unequivocally) determined by the chip-thickness as Alden supposed".

At this point a question of semantics arises over the definition of grinding wheel wear. The G-ratio is in fact a measure of the efficiency of the grinding operation where the objective is maximum metal removal with minimum wheel wear. In finish grinding, which is considered here, the abrasive cost usually represents an insignificant contribution to the overall expense of the grinding operation. In fact, more abrasive is used in dressing the wheel than during grinding. This was clearly recognized by both Alden and Woxen.

From an analytical point of view, it is probably better to consider wheel wear as the weight (or volume) of abrasive removed for a given length of travel of the wheel periphery. This is consistent with conventional practice in the general treatment of other wear systems.<sup>(3)</sup> Alden may have thought of wear in this way, in which case his belief that grinding wheel wear is determined from the grain depth of cut has never been really explored.

Most experimental studies of grinding wheel wear consist of measuring the G-ratio and the specific energy (power consumed/metal removed) for a particular set of grinding conditions. While this approach has enjoyed limited success in optimization of grinding conditions, very little has been learned about the fundamental aspects of grinding wheel wear. Furthermore, small changes in grinding conditions often lead to large unexplainable differences in the G-ratio.

Tarasov<sup>(4)</sup> used this approach to investigate the grindability of tool steels. He concluded that "the power or energy consumed in grinding cannot

be used to predict the grindability (G-ratio) of tool steels, since these quantities can be the same for steels known to be extremely difficult to grind as for those comparatively easy to grind." On the other hand, he did obtain some correlations between the alloy content of the steel and its G-ratio.

Essentially the same approach was taken by Backer and Merchant<sup>(5)</sup> who measured the G-ratio, grinding forces, and specific energies for several grades of aluminum oxide wheels on steel and cast iron. Attempts to correlate the G-ratio with specific energy, chip area, chip length, and cutting speed were unsuccessful.

For mechanisms of grinding wheel wear have been proposed by Peklenik<sup>(6,7)</sup>.

1. Pressure softening of the grain due to high temperature producing wear flats
2. Splintering of individual crystals from the grain
3. Partial grain dislodgement
4. Complete grain dislodgement

The first of these is dulling of the grain. The second and third are types of grain fracture, and the fourth is bond fracture.

Peklenik considered the wear flats in grinding to be analogous to the flank wear of a cutting tool. The dulling of the grains was quantitatively expressed by the fraction of the total active area of the grinding wheel on which wear flats appear. This was measured by running carbon paper between the grinding wheel and a piece of glass. A replica of the wear flats is transferred to the glass as black carbon spots. The wear flat area is

determined with a planimeter from an enlarged photograph of the glass.

The tests showed that when a given wear flat area was reached, burning of the steel workpiece occurred. This critical wear flat area was found to be between 5 and 10 per cent, the larger wear flat area corresponding to wheels of smaller grain size. Therefore the wear flat area was proposed as a criterion of grinding wheel tool life ("Verschleisskriterium").

Yoshikawa<sup>(8,9)</sup> arrived at essentially the same conclusion. In his tests the wear flat area was determined from photographs of the grinding wheel taken through a microscope. With the proper lighting, the wear flats exhibit a mirror-like effect and stand out brightly over the dark background of the rest of the wheel. The white traces in the photographs corresponding to the wear flats were cut out and weighed. The ratio of their weight to the weight of the original photograph determined the wear flat area per cent.

At a critical wear flat area of 8 per cent, a sharp rise in the grinding forces occurred. For smaller wear flat areas, the grinding forces were found to be essentially constant. (This last observation is contrary to results presented in this thesis and will be discussed in detail.) He concluded that the grinding life depends on an increase of wear flat area due to attrition and a decrease of wear flat area due to fracture.

Tsuwa<sup>(10, 11)</sup> investigated the progress of individual wear flats by observing the profile of the grain tips. Both the breadth and number of wear flats were measured. The changing nature of the cutting edges were

attributed to

1. Attritious wear
2. Grain breakage
3. Dig out (bond fracture)
4. Newly appeared grains

The first and fourth increase the wear flat area, the second and third decrease it.

A photoelectric device was also developed to automatically determine the number and area of wear flats on the wheel.<sup>(11)</sup> The number of wear flats was determined from the number of light peaks reflected from the duration of the light peaks.

Tsuwa et al<sup>(12, 13)</sup> made numerous detailed observations of the wear flat surfaces. Wear flats were found to develop on the vitreous bond as well on the grain. The ratio of bond to grain wear flat areas was approximately equal to the relative amounts of bond and grain in the wheel.

Two types of surfaces were observed on the worn grain. The first is smooth and has striations parallel to the grinding direction. The other contains a network of cracks, and is quite rough. At the beginning of wear only the first region appears. As the wear flat grows, the second region suddenly appears at the trailing edge, presumably where the temperature is greatest.

Attritious wear was also measured by Hahn<sup>(14)</sup> and Lindsay<sup>(15)</sup> for controlled force (constant normal force) internal grinding. Wear flat areas were determined from planimeter measurements on microphotographs of the



wheel surface. As grinding proceeded, the increasing wear flat area was accompanied by a proportional decrease in the metal removal rate. It was also reported <sup>(16)</sup> that the natural roughness of the wear flat surface corresponded to the best surface finish obtainable on the workpiece.

The dressing technique can have a strong influence on the size of the wear flats observed. Lindsay <sup>(15)</sup> found that when a coarser dressing technique (higher infeed velocity of dressing tool) was used, less wear flat area was observed on the wheel. A finer dressing technique was believed to dress a larger initial wear flat area on the wheel.

D.K. Bruckner <sup>(17)</sup> showed that increasing wear flat areas were accompanied by increased radial wheel wear. Peklenik's procedure <sup>(7)</sup> was used for the wear flat measurements. For low alloy and structural steels, the radial wheel wear before redressing amounted to only about one-tenth of a grain dimension. From this it was concluded that complete grain dislodgement (bond fracture) was very unlikely to be a significant form of grinding wheel wear.

The attritious wear of abrasive rubbing against the workpiece surface occurs at high temperatures where the wear rate should depend on the chemical interaction between the grain and workpiece materials. Goepfert and Williams <sup>(18)</sup> investigated the attritious wear of single point tools of aluminum oxide and silicon carbide abrasive against various metallic materials. Qualitative assessment of chemical interaction was independently obtained from metallographic observation of the reacting material pairs which had been placed in contact and heated. In general those combinations

with higher wear rates also had more extensive reaction. These results were not applied to interpreting the overall wear of grinding wheels.

In this same paper, the effect of grain toughness on the G-ratio is also indicated. Grain toughness is an arbitrary measure of the breakdown resistance of the material under impact loading, a high toughness number signifying a low percentage breakdown of particles. The G-ratio was found to increase with toughness. However, this result is of limited value since neither the test conditions nor numerical results are reported.

The general shape of the radial wheel wear curves has been found by Backer and Krabacher<sup>(19)</sup> and Grisbrook et al<sup>(20)</sup> to consist of three regimes. In the first regime there is a high initial wear rate which decreases with time. This is followed by a more or less constant wear rate in the second regime and an increasing wear rate in the third regime. The same type of wear rate curve is often found in other situations, (e.g. wear lands on cutting tools, ball bearing wear,) where the three wear regimes are called run-in, run-with, and run-out.

Pattinson and Chisholm<sup>(21)</sup> considered the effect of dressing on the wear in the first and second regimes. With coarser dressing technique (larger crossfeed velocity of dressing diamond) the initial wear rate of the wheel is higher. In the second regime, however, the wear rate appeared to be unaffected by the dressing technique.

Grisbrook et al<sup>(20)</sup> stated that the increasing rate of wheel wear in the third regime is due to bond fracture, where whole grits are being dislodged from the grinding wheel. No experimental evidence was presented to support this contention.

Colding<sup>(22)</sup> attempted to correlate grinding wheel wear with the "grinding equivalent", which is the ratio of the length of the chip to its cross-sectional area. The only reasoning which underlies a possible connection between the wheel wear and grinding equivalent is that a somewhat analogous chip equivalent (the ratio of total engaged cutting edge length to the cross-sectional area of the chip, before metal removal) was used with some success in correlating the tool life for milling and turning. Using Wöxén's data, Colding did obtain, on a log-log plot, a linear relationship between the G-ratio and the chip equivalent. Other data did not provide such a neat correlation.

Yoshikawa and Sata<sup>(23)</sup> took a new approach to the problem of grind-wheel wear. They classified the wheel wear as

1. Attritious wear
2. Mechanical fracture of grains (grain fracture)
3. Fracture of bond bridges (bond fracture)

The third type of wear was theoretically considered from the standpoint of delayed fracture of brittle materials. Analytical results indicate that the rate of bond fracture varies linearly with grinding time and exponentially with the stress on the bond. The bond stress is assumed to vary linearly with the resultant force per grain.

Experimental verification of the effect of grinding time and force on the rate of bond fracture was obtained for a weakly bonded wheel (F-grade). With a soft wheel such as this, the average wheel wear particles are only slightly smaller than the grains used in the wheel production.

Virtually all the wear is due to bond fracture.

In a later paper, Yoshikawa<sup>(24)</sup> attempted to generalize this approach for harder grades of wheels. The overall wear was analytically determined as the sum of grain fracture and bond fracture particles. The predictions were partially supported by experiments using grinding wheels of different grades. The complex form of the analytical expressions preclude their practical application.

The theoretical analysis presented in these last two papers might be questioned on several points. However, it is more important to realize that this approach is the only instance in the literature where an attempt was made to come to grips with the complex problem of grinding wheel wear in fundamental terms. A similar approach to the problem is used in this thesis.

### III. EQUIPMENT, MATERIAL, PROCEDURE, AND PARAMETERS

#### 3.1 Introduction

Numerous experimental techniques and parameters have been devised to characterize the behavior of grinding wheels and the grinding process. Yet there are hardly any routine tests or standardized symbols which have been adopted by the various laboratories engaged in basic grinding research. In some instances, apparent contradictions appear in the literature where different techniques were used to measure what was thought to be the same physical value. Therefore, it is especially important in grinding research to closely identify experimental results with the methods by which they were obtained.

In this section the equipment, materials, procedures and some of the parameters used in this investigation are discussed in some detail. These are also compared to similar experimental techniques used by other investigators.

#### 3.2 Equipment

The experimental apparatus used in this investigation is shown in Figure 2. All the tests were run on a Norton 6 x 18 surface grinder using 8 inch diameter wheels (8 inch diameter x 1/2 inch wide and 1 1/4" bore) on a 1/4 inch wide workpiece under plunge cut conditions (no crossfeed). This machine has a D.C. drive variable speed spindle and

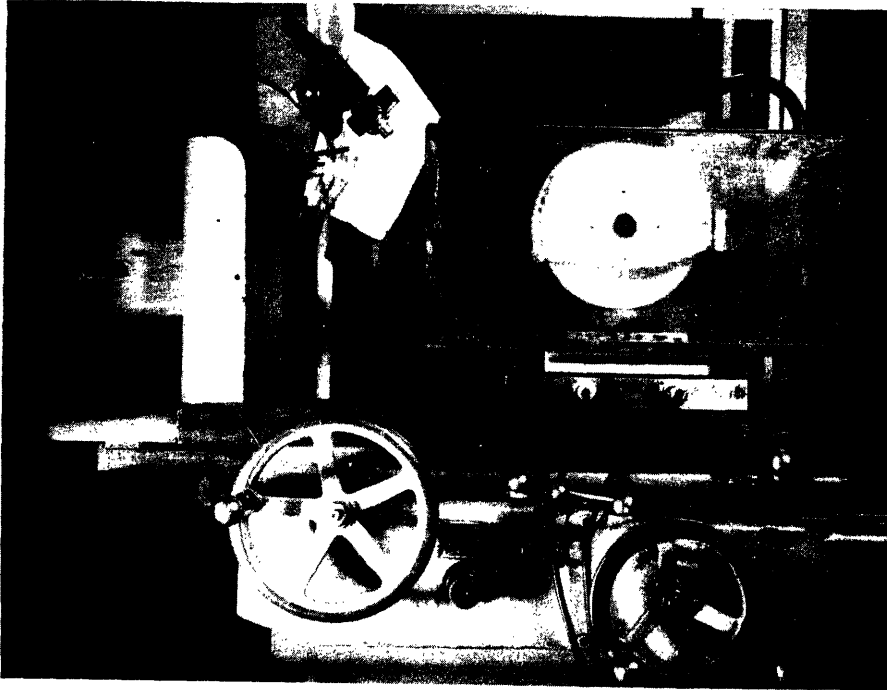


Figure 2. Photograph of the equipment. Note the microscope which can be positioned to view the wear flats and the box for collecting the wheel wear and chips.

a variable speed hydraulic drive table. Most tests were run at a wheel speed  $V = 6250$  ft/min. with a table speed  $v = 8$  ft/min., and a down feed  $d = .001$  inch.

Both the horizontal and vertical components of the grinding force  $F_H$  and  $F_V$  were measured with a very stiff and sensitive semiconductor strain gage dynamometer connected to a Sanborn Model 150 recorder. Semiconductor strain gages are about 50 times more sensitive than the conventional wire gages. This dynamometer has a stiffness of approximately 700,000 pounds per inch, and thus is about 50 times more rigid than the grinding machine. Force differences as small as .02 pounds can be detected.

Grinding wheel wear was determined from the weight of wear particles generated in a given number of passes. The wear particles were collected together with the metal removed and ultimately separated by chemical means. The particles were then weighed and sieved. Details of these procedures are given below.

With a microscope attached directly to the machine, both the wear flat area and the number of active grains per unit area were determined without removing the wheel from the spindle. The details of the procedures used for these measurements are discussed below.

Surface finish measurements were made with a Cleveland Roughness Meter Model BK6101 (not shown in Figure 2). With this device, a hand held instrument was traversed along the workpiece surface. Measurements were taken intermittently without removing the workpiece from the dynamometer. The results, indicated on a meter, were

estimated to 1 microinch A.A. (arithmetic average) below a surface finish of 20 microinches A.A. and to 5 microinches A.A. with coarser finishes. Although there were more refined instruments available for obtaining finer surface finish measurements, the accuracy of this instrument was more than sufficient for this investigation.

### 3.3 Grinding Wheels

The grinding wheels furnished by Norton Company for this investigation are described in Table 1. These wheels vary only in grade which is determined by the amount of vitreous bonding material in the wheel. The abrasive is Norton's 32 Alundum (32 A), a light gray colored single crystal aluminum oxide of high purity which is widely used for grinding steel. The 46 grain size corresponds to a mean grain diameter of about .015 inch.

### 3.4 Workpiece Materials

The workpiece materials are listed in Table 2 together with their chemical composition and room temperature hardness. All these materials were used for the attritious wear studies. Only the 1018 and 52100 steels were used for the fracture wear studies. The specimens were 1/4 inch wide and initially 2 inches high. The 1018 and 52100 steel specimens were 4 inches long, and the other specimens were 2 inches long.



### 3.5 Parameters

#### 3.5.1 Grinding Forces and Energy

As previously mentioned, both the horizontal and vertical components of the grinding forces,  $F_H$  and  $F_V$ , were measured with a semiconductor strain gage dynamometer. This instrument was sufficiently stiff so that it would have had virtually no influence on the grinding process itself.

In the past, grinding forces have been typically measured with dynamometers using conventional wire strain gages. To achieve adequate sensitivity, these devices are rather flexible. For instance, Marshall and Shaw<sup>(25)</sup> report using a dynamometer with a stiffness approximately equal to that of the machine itself. This in effect cuts the stiffness of the grinding system in half. Machine stiffness is a significant factor in grinding, and there is a concerted effort today to build very rigid grinding machines.

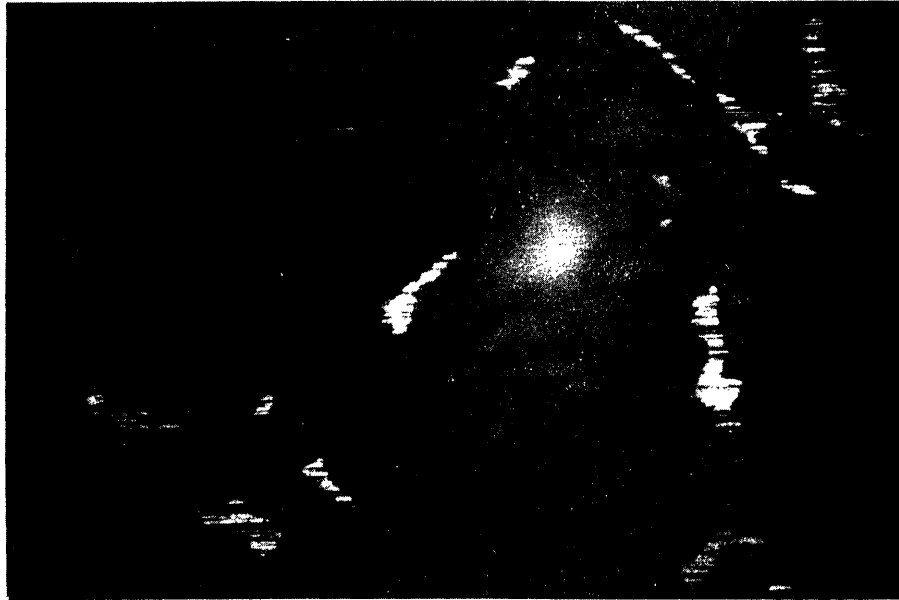
The grinding force measured by the dynamometer represents the sum of the forces between the active grains and the workpiece. The tangential component of the grinding force can be used to compute the specific grinding energy,  $u$ , which is defined as the energy required to remove a unit volume of material. This parameter is widely used in metal cutting research. For surface grinding with wheel speeds much greater than table speeds, the horizontal force,  $F_H$ , multiplied by the wheel velocity,  $V$ , is the total power input.

With a high G-ratio, the metal removal rate is the product of the table speed,  $v$ , the downfeed or wheel depth of cut,  $d$ , and the width of cut,  $b$ . The specific grinding energy is given by the ratio of the power input to metal removal rate.

$$u = \frac{F_H V}{v b d} \quad (3.1)$$

### 3.5.2 Per Cent Wear Flat Area

The attritious wear of the grain rubbing on the workpiece surface leads to the development and growth of wear flats on the active grains in the wheel. The percentage of the total area was measured with a microscope attached directly to the grinding machine. This microscope had a self contained illuminator with a light coming directly through the objective lens. When the microscope was focussed normal to the wheel surface, the wear flats reflected light directly back through the microscope. The remainder of the wheel surface reflected the light in random directions and appeared quite dark. A photograph of a typical observation is shown in Figure 3. The fraction of the total viewing area covered with the wear flats was easily estimated with the aid of a fine grid on a reticle mounted in the eyepiece. A minimum of ten locations chosen at random on the face of the wheel were used for each measurement.



35 X

Figure 3. Microphotograph of wear flats. Wheel - 32A461I8VG, workpiece - 1018 steel,  $V = 6250$  ft./min.,  $v = 8$  ft./min.,  $d = .001$  in. Taken after 60 passes.

The main advantage of this technique for wear flat area measurements, as compared to most of those described previously in this thesis (see Literature Review), is its efficiency and simplicity. Unlike the other methods, it is not necessary to take numerous photographs from which to work. It is possible to obtain a data point here in a few minutes where the other methods normally require hours of work, and the amount of data previously gathered has been rather limited.

### 3.5.3 Active Grains per Unit Area

There have been numerous attempts to measure the effective number of cutting points per unit area (or their mean spacing) in the surface of a grinding wheel (6, 10, 11, 14, 15, 21, 23, 24, 26, 27, 28). This parameter is usually confused with the number of active grains per unit area, the number of wear flats per unit area, or some other measurement which is related to a particular experimental procedure. The tacit assumptions are that there can be only one cutting point per grain, one wear flat per grain, and one cutting point per wear flat. None of these assumptions are justified.

In the present investigation, the number of active grains per unit area in the surface of the grinding wheel is a particularly important parameter. To illustrate, it is used together with the grinding force and wear flat measurements for the calculation of the average grinding force and wear flat area per active grain.

The number of active grains was experimentally determined with the microscope together with the wear flat measurements previously described. By lighting the wheel surface at a glancing angle, still viewing normal to the surface, the grain corresponding to a particular wear flat could be seen. The total number of grains on which there were wear flats divided by the viewing area was the number of active grains per unit area. Numerical results obtained in this manner were typically lower, by a factor of two or more, than measurements reported by other researchers on similar grinding wheels. This was, of course, to be expected. A single grain may have more than one wear flat and more than one cutting point.

#### 3.5.4 Grinding Wheel Wear

Grinding wheel wear is usually expressed by the G-ratio, which is defined as the volume ratio of metal removed to wheel worn. The volume of wheel worn is given by the product of the decrease in wheel radius, the circumference of the wheel, and the width of the wheel used for grinding. The actual measurement of the decrease of wheel radius is usually made with a micrometer.

For finish grinding, the radial wheel wear before redressing typically amounts to about one-tenth of a grain dimension. It will be shown that most of the wear (by weight) consists of particles which are almost as large as the initial grains. Therefore most of the wear consists of particles whose average diameter is much larger

than the decrease in wheel radius, and the measurement of the wear in this way does not give a true indication of the amount of abrasive removed from the wheel. This would account, at least in part, for the lack of success in correlating the radial wheel wear (or G-ratio) with other parameters of the grinding operation.

In this thesis, the overall grinding wheel wear was determined from the weight of grinding wheel wear particles. A special box-like collector described above was constructed which enabled virtually all the wear debris to be collected. (See Figure 2) The interior of this container was coated with white petrolatum grease which caught the debris as it was generated. The wheel wear particles were ultimately separated by dissolving away the grease in boiling trichlorethylene and the chips in aqua regia acid solution which does not attack aluminum oxide. Wheel wear particles were sieved and weighed on an electric balance to determine the total wear and particle size distribution.

#### 3.5.5. Per Cent Bond Fracture

Grinding wheel wear particles are generated from the fracture of the grain at the bond, fracture within the grain, and rubbing of the grain on the workpiece surface. These are respectively referred to as bond fracture, grain fracture, and attrition. Bond fracture wear particles are almost as large as the grains used in the wheel manufacture. Grain fracture particles are somewhat smaller, about

half as large as the grains. Attritious wear particles are orders of magnitude smaller. Experimentally, most of the grinding wheel wear is found to consist of particles almost as large as the initial grains, and only about five per cent of the wear consists of particles small enough to be caused by attrition. In other words, about ninety-five per cent of the total wear is generated by either bond fracture or grain fracture.

With this in mind, a statistical approach was devised to determine the percentage of the total wear due to bond fracture. It was based on the particle size distributions for both the wear particles and the grains used for production of the wheel. This statistical approach was also applied to the analysis of abrasive particles generated by dressing the wheel. The following assumptions were made:

1. There is only one bond fracture per grain.
2. The total wear is proportional to the number of bond fractures.
3. The largest particles are due to bond fracture.
4. The grain and bond fracture particles have the same density.
5. The weight of a grain or bond fracture particle is proportional to the cube of the average particle diameter as determined by sieving.
6. The contribution to the total wear by particles of bonding agent is negligible.

Calculation of the percentage of total wear due to bond fracture (hereafter called "per cent bond fracture") with the assumptions stated above was based on the following line of reasoning. A given weight

of wheel wear,  $w$ , corresponds to a given number of whole grains,  $M$ . Let  $m$  equal the number of grains per unit weight of grinding wheel. This is experimentally determined by sieving a sample of abrasive used in manufacturing the wheel.  $M$  is obtained by multiplying  $m$  by  $w$ .  $M$  is also the number of bond fracture particles in  $w$  milligrams of wear. The ratio ( $\times 100$ ) of the weight of the  $M$  biggest particles to the total wear " $w$ " is equal to the per cent bond fracture,  $B$ .

The per cent bond fracture also represents the weight of an average bond fracture particle compared to the weight of an average whole grain. With the per cent bond fracture  $B$  expressed in decimal form ( $B/100$ ), its cube root is the ratio of the average bond fracture particle diameter to the average whole grain diameter.



#### IV. DRESSING

##### 4.1 Introduction

Most grinding operations are very sensitive to the manner in which the wheel is dressed. This is especially true in the case of precision grinding where the depths of cut are small and the radial wheel wear amounts to only a small fraction of the mean grain diameter.

In this investigation, two different dressing procedures were used which are referred to as "coarse" and "fine". Coarse dressing was accomplished by passing the flat side of a pyramidal diamond across the wheel face with .001 inch radial infeed at 3 ft/min. cross-feed at the same wheel/speed used for grinding. The diamond was inclined 13 degrees towards the trailing edge of the wheel. This procedure was repeated five times beyond what was necessary for truing the wheel: typically a total of ten or fifteen passes were taken. The diamond was rotated 90 degrees after each test in order to maintain its shape.

The fine dress was achieved in a similar manner but with two additional "spark-out" passes (no downfeed) also at 3ft/min crossfeed velocity. Although differences between these two dressing procedures may appear to be slight, substantial differences in grinding action were observed.

The number of active grains per unit area and the initial wear flat area on the wheel face were determined for both dressing techniques using

the methods previously described. Prior to making these measurements, a single grinding pass across the 1018 steel workpiece was taken. This was necessary in order to clearly view the wear flats on the grains.

The particle size distribution was also obtained for particles removed from the wheel during a coarse dress pass. The per cent bond fracture was calculated and was related to the wheel grade and the number of active grains per unit area.

#### 4.2 Results

The experimental results are listed in Table 3 and shown in the graphs in Figures 4-8.

From Figures 4 and 5 it is seen that harder wheels and finer dressing produce more active grains per square inch and a larger initial wear flat area. Between the G and K grade wheels (3.1 and 8.6 per cent bonding agent respectively) there is about a factor of three increase in the number of active grains, and a factor of four increase in wear flat area. These parameters are about 15 per cent greater with the fine dress than with the coarse dress.

The average wear flat area per grain is shown in Figure 6 as a function of wheel grade and dressing condition. This is obtained by dividing the wear flat area per square inch ( $.01 \times$  per cent wear flat area) by the number of active grains per square inch. The wear flat area per grain is constant for the H through K grade wheels at

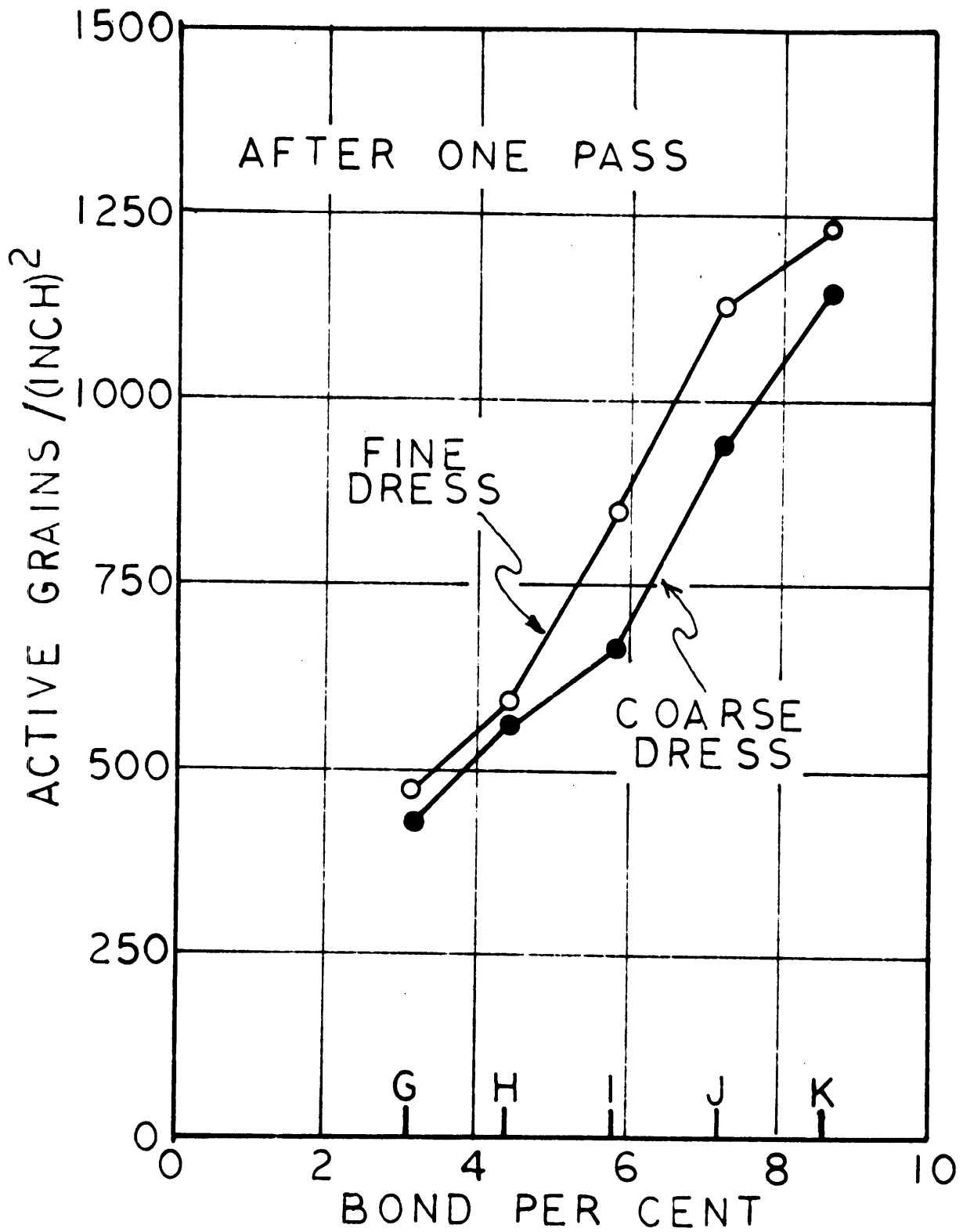


Figure 4. Number of active grains/inch<sup>2</sup> versus bond per cent for fine and coarse dressing. (The letters denote wheel grades.)

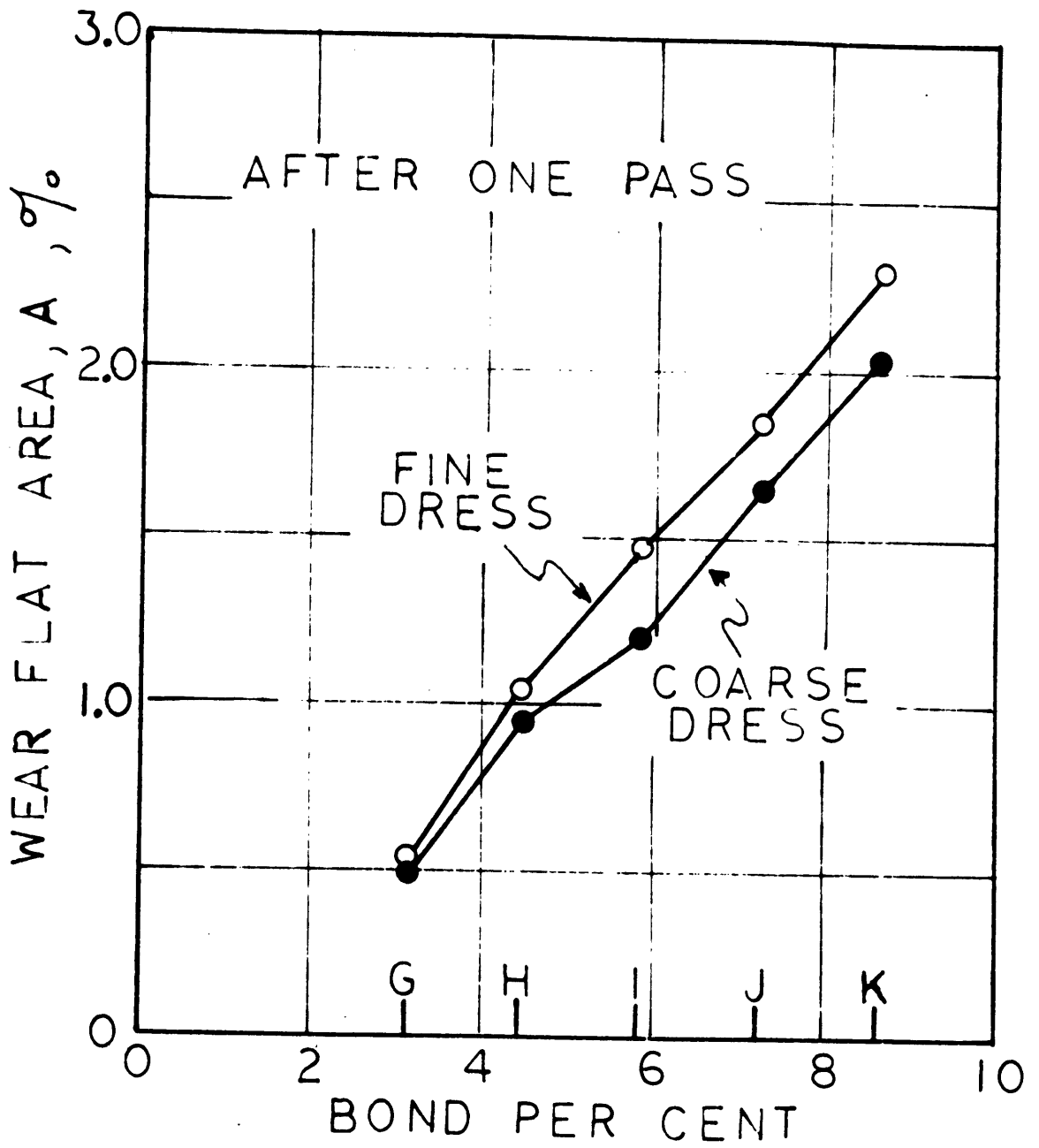


Figure 5. Wear flat area versus bond per cent for fine and coarse dressing. (The letters denote wheel grades.)

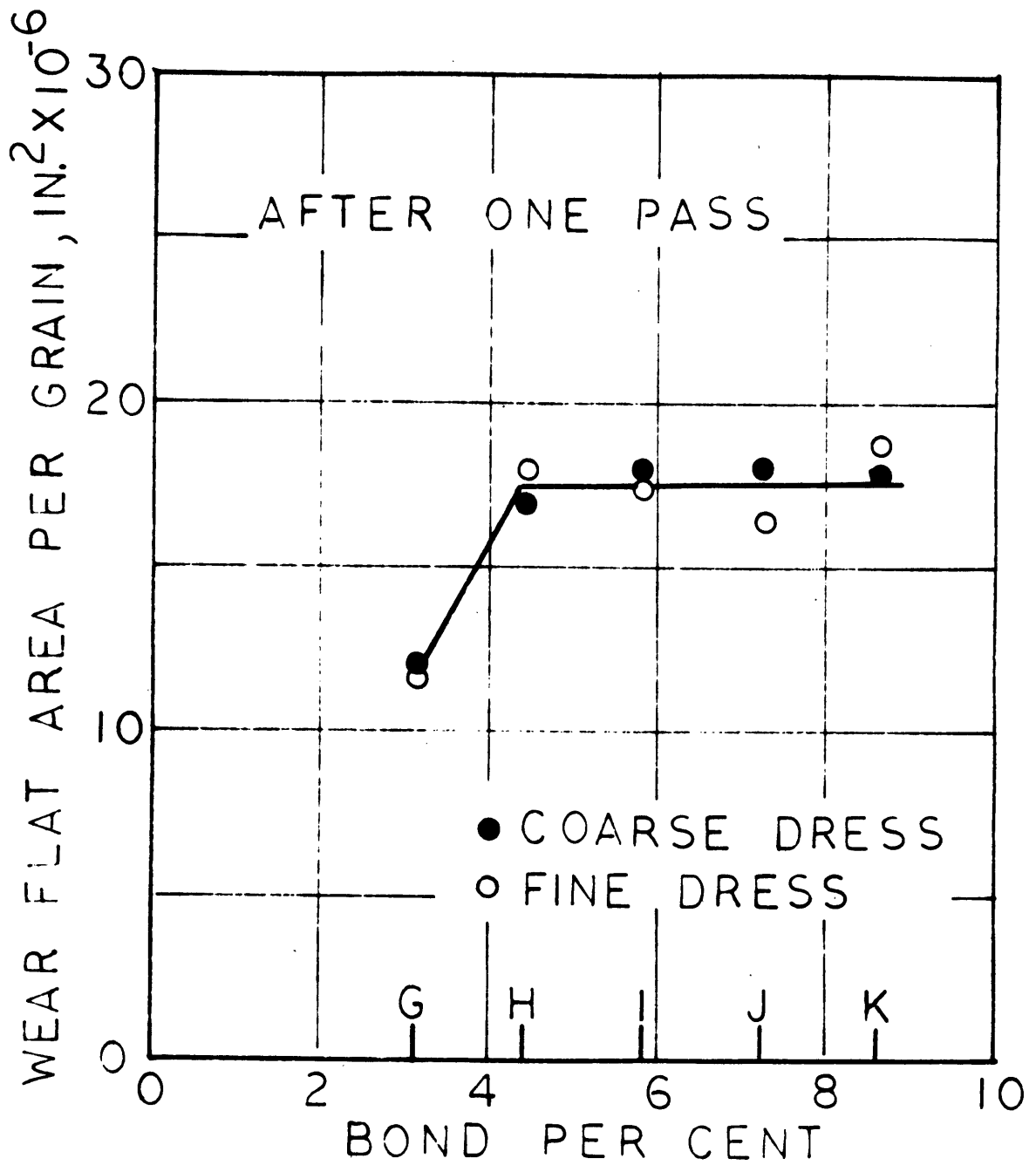


Figure 6. Wear flat area per grain versus bond per cent for fine and coarse dressing. (The letters denote wheel grades.)

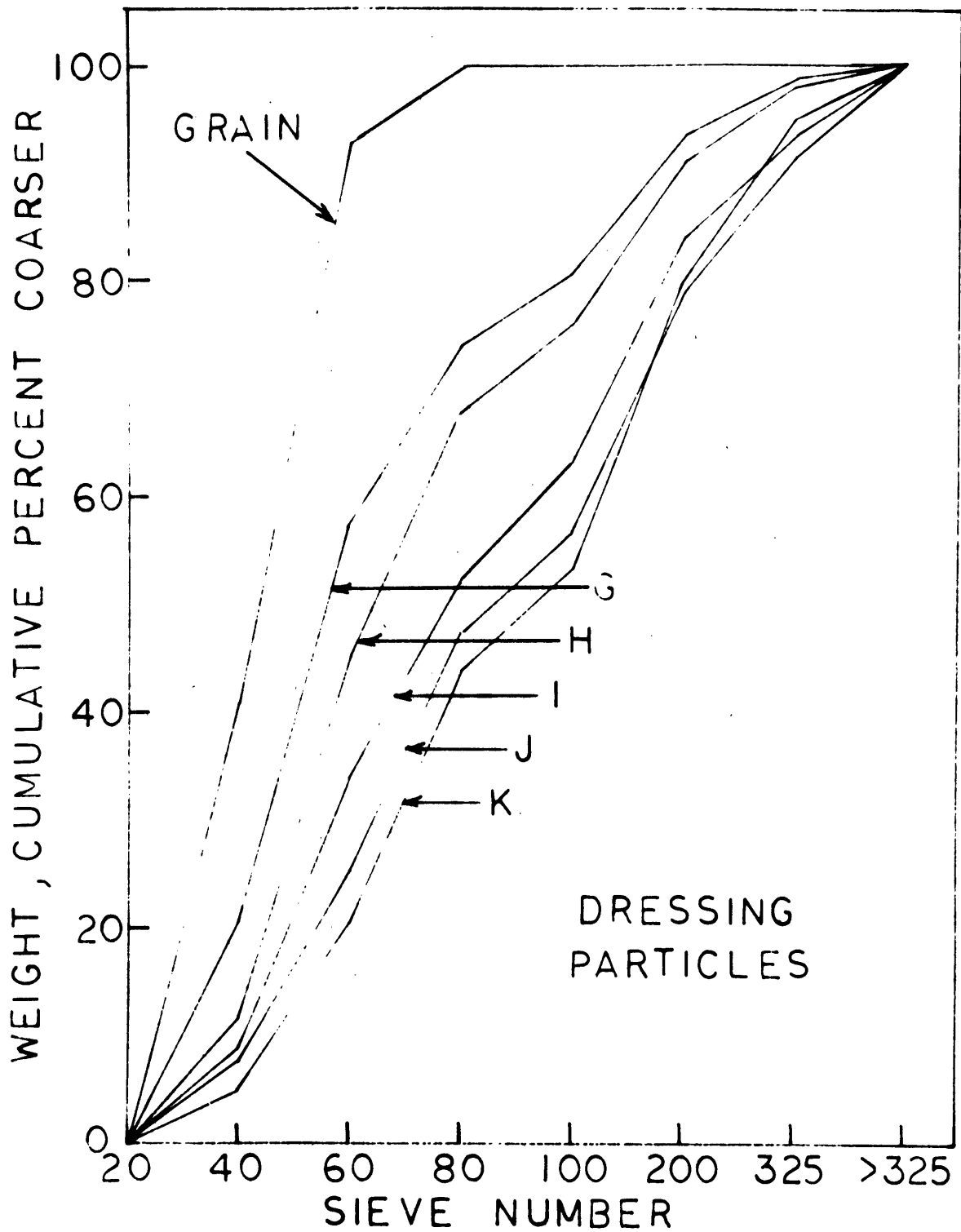


Figure 7. Particle size distribution for dressing particles and abrasive grain. (The letters denote wheel grades.)

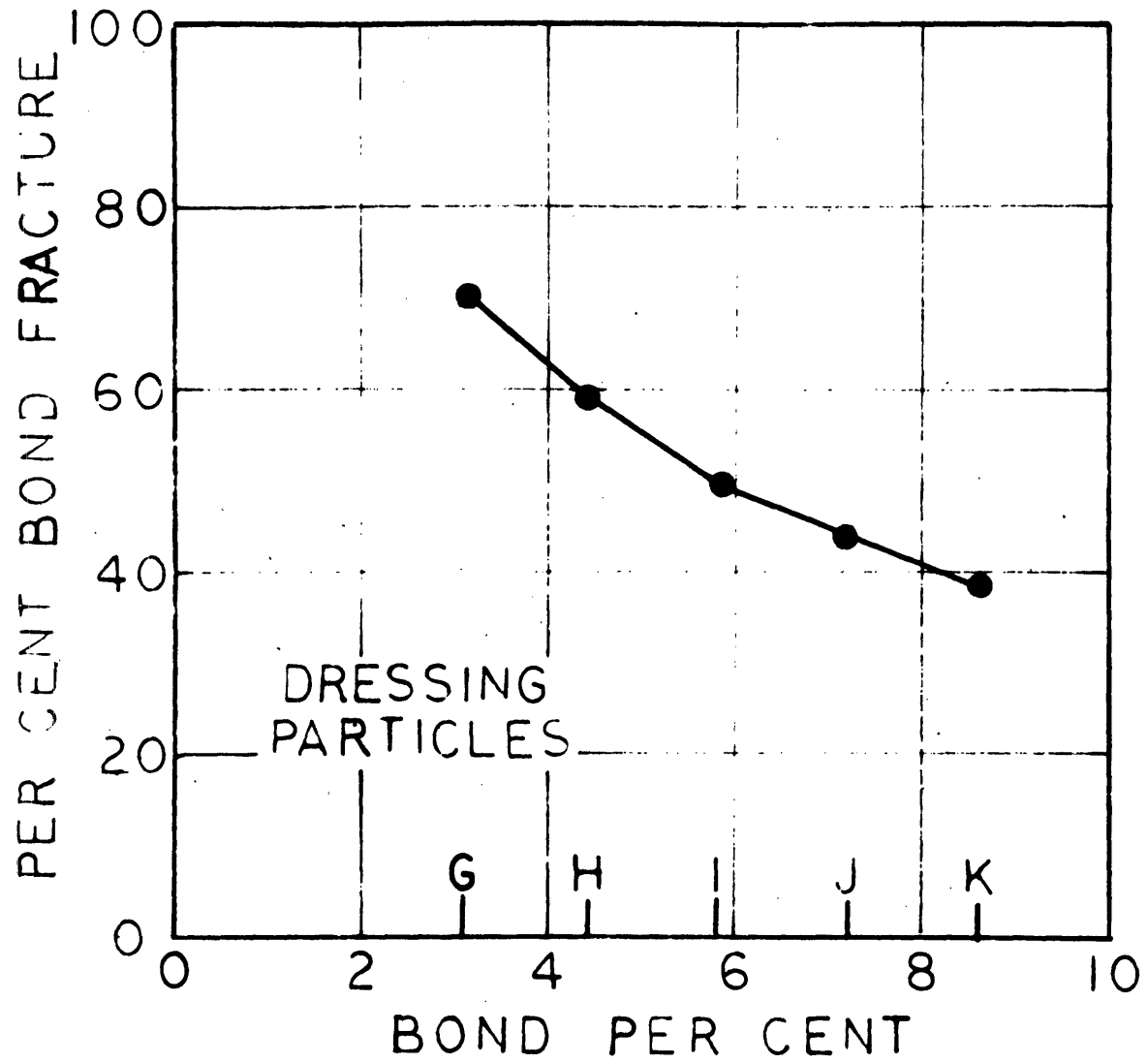


Figure 8. Per cent bond fracture versus bond per cent for dressing particles. (The letters denote wheel grades.)

about  $17 \times 10^{-6}$  inch<sup>2</sup>, and about one-third lower for the G wheel. The wear flat area per grain for the harder wheels represents only about 8 per cent of the grain cross-sectional area which is determined from the square of the mean grain diameter.

Figure 7 shows the particle size distribution for wheel particles removed during dressing for the various grades of wheel. The screen openings corresponding to the sieve numbers are given in Table 4. For comparison, the distribution is also presented for the 32A46 grain (32 Alundum, 46 grain size) used in production of the wheels. These distributions are plotted on a cumulative basis from larger to smaller particles (smaller to larger sieve numbers). A higher elevation of the curve corresponds to less fragmentation and larger particles.

The results clearly show that there was more fragmentation when dressing the harder grade wheels. This can also be seen in Figure 8 where the per cent bond fracture, which is calculated from the particle distributions in Figure 7, is plotted for the various wheel grades.

#### 4.3 Discussion

The surface of the grinding wheel is defined by the tips of the active grains. In order for a grain to be "active", it must be close to the wheel periphery, say within  $10^{-5}$  inch which approximates the chip thickness. If a wheel is dressed in such a manner as to decrease the height deviations among the tips of the outermost grains, there are likely to be more active grains in the surface of the wheel.



It has been shown (see Figures 4 and 8) that the harder wheels tend to have smaller dressing particles and more active grains. Smaller particles are to be expected since grains more firmly held with larger amounts of bonding agent are more susceptible to fragmentation prior to total dislodgement. The number of active grains should increase with increasing wheel hardness since the smaller particles leaving the wheel would minimize the height deviations among the grains left on the wheel surface. This is clearly illustrated in Figure 9 which is a crossplot of the active grains per square inch and 100 minus the per cent bond fracture. Zero on the abscissa corresponds to 100 per cent bond fracture (an infinitely soft wheel) with only whole grains removed by dressing.

The extension of this curve almost intersects the origin. This makes sense from a physical standpoint. In Appendix A it is shown that the potential number of active grains is about  $3240/\text{inch}^2$ . For an infinitely soft wheel this is also the number of grain tips expected to extend to within one grain dimension of the wheel periphery. With the wheel periphery defined by the center of the wheel and the tip of the outermost grain, assuming the height distribution of the grain tips is random, the probability that any of the potentially active grains is active (within  $10^{-5}$  of the wheel periphery) is equal to  $10^{-5}$  divided by the mean grain diameter (mean grain diameter = .015 inch) or .0066. The expected number of active grains per square inch for 100 per cent bond fracture is then  $.0066 \times 3240 = 22$ , which is very small.

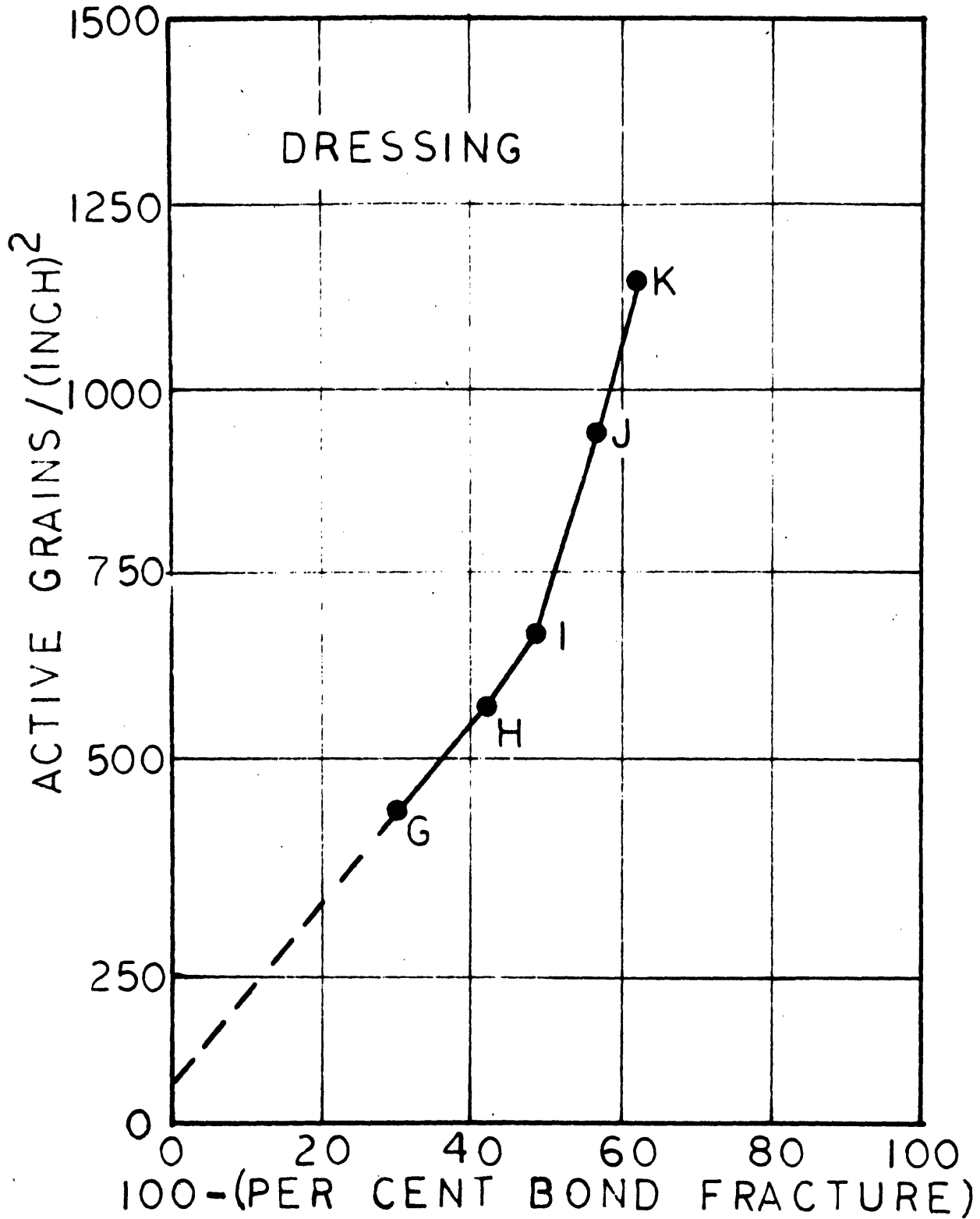


Figure 9. Number of active grains per square inch versus 100 minus per cent bond fracture for dressing particles. (The letters denote wheel grades.)

PAGES (S) MISSING FROM ORIGINAL

PAGE 35 MISSING

## V. ATTRITIOUS WEAR AND GRINDING FORCES

### 5.1 Introduction

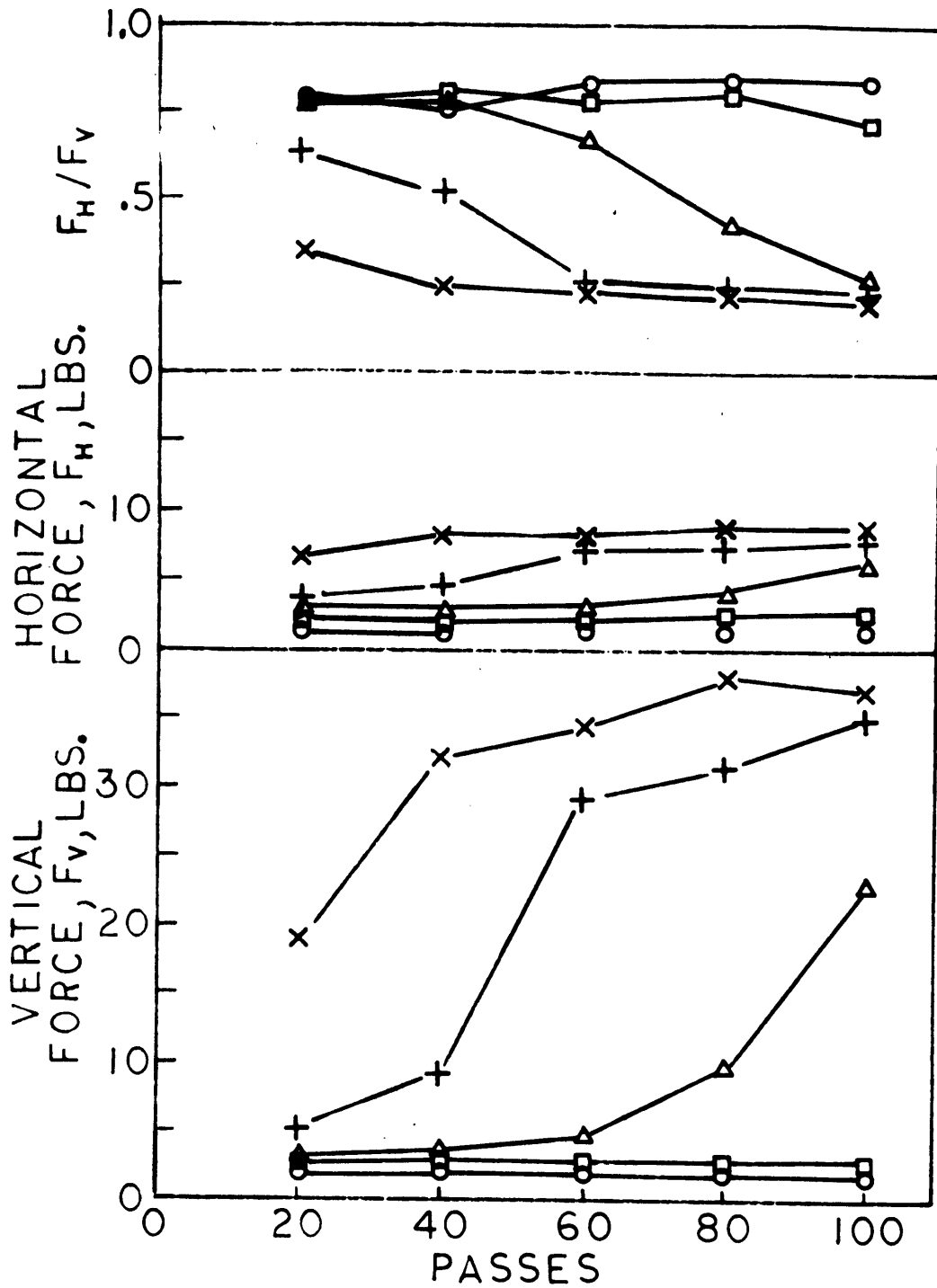
Attritious wear in grinding refers to the development and growth of wear flats on the tips of the active grains. This type of wear is measured by the percentage of the wheel surface covered with wear flats.

In the previous section it was seen that wear flats are dressed on to the wheel and therefore, in this sense, the initial attritious wear is not zero. While the wear flat area will, in general, increase as grinding proceeds, this is not a necessary requirement since fracture wear can diminish the wear flat area.

Grinding forces are measured with the semiconductor strain gage dynamometer previously described, and each data point is the average of an "up" and "down" pass. "Up" grinding refers to the condition where the workpiece velocity,  $v$ , is in the opposite direction to the wheel velocity,  $V$ , at the grinding area. "Down" grinding refers to the opposite table motion. In the present series of tests, the grinding forces were only slightly affected by the direction of the workpiece motion, the "down" grinding forces being at most 10 per cent greater at the largest wear flat area.

### 5.2 Results

Experimental results are presented in Tables 5 and 6 and Figures 10-14 for the 1018 steel with the fine and coarse dressed wheels. Figures 10 and 12 show the variation in the grinding forces and force ratio and



1018 STEEL, FINE DRESS

○ G      □ H      △ I      + J      × K

Figure 10. Grinding forces and force ratio versus number of passes for 1018 steel workpiece, fine dress,  $V = 6250$  ft./min.,  $v = 8$  ft./min.,  $d = .001$  in. (The letters denote wheel grades.)

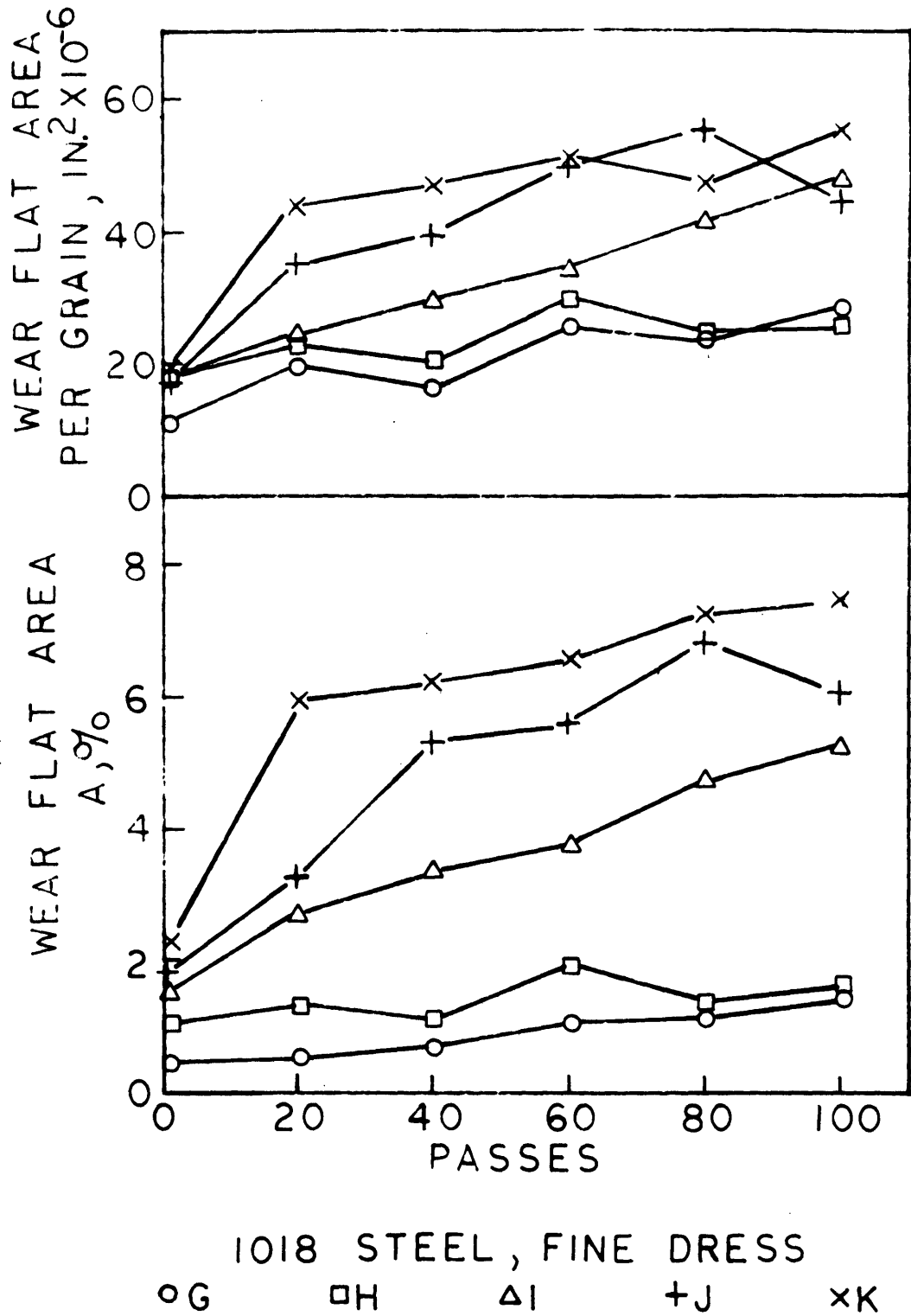
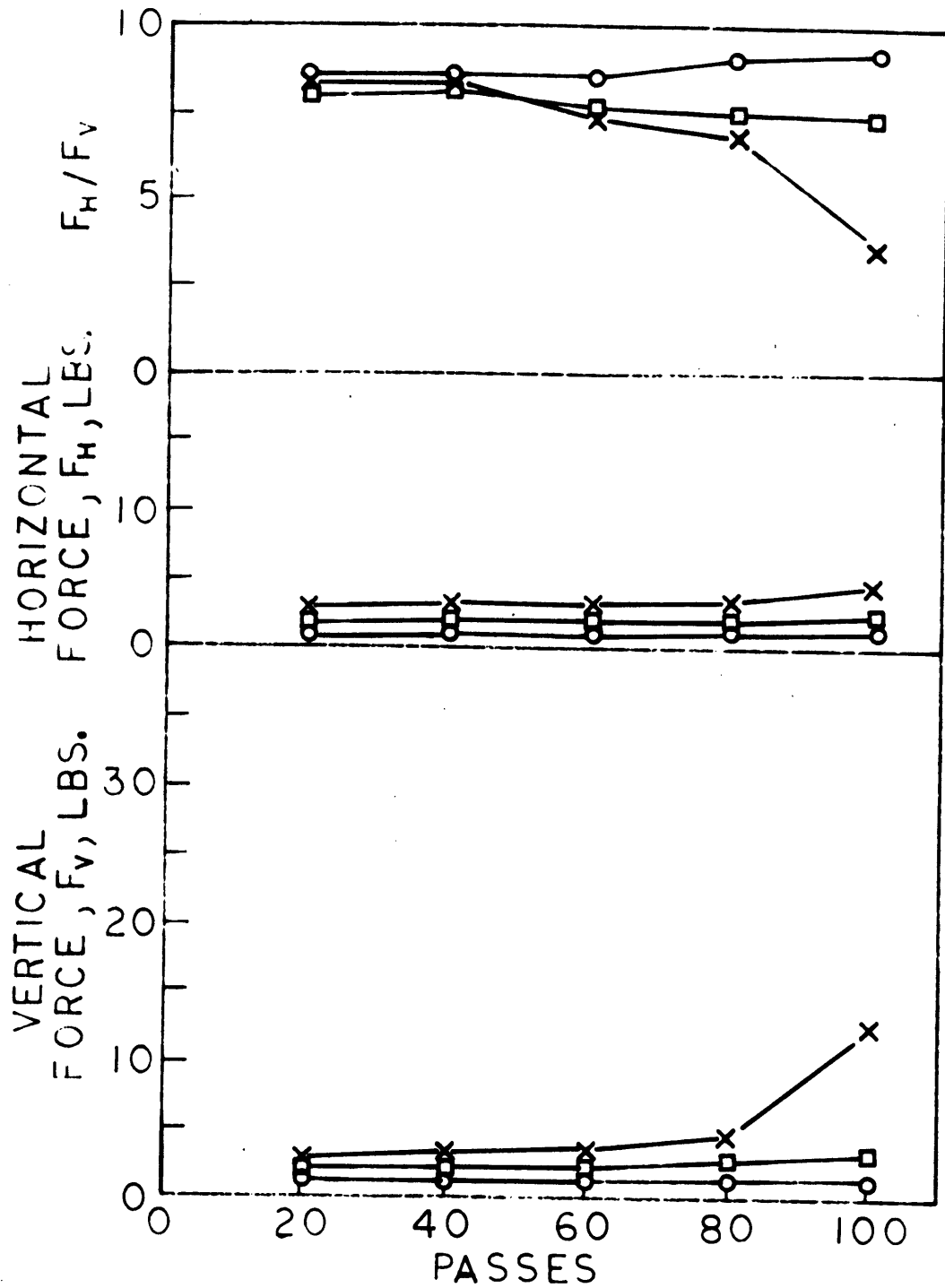
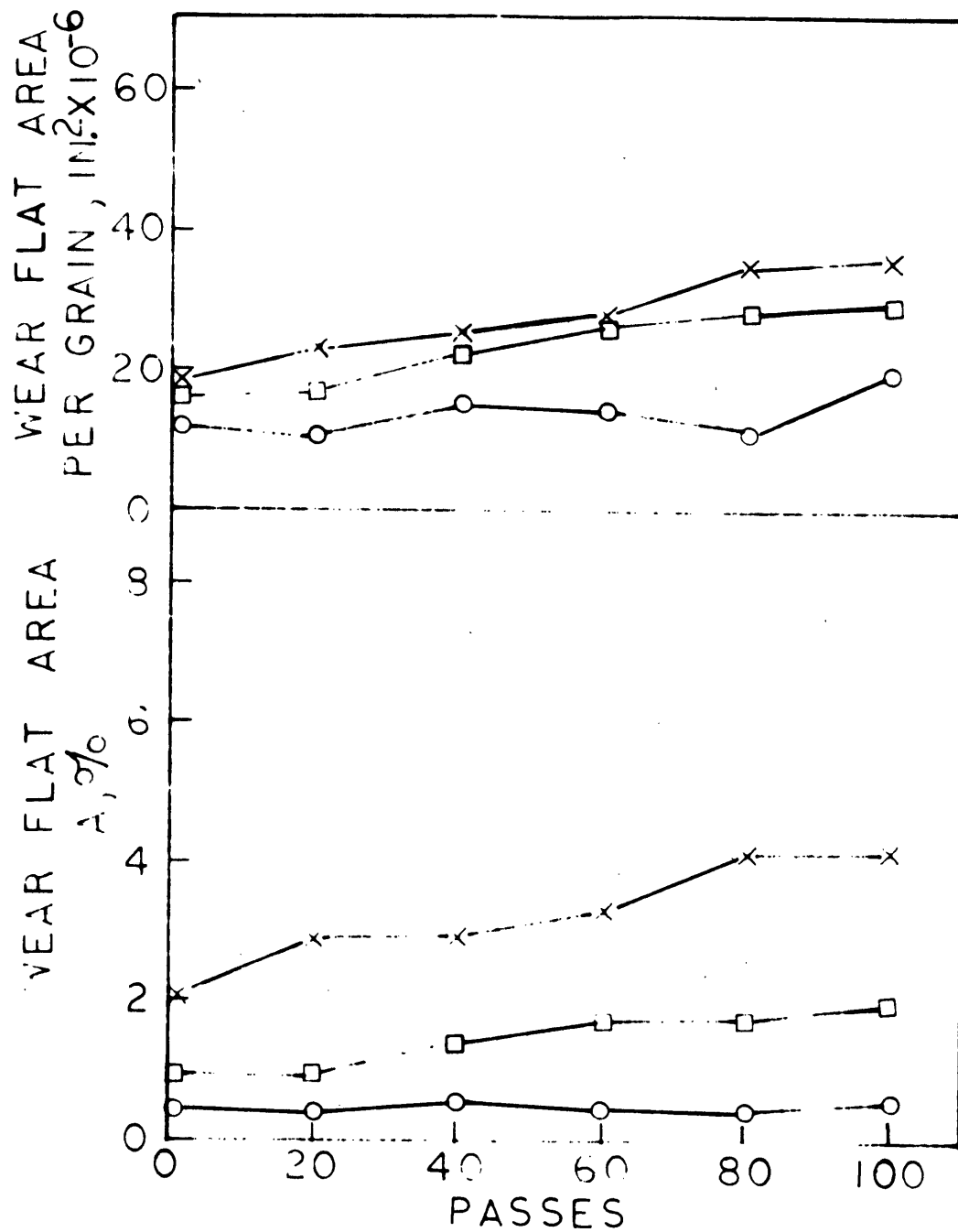


Figure 11. Per cent wear flat area and wear flat area per grain versus number of passes for 1018 steel workpiece, fine dress,  $V = 6250$  ft./min.,  $v = 8$  ft./min.,  $d = .001$  in. (The letters denote wheel grades.)



1018 STEEL, COARSE DRESS  
 ○ G      □ H      × K

Figure 12. Grinding forces and force ratio versus number of passes for 1018 steel workpiece, coarse dress,  $V = 6250$  ft./min.,  $v = 8$  ft./min.,  $d = .001$  in. (The letters denote wheel grades.)



1018 STEEL , COARSE DRESS

○G      □H      ×K

Figure 13. Per cent wear flat area and wear flat area per grain versus number of passes for 1018 steel workpiece, coarse dress,  $V = 6250$  ft./min.,  $v = 8$  ft./min.,  $d = .001$  in. (The letters denote wheel grades.)



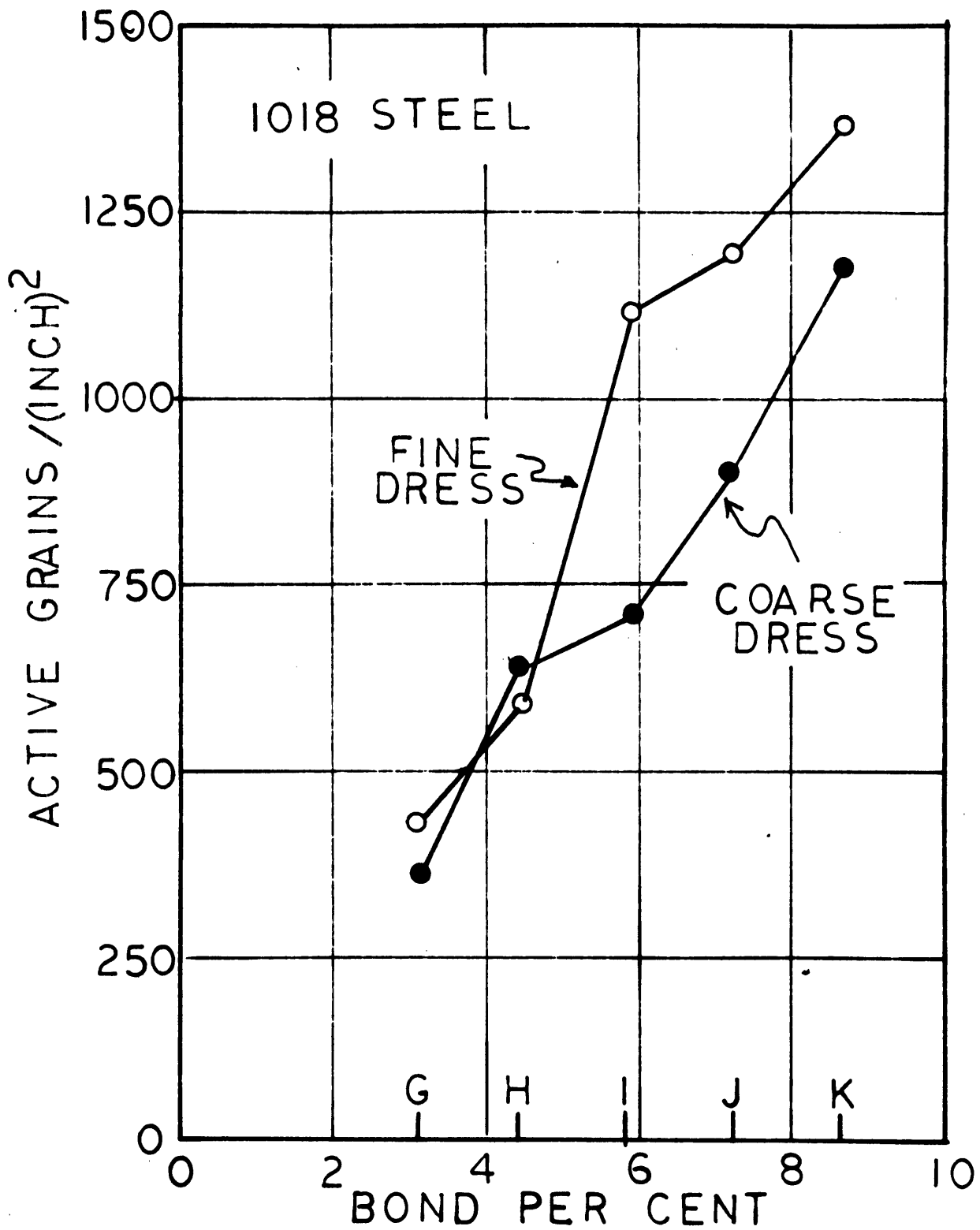
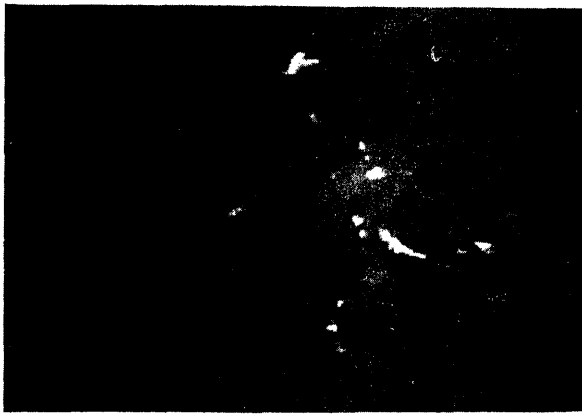


Figure 14. Number of active grains/inch<sup>2</sup> versus bond per cent for 1018 steel workpiece,  $V = 6250$  ft./min.,  $v = 8$  ft./min.,  $d = .001$  in. (The letters denote wheel grades.)

Figures 11 and 13 the variation in wear flat areas as a function of the number of passes for the different grades of wheels. The wear flat area data points for 1 pass, Figures 11 and 13, are those presented in the previous section in Table 3. To simplify the graphs, only the results for the G, H, and K wheels are plotted in Figures 12 and 13. The number of active grains was more or less constant as grinding proceeded, and therefore, the average values are presented in Figure 14 for the different wheel grades and dressing techniques.

The grinding forces in Figures 10 and 12 are characteristically higher for the harder grades of wheels. With the harder wheels a transition appears where the grinding forces increase rapidly, the rate of increase being about seven times greater for the vertical as compared to the horizontal force component. This transition is more readily obtainable with the finer dressing technique where it occurs almost instantaneously for K-grade wheel, after about 35 passes for the J-grade wheel, and after about 60 passes with the I-grade wheel. At this point workpiece "burn" is observed where the ground surface takes on a bluish tempering color.

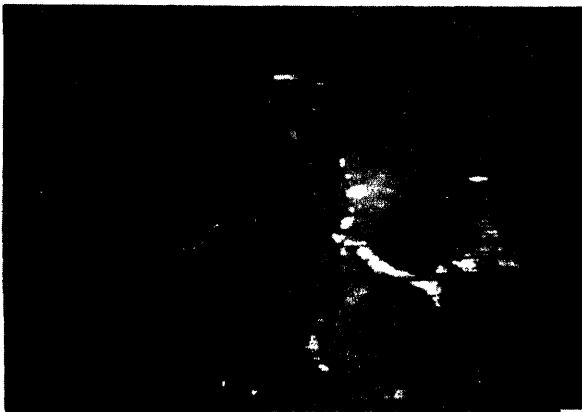
The wear flat area measurements in Figures 11 and 13 follow the same general trend as their corresponding force measurements. As previously stated, the number of active grains per unit area for each wheel was found to be relatively unchanged as grinding proceeded. Therefore increases in the wear flat area with the number of passes would be expected to be primarily due to the growth of existing wear flats rather than the development of new ones. This can in fact be seen in Figure 15 where photographs of the same area of



20 passes



40 passes



60 passes



80 passes



100 passes

20X

Figure 15. Microphotographs of wear flats after 20, 40, 60, 80, and 100 passes. Wheel - 32A461I8VG, workpiece - 1018 steel, fine dress,  $V = 6250$  ft./min.,  $v = 8$  ft./min.,  $d = .001$  in.

a grinding wheel are shown after 20, 40, 60, 80, and 100 passes.

Although little variation was noted in the number of active grains as grinding proceeded, substantial differences were found for wheels of different grades, the harder wheels exhibiting more active grains. A smaller increase was generally obtained with finer dressing. These results, presented in Figure 14, are substantially the same as those previously presented in Figure 4.

Figure 16 presents cross plots of the horizontal and vertical components of the grinding forces,  $F_H$  and  $F_V$ , each plotted against the per cent wear flat area,  $A$ . The data for all grades of wheels using both dressing techniques fall on a single curve consisting of two straight line segments of different slopes. The straight lines in this figure were obtained by the method of least squares with the force taken as the error free variable. The intersection of these two straight line segments, at about 3.6 per cent wear flat area, corresponds to the transition above which workpiece "burn" is observed. Data points used for determining this section of each of the curves were the ones where burning was actually observed, as indicated in Tables 5 and 6.

The relationship between the grinding forces and the per cent flat area was also obtained for the other workpiece materials listed in Table 2 for the same grinding conditions, and for 1018 steel with both the wheel speed and table speed decreased by a factor of 2. These results are presented in Figures 17-23 and Tables 7-13.

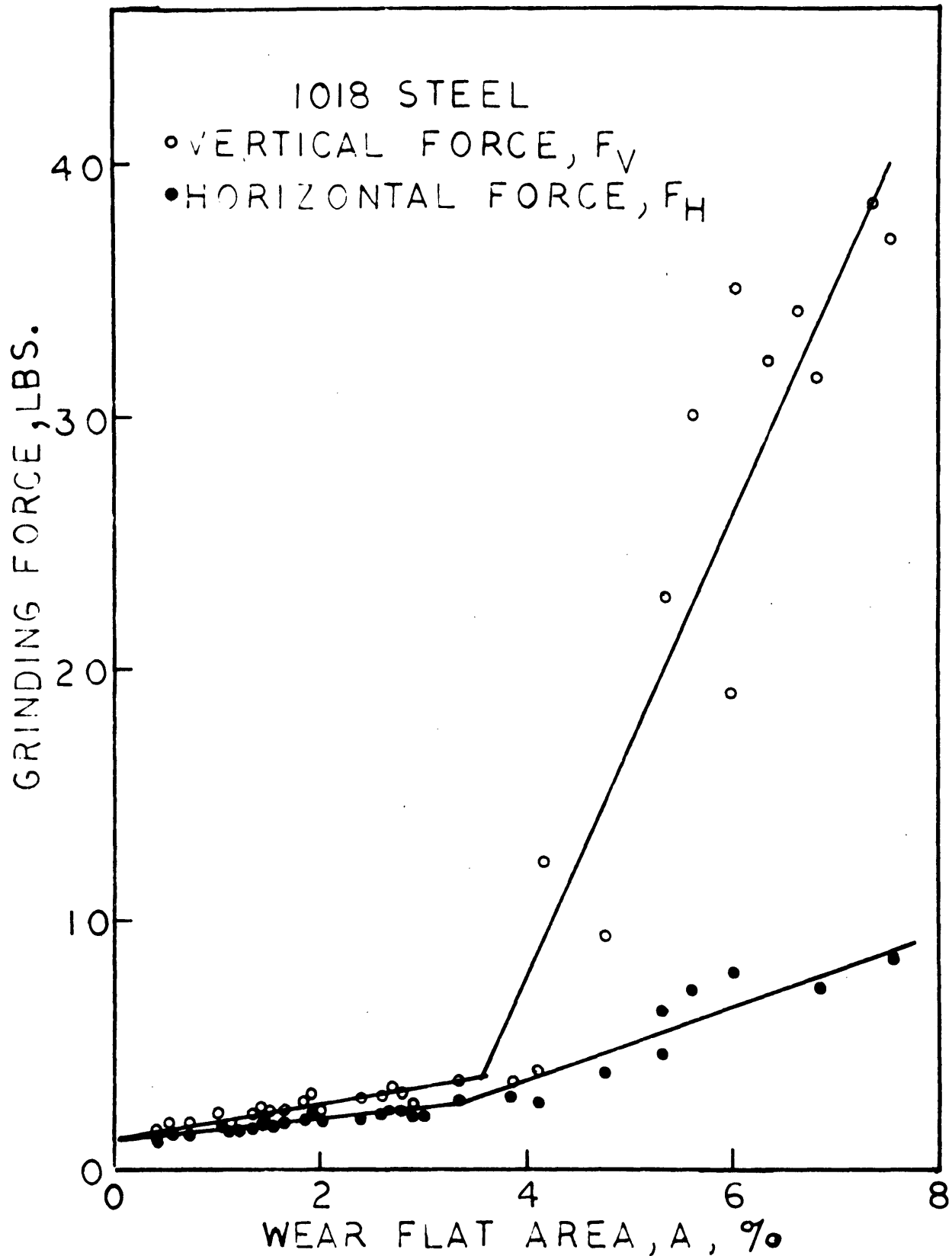


Figure 16. Grinding forces versus wear flat area for 1018 steel, fine and coarse dress,  $V = 6250$  ft./min.,  $v = 8$  ft./min.,  $d = .001$  in. (The letters denote wheel grades.)

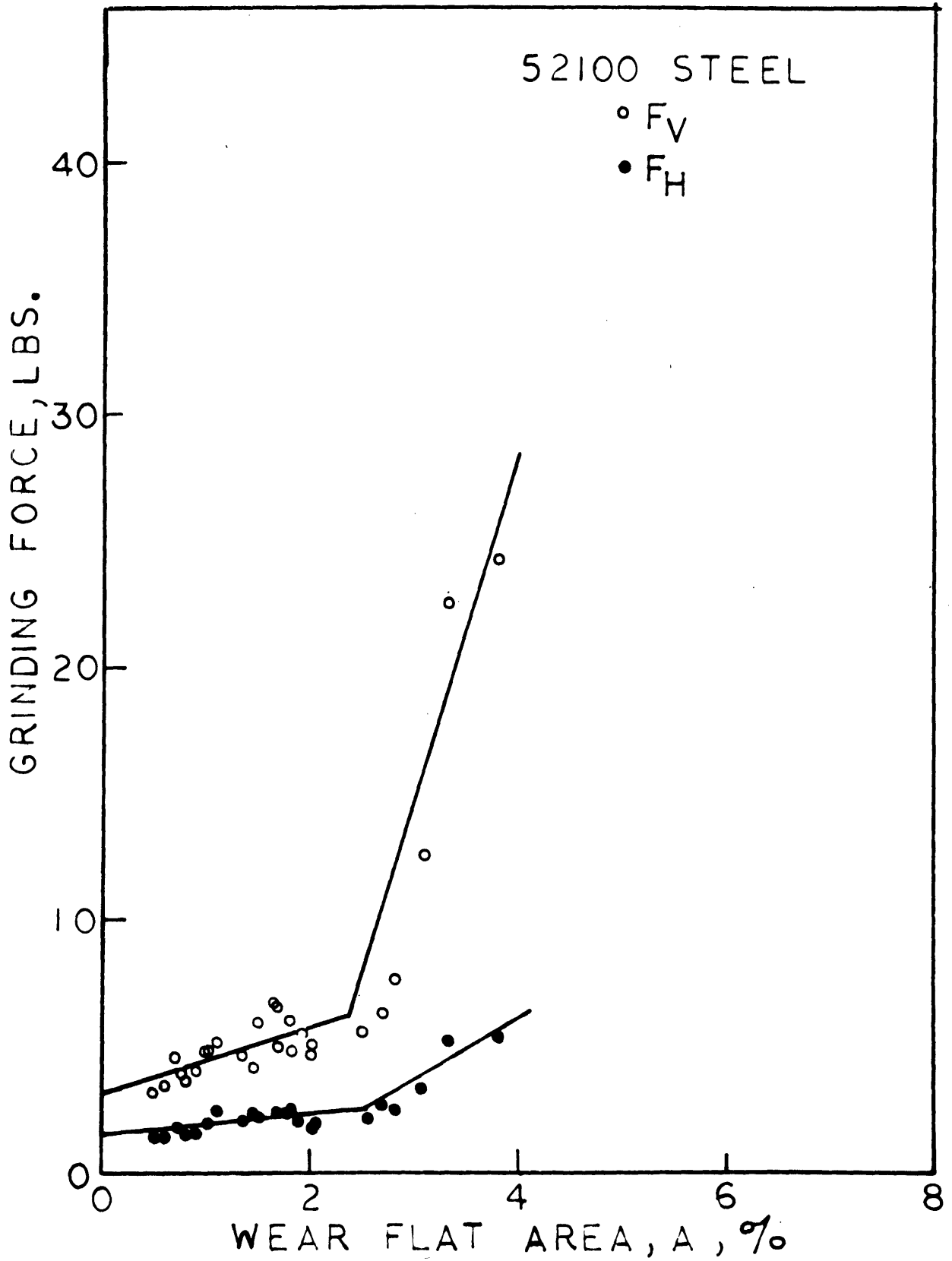


Figure 17. Grinding forces versus wear flat area for 52100 steel, fine dress,  $V = 6250$  ft./min.,  $v = 8$  ft./min.,  $d = .001$  in.

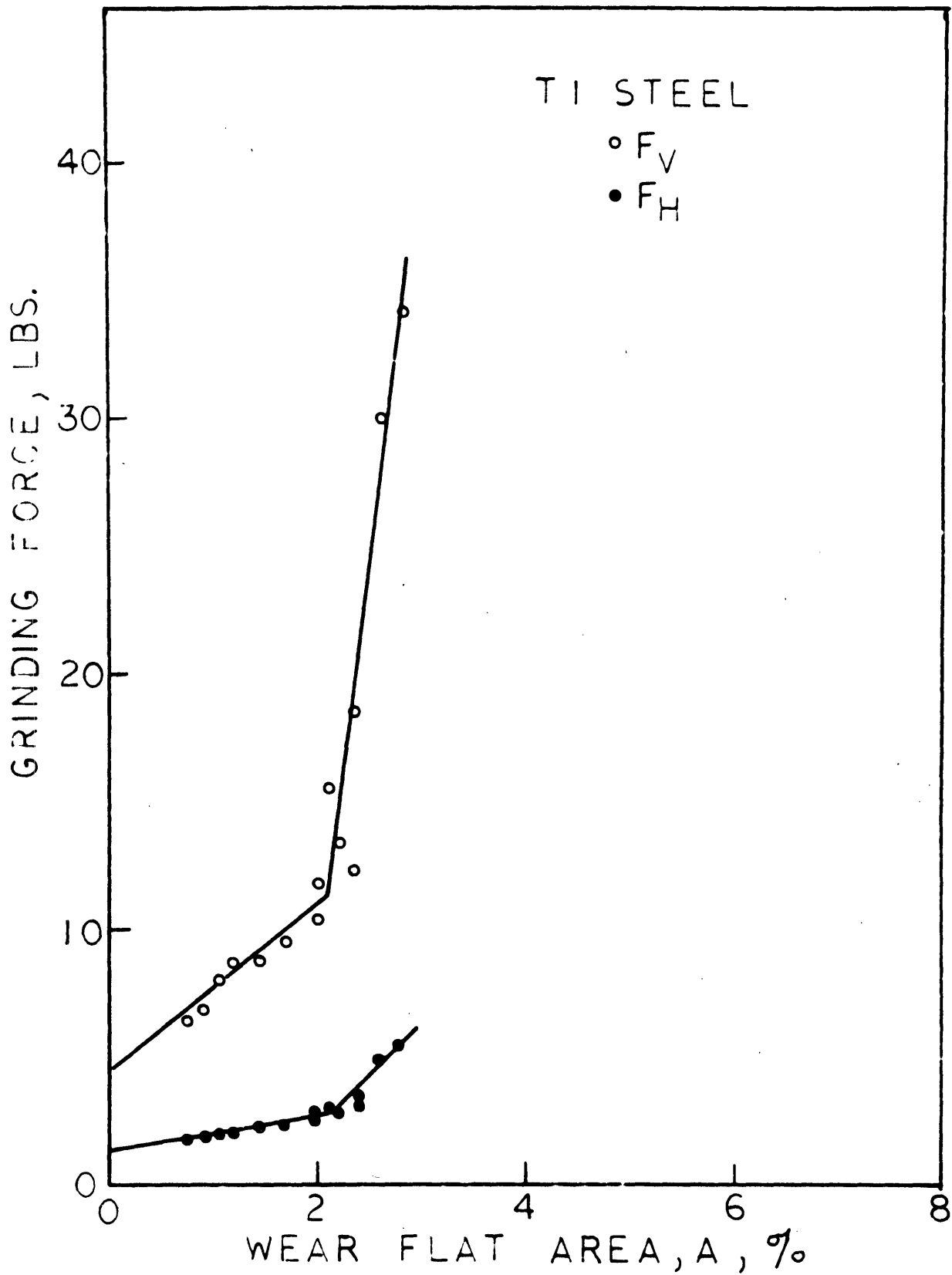


Figure 18. Grinding forces versus wear flat area for T1 steel, fine dress,  $V = 6250$  ft./min.,  $v = 8$  ft./min.,  $d = .001$  in.

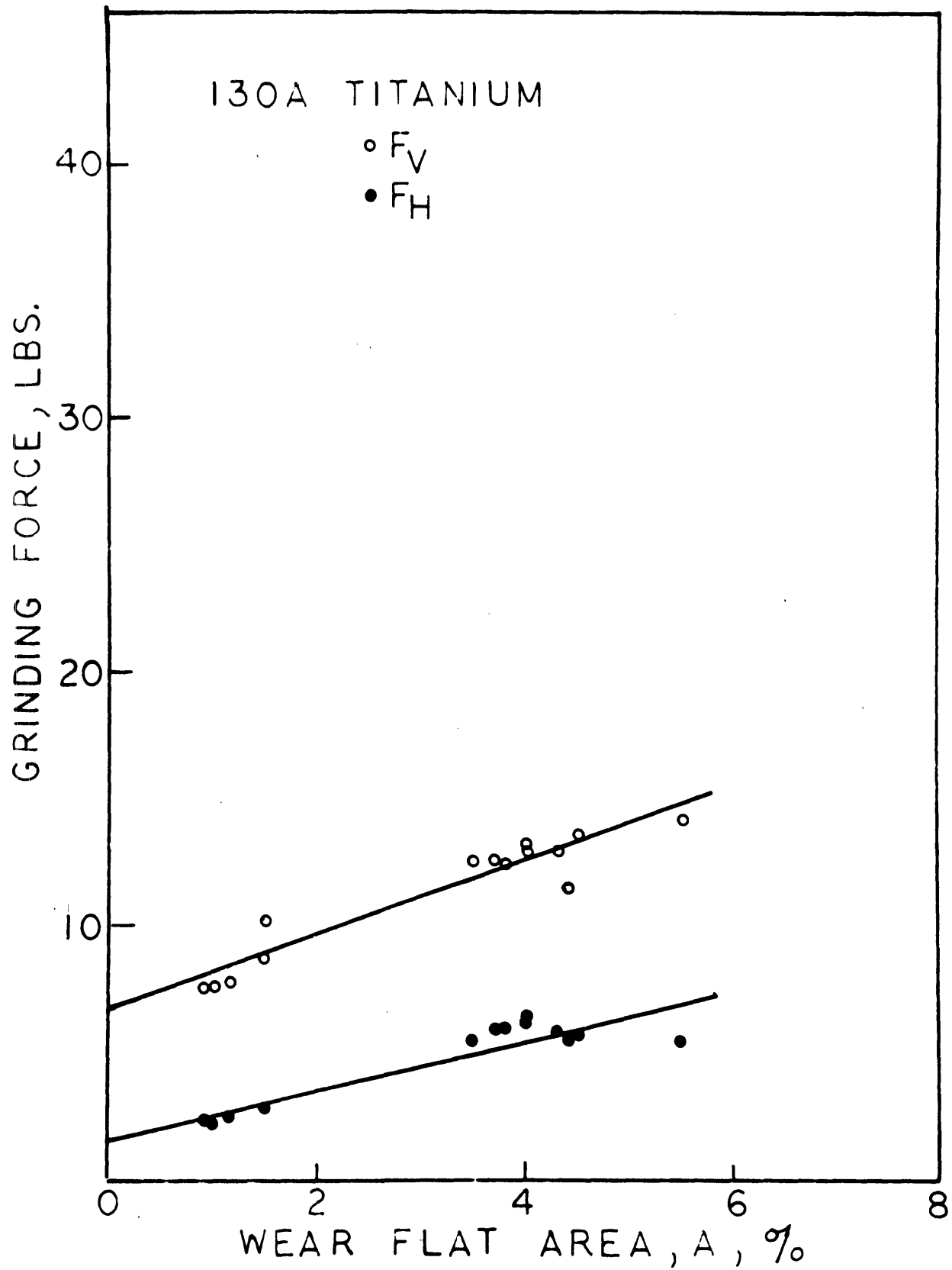


Figure 19. Grinding forces versus wear flat area for 130A titanium, fine dress,  $V = 6250$  ft./min.,  $v = 8$  ft./min.,  $d = .001$  in.



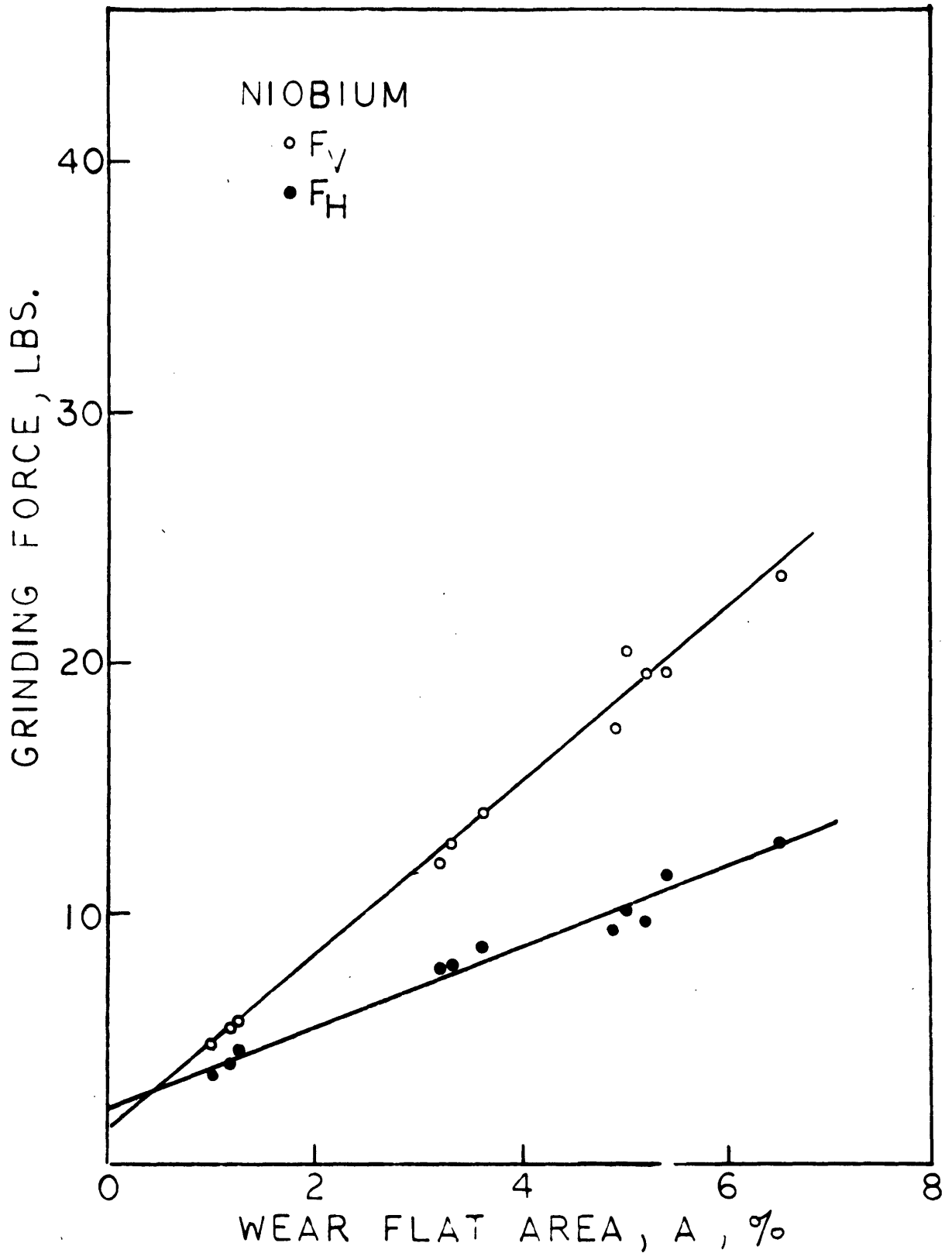


Figure 20. Grinding forces versus wear flats area for niobium, fine dress,  $V = 6250$  ft./min.,  $v = 8$  ft./min.,  $d = .001$  in.

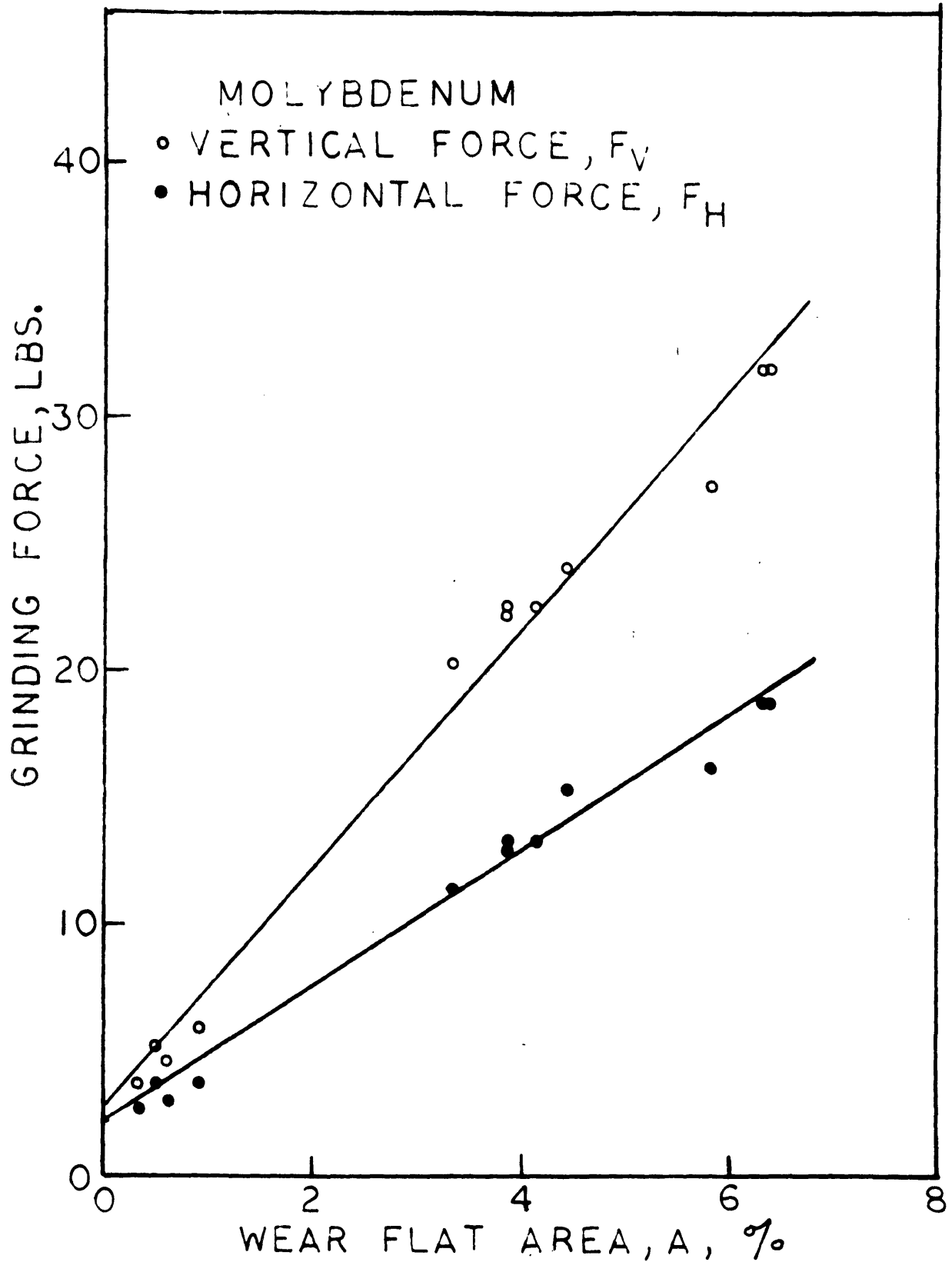


Figure 21. Grinding forces versus wear flat area for molybdenum, fine dress,  $V = 6250$  ft./min.,  $v = 8$  ft./min.,  $d = .001$  in.

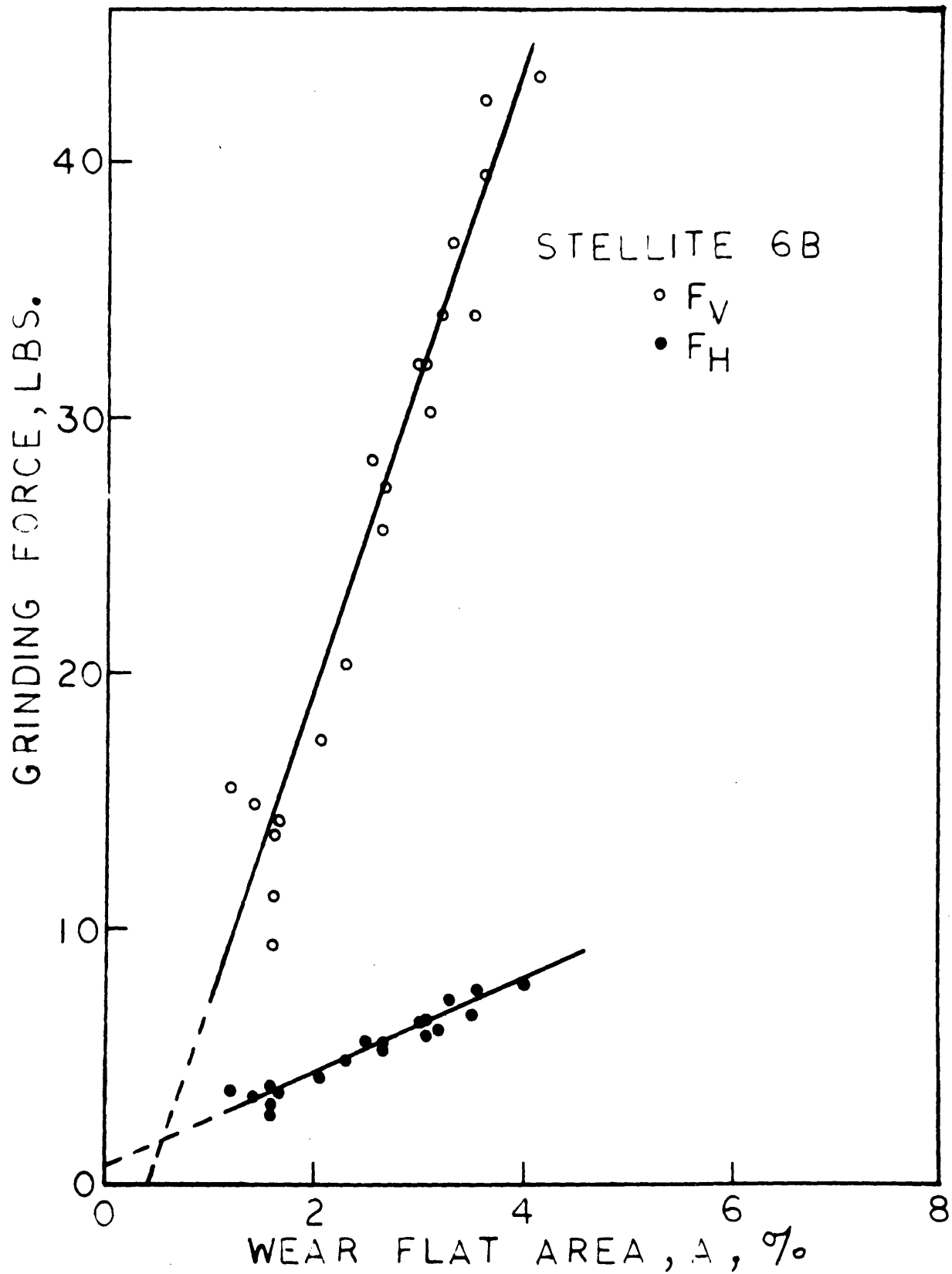


Figure 22. Grinding forces versus wear flat area for Stellite no. 6B, fine dress,  $V = 6250$  ft./min.,  $v = 8$  ft./min.,  $d = .001$  in.

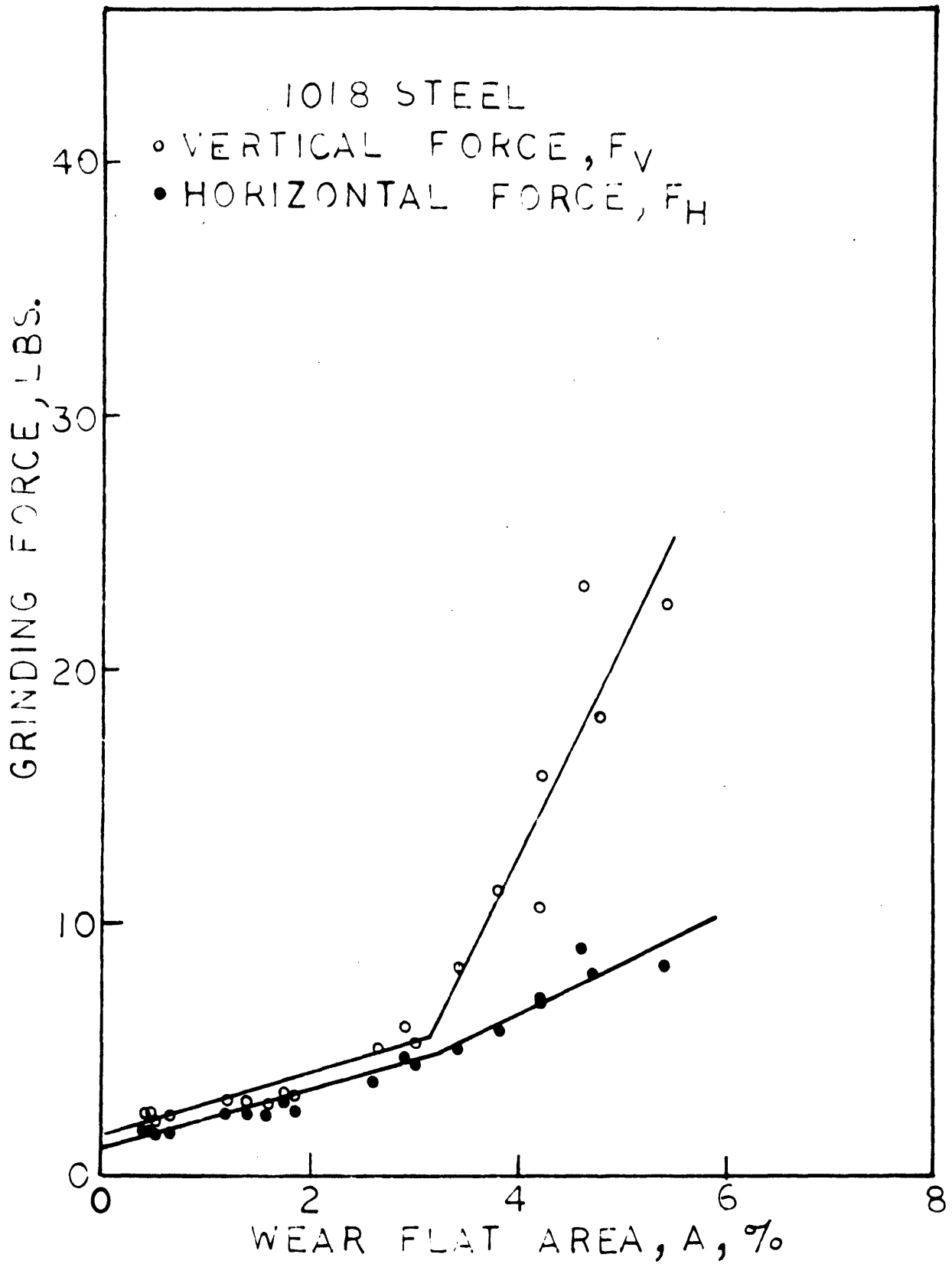


Figure 23. Grinding forces versus wear flat area for 1018 steel, fine dress,  $V = 3125$  ft./min.,  $v = 4$  ft./min.,  $d = .001$  in.

For the steel workpieces (Figure 17, 18 and 23) the same general behavior was observed as in Figure 16, and workpiece burn was always observed beyond the transition. The results for the other materials, Figures 19-22, all fell on a single straight line.

An attempt was made to grind a number of other materials including nickel, cobalt, copper, bronze, brass, and aluminum. For these materials, the phenomenon commonly referred to as "loading" occurred where fragments from the workpiece would stick to the wheel and prevent normal grinding action. With the exception of the cobalt, no grinding sparks were observed. Under these conditions, it was impossible to obtain any meaningful data.

### 5.3 Discussion

The experimental results for the force vs. wear flat area relationships; with the exception of those for the Stellite, are consistent with the following interpretation. The vertical and horizontal grinding forces are both made up of two components, one due to cutting and one due to sliding on the wear flats.

$$F_V = F_{VC} + F_{VS} \quad (5.1)$$

$$F_H = F_{HC} + F_{HS} \quad (5.2)$$

This is illustrated in Figure 24. The chip mechanics and therefore the cutting force components are assumed to be unaffected by the size of the wear flats. At zero wear flat area, the sliding forces are zero and the grinding forces are equal to the cutting force components,  $F_{VC}$  and  $F_{HC}$ .

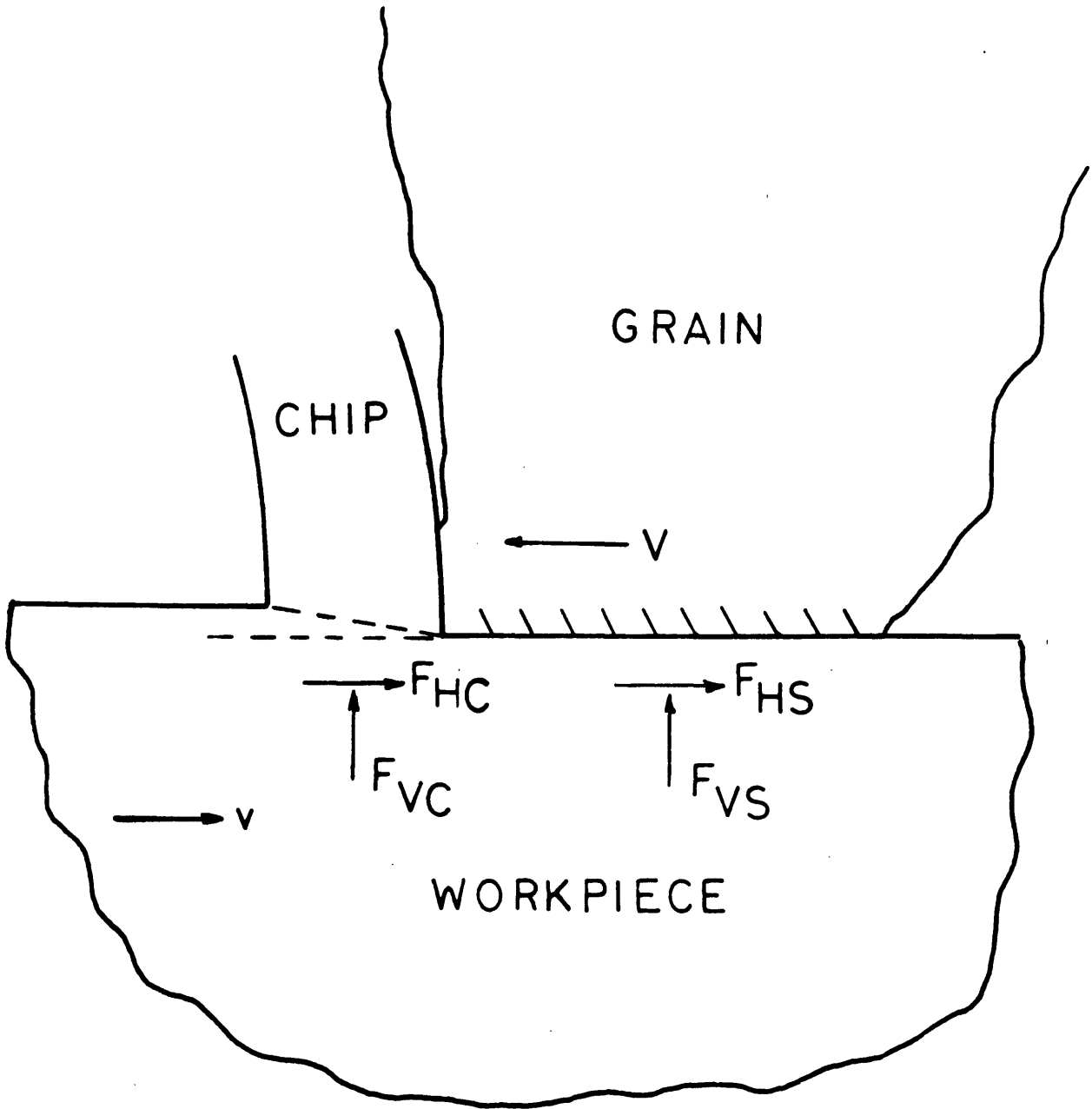


Figure 24. Illustration of chip formation and the cutting and sliding force components.

The linear increase of the vertical force with wear flat area (only up to the transition for steels) indicates that the average contact pressure  $\bar{p}$  between the wear flats and workpiece is constant. Since the horizontal force also increases linearly with wear flat area, the coefficient of sliding friction  $\mu$  is also constant. Defining  $a_R$  as the real area of contact between the wheel and the workpiece, equations 5.1 and 5.2 then become

$$F_V = F_{VC} + a_R \bar{p} \quad (5.3)$$

$$F_H = F_{HC} + \mu a_R \bar{p} \quad (5.4)$$

The actual wear flat pressure can be calculated from the slope  $\frac{dF_v}{dA}$  and a consideration of the grinding geometry, Figure 25. The apparent area of contact between the wheel and the workpiece,  $a_A$ , is given by the expression

$$a_A = l_c \times b \quad (5.5)$$

where  $l_c$  is equal to the undeformed chip length<sup>(29)</sup>

$$l_c = \sqrt{D d} \quad (5.6)$$

and  $b$  is the width of the workpiece. The real area of contact between the wheel and the workpiece,  $a_R$ , is equal to the product of the fraction of the total area covered with wear flats and the apparent area of contact,

$$a_R = .01 A \times a_A \quad (5.7)$$

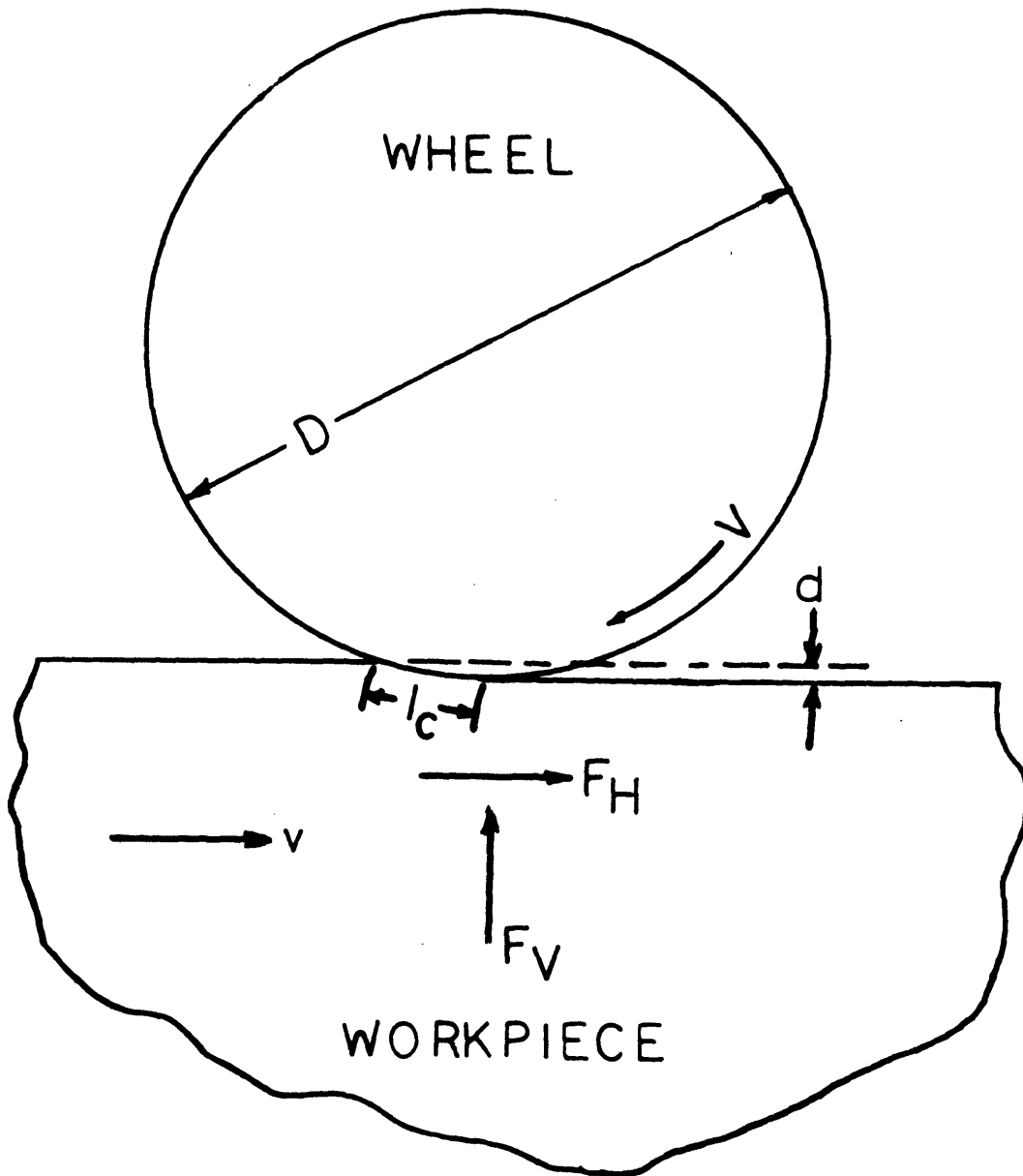


Figure 25. Illustration of the grinding geometry.



The average pressure  $\bar{p}$  is then

$$\bar{p} = \frac{dF_{VS}}{da_R} = \frac{dF_V}{da_R} = \frac{1}{.01 b \times l_c} \frac{dF_v}{dA} \quad (5.8)$$

The friction coefficient  $\mu$  is given by

$$\mu = \frac{F_{HS}}{F_{VS}} = \frac{dF_H/dA}{dF_V/dA} \quad (5.9)$$

The same interpretation can also be applied to other types of grinding operations. Story<sup>(30)</sup> has recently shown that forces obtained with coated abrasives, for both fixed feed and constant force grinding, can be considered as the sum of cutting and sliding components. Although the origin of the sliding forces is not discussed, presumably they are related to the size of the wear flats.

Hahn<sup>(14)</sup> has found that for controlled force cylindrical grinding ( $F_V$  is constant), the metal removal rate decreases in direct proportion to the increase in the wear flat area. This can be explained by assuming that the average wear flat pressure is constant and the fraction of the controlled vertical force employed in the cutting action,  $F_{VC}/F_V$ , is proportional to the metal removal rate. From Hahn's data on 52100 steel, I calculate the average wear flat pressure to be about 7000 lbs./in.<sup>2</sup>.

Yoshikawa<sup>(8)</sup> has stated that below the transition, the grinding forces are constant and independent of the wear flat area. A closer examination of his data reveals that this is not true. Force vs. wear flat area curves were presented only for the harder grades of wheels and the grinding forces measured in the first few passes were incorrectly assumed to correspond to

zero wear flat area. (See Figure 5). He did obtain smaller grinding forces with soft wheels but no wear flat area measurements were reported for these.

An analogous situation has been observed in the case of turning where the cutting forces are found to increase linearly with the area of the wear land (31, 32, 33, 34). Zorev<sup>(34)</sup> has pointed out that the contact pressure between the wear land and the workpiece "can be considered elastic since the plasticity condition is fulfilled only at the cutting edge where the contact stresses reach a maximum".

To visualize this more clearly consider the wear land as a punch with a plane base on an elastic semi-infinite plane, Figure 26, where P is the total contact force per unit width, 2 a is the contact length, and x is the local variable. The elastic pressure distribution under the punch is given by the formula<sup>(35)</sup>

$$p \left( \frac{x}{a} \right) = \frac{P}{a} \sqrt{\frac{1}{1 - \left( \frac{x}{a} \right)^2}} \quad (5.10)$$

Thus at the corners of the punch,  $x = \pm a$ , the pressure is infinite. However, in reality, there is plastic deformation in these regions, and the pressure will approximately follow the dotted lines reaching the full indentation hardness H at the corners of the punch<sup>(35)</sup>. In the discussion which follows, the size of the plasticity region is assumed to be much smaller than a.

In the case of a wear land on a cutting tool or the wear flat on a grain, full plasticity will probably be reached only at cutting edge ( $x = - a$ ) and the pressure towards the trailing edge,  $x = + a$ , would be

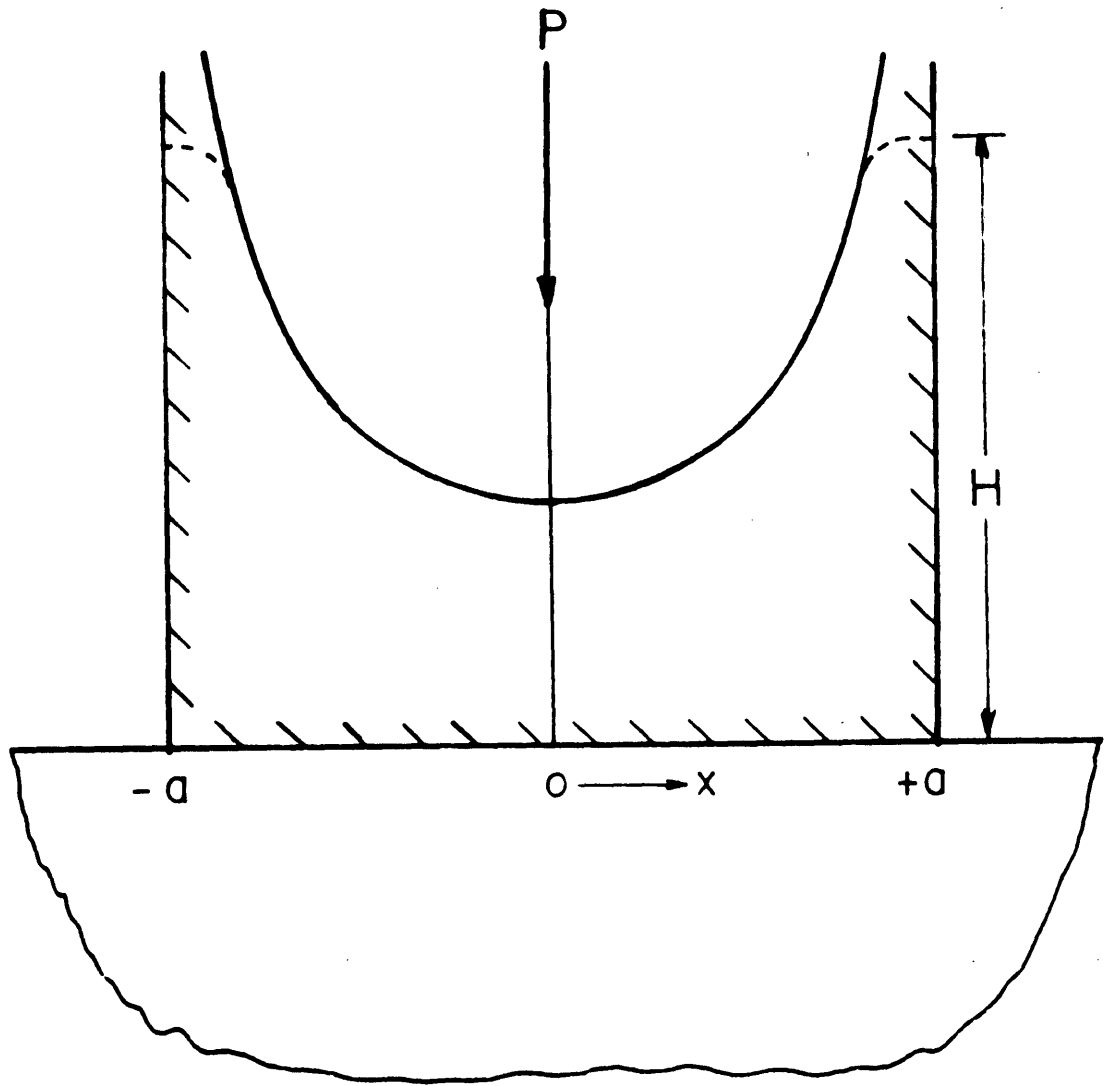


Figure 26. Pressure distribution due to contact between a punch and a semi-infinite elastic solid.

less than H. In this case, the pressure distribution is given by an expression of the form

$$p \left( \frac{x}{a} \right) = \frac{P}{2a} f \left( \frac{x}{a} \right) \quad (5.11)$$

and

$$\bar{p} = \frac{P}{2a} \quad (5.12)$$

If the shape of the pressure distribution  $f\left(\frac{x}{a}\right)$  is independent of the size of 'a' and the boundary condition at  $x = -a$  is fixed by the hardness H, then equation 5.11 is also independent of 'a'. The average pressure is then constant and proportional to the workpiece hardness H.

In Figures 16-23, the straight lines were determined by the method of least squares with the force taken as the error free variable. These results are summarized in Table 14 together with the standard errors, correlation coefficients c, cutting forces, cutting force ratios  $(F_{HC}/F_{VC})$ , specific cutting energies  $u_c$ , and the frictional energy flux on the wear flats  $q_f$ . The specific cutting energy is given by

$$u_c = \frac{F_{HC} V}{vd} \quad (5.13)$$

and the frictional energy flux by

$$q_f = \mu \bar{p} V. \quad (5.14)$$

Note that the correlation coefficients are close to unity which means that the straight line approximation is valid.

Figure 27 shows a cross plot of the specific cutting energy and the average wear flat pressure. Materials which require a larger cutting energy generally experience a greater contact pressure. In line with the previous discussion, such a correlation would be expected to be valid only to the extent that the cutting energy describes the plasticity condition under the cutting edge of the grain. The results for the T 1 high speed steel fall outside this general relationship possible because of its high alloy content. At the peak temperature generated at the chip which is near the melting temperature of the workpiece, the alloy content of the steel should be relatively unimportant and the T1 steel requires about the same cutting energy as 1018 steel. At the lower temperature under the cutting edge, the alloy content becomes significant and T1 would be relatively harder than mild steel. Calculation of the grinding temperatures are presented in the next section.

With the 1018 steel run at half the speed, the cutting energy is approximately the same as that found at the higher speed. However, the contact pressure is about twice as big. This suggests a dynamic effect whereby decreased grinding speeds raise the contact pressure and, in effect, move the curve in Figure 27 to the right, possibly far enough so that it will intersect the origin. This dynamic effect could account for the improved grinding performance which has been observed at very high grinding speeds (36).

When the specific cutting energy is plotted against the melting temperature of the workpiece material (Figure 28) the result is approximately linear with the curve passing through the origin. (Melting temperatures for the

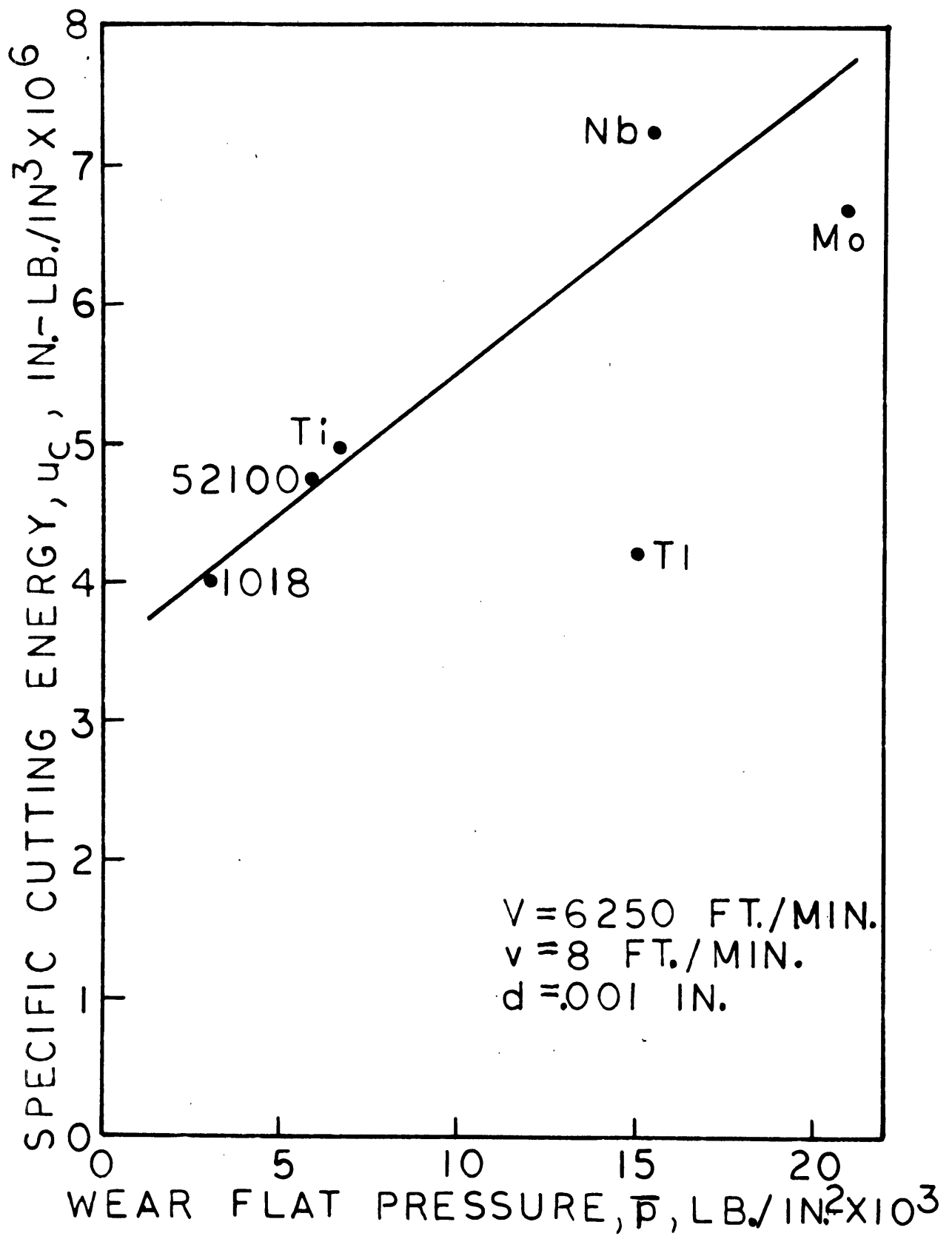


Figure 27. Specific cutting energy versus wear flat pressure.

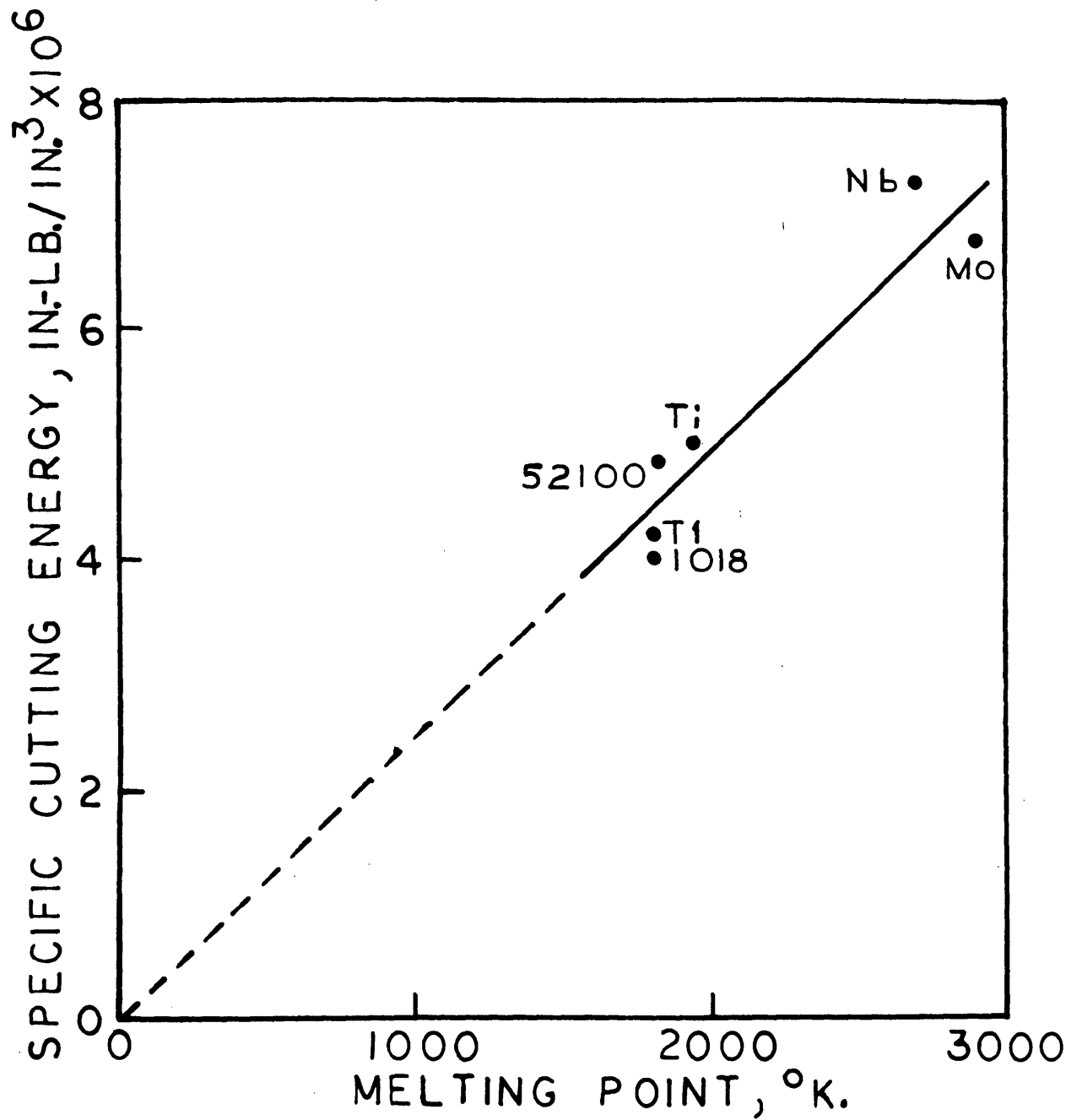


Figure 28. Specific cutting energy versus melting point of the workpiece.

alloys are given by the melting temperatures of their base metal). This result is not altogether unexpected since a high melting temperature signifies strong bonding. It can also be seen that all the steel alloys require roughly the same cutting energy. At the high temperatures generated in grinding chip formation, which will be shown to be near the melting temperature, the effect of alloying and prior heat treatment should be relatively unimportant.

It is interesting to note that all the metals which were found to load the wheel have a melting temperature below that of iron. Hence no data points are given in Figure 27 for the lower end of the curve. Why wheel loading should occur with these materials is not understood.

Workpiece burn, which appears at a critical wear flat area for a particular steel, is characterized by sharply increasing grinding forces and bluish tempering colors on the workpiece. In addition to this, a flash or ridge of material is also observed to form along the edge of the workpiece which indicates that some of the material to be removed is ploughed aside by the grains instead of being formed into chips. Metallurgical examination of burned workpieces by Littman<sup>(37)</sup> and Tarasov<sup>(38)</sup> have shown that the surface layers are over tempered and softened. The burn color is the result of surface oxidation at high temperature. Apparently this metallurgical softening, and non-metallurgical softening due to the high temperatures in grinding, lead to a fully plastic condition under some of the wear flats, and the slope of  $F_v$  vs.  $A$  beyond the transition would correspond to the hardness under the grain. These pressures are about 10 times greater than the average wear flat pressures below the transition. The



drop in friction coefficient above the transition (Table 14) is also to be expected.

Littman<sup>(37)</sup> has empirically found that the surface temperature in grinding  $T_G$ , is uniquely related to the energy input per unit area of work surface ground, or

$$T_G \propto \frac{F_H V}{l_c b} \quad . \quad (5.15)$$

Referring to Figures 16, 17, 18 and 23 it is seen that the transition did occur at approximately the same energy input rate ( $F_H V$ ) or in other words, the workpiece burn did commence at approximately the same temperature in all four cases.

With the Stellite workpiece a flash of material also forms as in the case of steel workpiece burn. Looking at Figure 22, the extension of the vertical force curve to zero wear flat area would result in a negative value of the force,  $F_{VC}$ . In reality this could not exist and the curve must turn toward a positive value. The wear flats grew so fast when grinding this material that data below a wear flat area of about 1 per cent could not be obtained. Considering the shape of this force curve and the flash formation, the grinding mechanism here is probably the same as that for steel beyond the transition.

## VI. GRINDING TEMPERATURES

### 6.1 Introduction

Some of the most serious problems in the grinding process are caused by grinding heat. Grinding burn with steel is associated with softening of the surface layer or in severe cases, softening followed by rehardening. Cracking is often observed in the ground surface as a result of the rapid cycle of heating and cooling. The desired dimensional accuracy may be difficult to obtain because of the thermal expansion of the workpiece. Control of these problems is usually accomplished by using coolant. However, a fundamental understanding of grinding heat and temperatures is needed to provide a broader approach to their solution.

It has been shown that the total grinding energy can be considered as the sum of frictional energy due to sliding on the wear flats and cutting energy due to chip formation (Figure 24). To be sure, part of the cutting energy is associated with frictional processes but this is not to be confused with the sliding energy considered here. As the wear flat area increases, the additional grinding energy required is dissipated as heat at the interface between the grain and the workpiece.

There has been some confusion about the concept of surface temperatures in grinding. Outwater and Shaw<sup>(39)</sup> used Jaeger's moving heat source theory (40) to calculate the temperatures on the shear plane of the chip. Their results are questionable insofar as the total grinding energy was assumed to be associated only with cutting ( $F_{HS} = 0$ ). Sato<sup>(41)</sup> used the

concept of an instantaneous heat source over the total grinding area (apparent area of contact) to determine an "average" surface temperature.

Littman<sup>(37)</sup> experimentally determined grinding temperatures by positioning a thermocouple at the bottom of a hole (.021 or .026 inch diameter) which extended nearly to the ground surface. Temperature measurements obtained in this way ( $T_G$  in equation 5.15) seem to be closely related to some metallurgical changes in the ground surface. However the cross sectional area of the hole was so large, compared to a grinding chip or wear flat, that the relationship between this temperature and the actual temperature distribution on the surface cannot be determined.

In this section, the distribution of surface temperatures in the vicinity of the chip and wear flat (for an isolated cutting point) will be calculated as the sum of two moving heat sources, one at the shear plane of the chip and the other on the wear flat. There is also an additional temperature rise due to all the other cutting points which is calculated as a single moving heat source equal to the apparent area of contact.

## 6.2 Geometry of Chip Formation

As a first step it is necessary to consider the geometry of chips formed in the grinding process. The details of the treatment of this subject can be found in reference (26). To a good approximation, the undeformed grinding chip can be considered as a long wedge of constant width as shown in Figure 29. The undeformed chip length  $l_c$  is given by

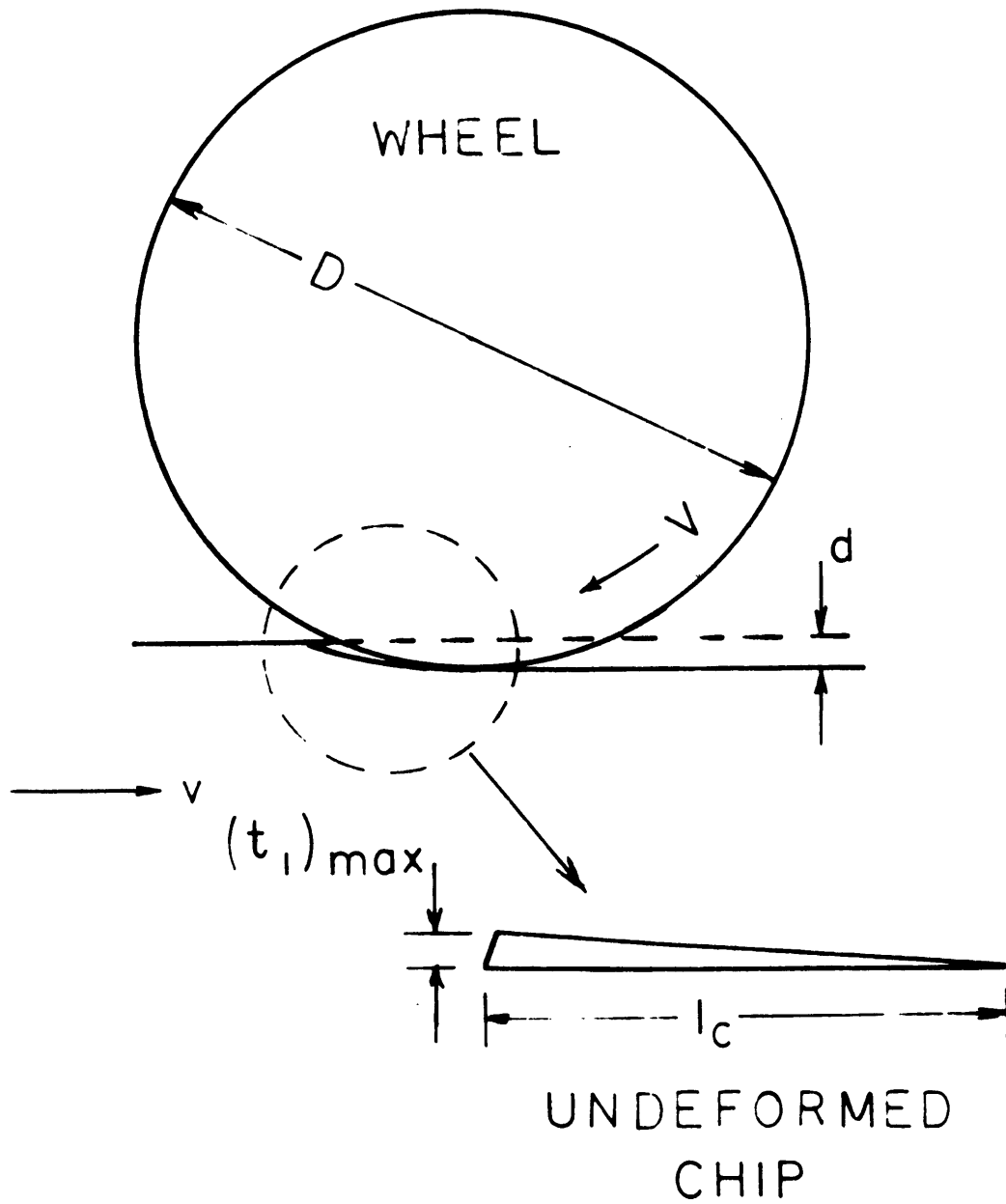


Figure 29. Geometry of the undeformed chip.

the chordal length

$$l_c = \sqrt{Dd} \quad (6.1)$$

and the maximum undeformed chip thickness by:

$$(t_1)_{\max} = \left( \frac{v}{VCr} \sqrt{\frac{d}{D}} \right)^{1/2} \quad (6.2)$$

where

D = wheel diameter

d = downfeed per pass

V = wheel speed

v = table speed

C = number of cutting points per unit area

r = ratio of width to thickness of undeformed chip

From taper section studies of ground surfaces<sup>(26)</sup>, the value for r, which is the ratio of underformed chip thickness to width, has been found to be about 15.

As previously discussed, the number of cutting points per square inch, C, has been often confused with other wheel parameters. The only direct measure of this value was achieved by Grisbrook<sup>(28)</sup> where the value of C was actually determined from the number of chips generated. For a 46 grit wheel, a typical value for C has been found to be about 6000 per square inch. This is higher than values obtained by other methods which supports the contention that there can be more than one wear flat per grain and more than one cutting point per wear flat.

For the present case ( $D = 8$  in.,  $d = .001$  in.,  $V = 6250$  ft./min., and  $v = 8$  ft./min.) equations 6.1 and 6.2 give

$$l_c = \sqrt{(8) (.001)} \approx .09 \text{ in.} \quad (6.3)$$

and

$$(t_1)_{\max} = \left( \frac{4 (8)}{(6250) (6000) (15)} \sqrt{\frac{.001}{8}} \right)^{1/2} = 25 \times 10^{-6} \text{ in.} \quad (6.4)$$

The dimensions of the undeformed chips are of course different from those of the chips actually produced. Grisbrook<sup>(28)</sup> has observed that the ratio of the real chip length to the undeformed chip length is about .1. Neglecting chip sideflow, this suggests that the ratio of the undeformed chip thickness  $t_1$  to the actual chip thickness  $t_2$  is also about .1. Further supporting evidence is given by Brown<sup>(42)</sup> who, for chips produced with single grains, found that this ratio is usually between .05 and .15, again .1 being a typical value. In other words, the chip produced is about 10 times thicker than the undeformed chip.

With this, the shear angle  $\phi$  in Figure 20 can be easily determined to be

$$\phi = \tan^{-1} .1 \quad (6.5)$$

or

$$\phi = 6^\circ. \quad (6.6)$$

### 6.3 Energy Partition

The grinding temperature distribution is calculated by considering the shear plane and wear flat areas as moving heat sources on the workpiece surface which move at a velocity equal to  $V$ . (Actually the velocity should be  $V \pm v$ , but since  $V \gg v$ ,  $v$  is neglected.) For this calculation it is necessary to know that heat fluxes which cross the shear zone AB and wear flat AD into the workpiece (Figure 30). That is, the fraction  $R_1$  of the cutting energy conducted to the workpiece at shear zone and the fraction  $R_2$  of the sliding energy conducted to the workpiece at the wear flat must be determined.

Experimental determination of these values is based on the following reasoning. Both  $R_1$  and  $R_2$  should be relatively unaffected by the size of the wear flats, and virtually all the sliding energy should be conducted to the workpiece as heat since the steel workpiece is a stationary heat source, has a much higher thermal conductivity than aluminum oxide, and has a much bigger volume. In turning,  $R_1$  is typically on the order of .20 but will probably be greater here due to the relatively small shear angle in grinding. The fraction of the total grinding energy conducted to the workpiece has been experimentally determined for 1018 steel by insulating the workpiece and measuring its average temperature rise after one pass by means of a thermocouple attached to the center of the workpiece. Wear flat areas were also measured. These results are listed in Table 15 and plotted in Figure 31, where the straight line relationship is obtained as expected. The fraction  $R_1$  is the value of  $R$  at zero wear

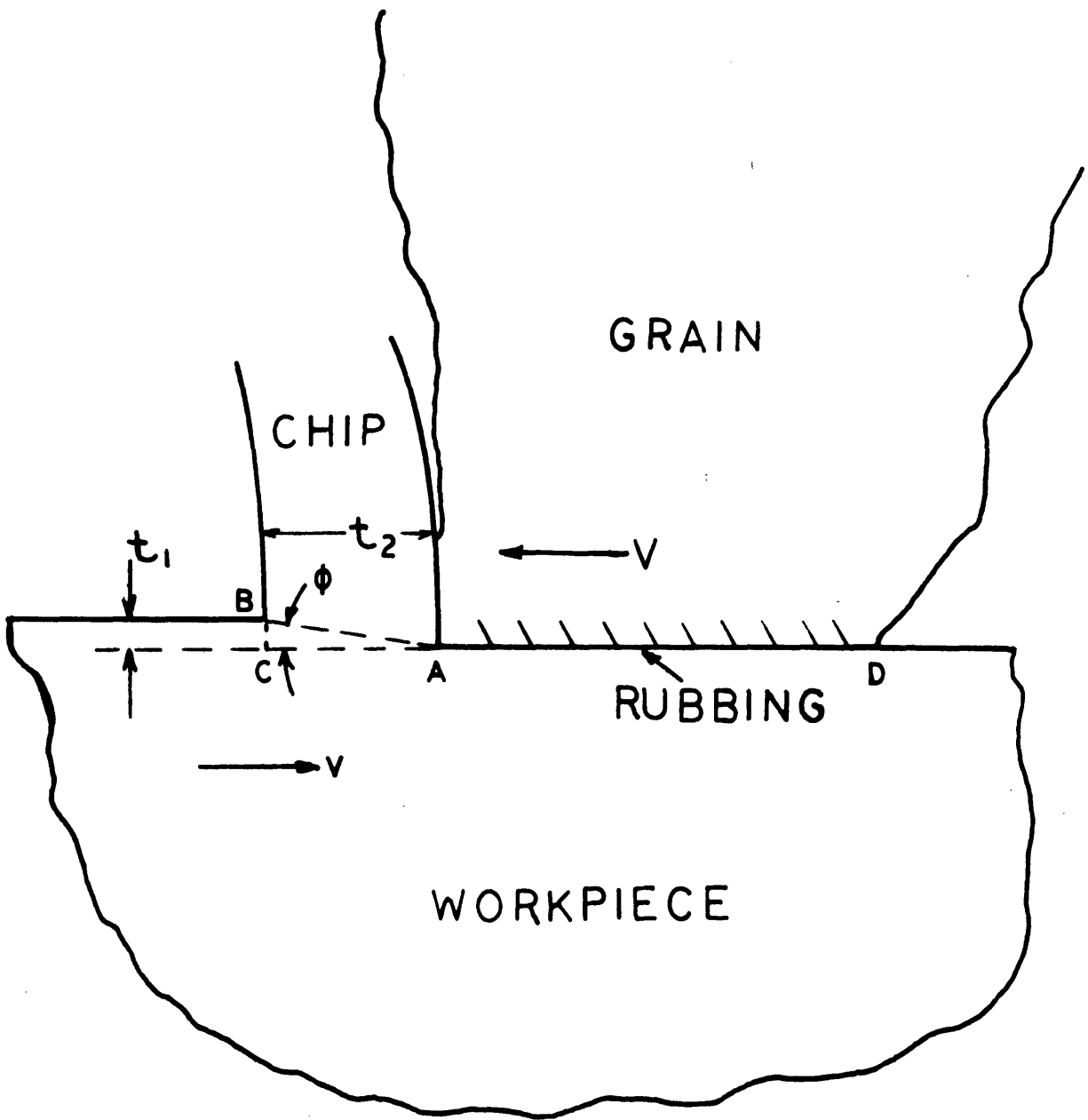


Figure 30. Geometry of chip formation.



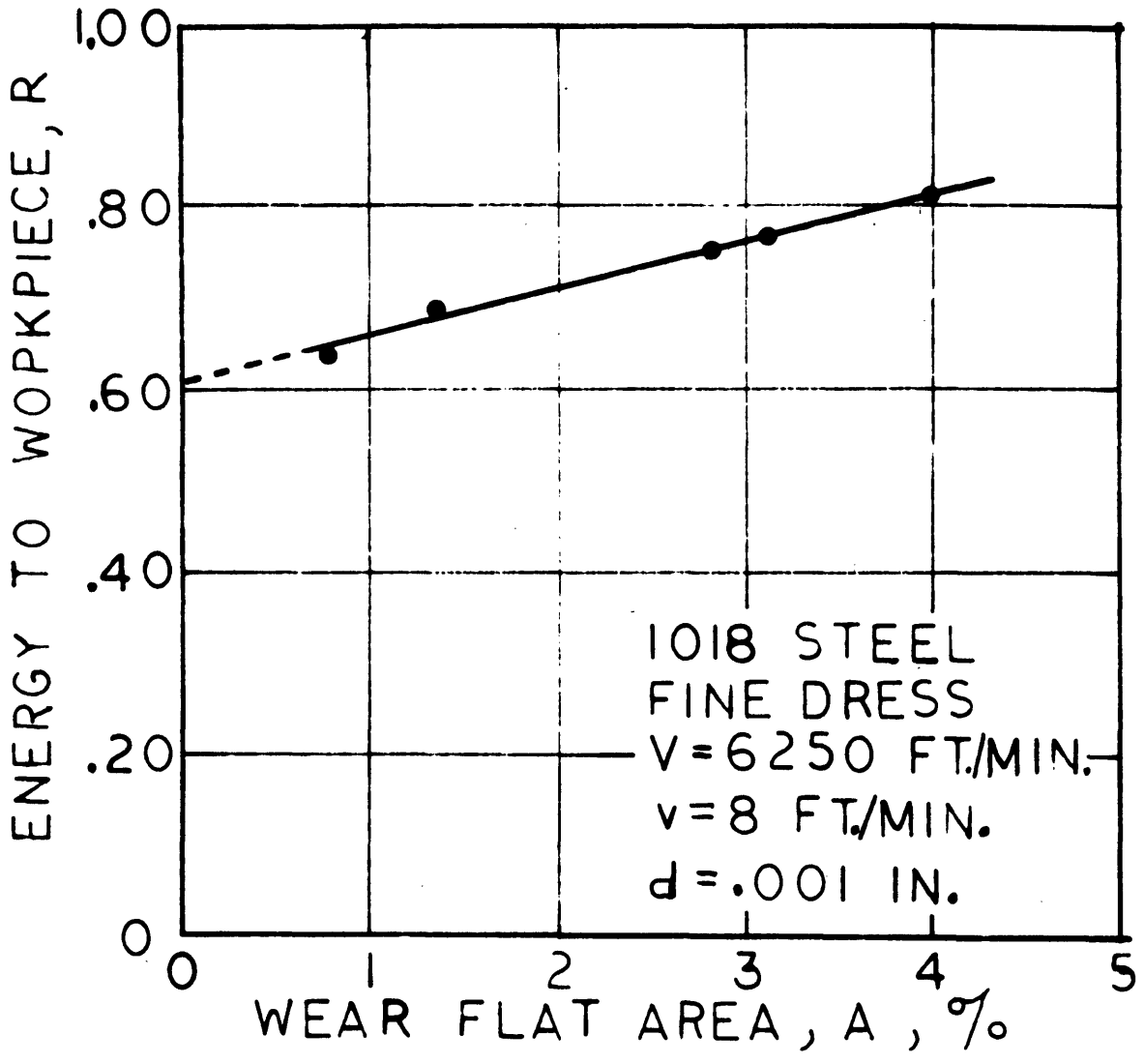


Figure 31. Fraction of grinding energy conducted to the workpiece versus the wear flat area.

flat area which is approximately equal to .61. Comparing the slope of this line with that of  $F_H$  vs  $A$  in Figure 16, the value of  $R_2$  is found to be equal to .97, or virtually all the sliding energy is conducted as heat to the workpiece. As a thermal analogy, this presents additional evidence to support the interpretation of the grinding forces as the summation of cutting and sliding components.

Sato<sup>(41)</sup> has measured  $R$  for cylindrical grinding also by measuring the temperature rise of the workpiece and has given a value of .85. Similar values have also been obtained by other Japanese researchers<sup>(42)</sup> and are in the same range as those presented here.

#### 6.4 Calculated Grinding Temperatures

Jaeger's theory of moving heat sources<sup>(40)</sup> will be used to calculate the temperature rise on the ground surface at the chip and wear flat for the 1018 steel near the transition ( $A = 3.5\%$  in Figure 16). This approach is based on the assumption that the thermal properties of the workpiece do not change with temperature. For the temperature ranges considered here, this is really not the case, and the variation of thermal properties with temperature are shown in Figure 32 for data taken from reference (44). However, a reasonable approximation to the actual situation can be obtained by using this constant property solution with the thermal properties evaluated at the average surface temperatures<sup>(39)</sup>. In the present case, the thermal properties at 1200°F will be used which will be found to be lower than the average temperature at the chip but higher than the average temperature on the wear flat.

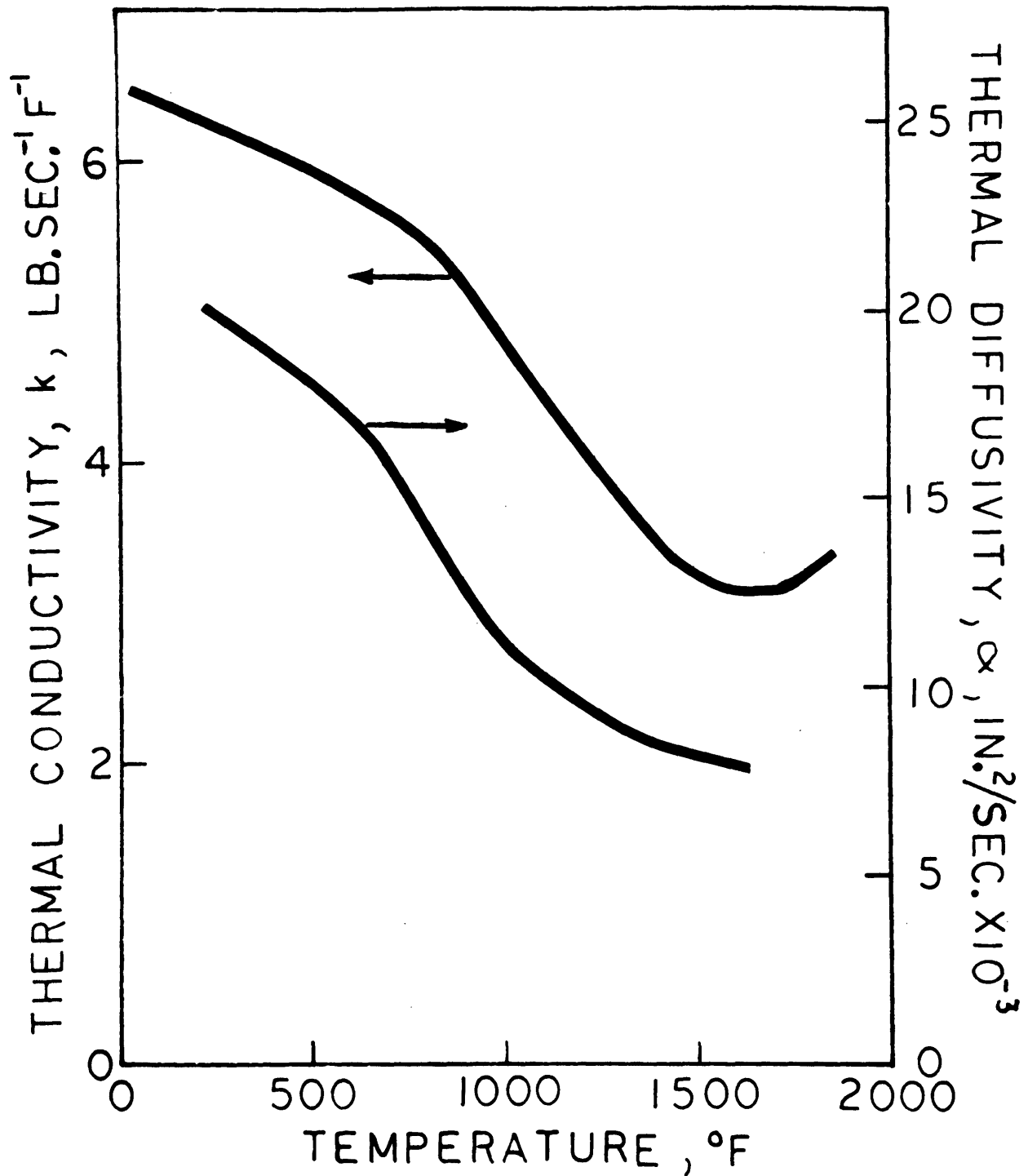


Figure 32. Variation of thermal conductivity and thermal diffusivity with temperature for mild steel. Data taken from Reference (44).

The temperature rise  $T_c$  due to the cutting energy is considered as a band source of width  $t_2$  moving along the workpiece surface at the wheel velocity  $V$ . Since the shear angle  $\phi$  is small (Figure 30) the band AB will be approximated by AC. The calculation will be performed where the cut is 50 per cent completed or  $t_1$  is half  $(t_1)_{\max}$ . Then the width of the band for this case,  $(t_2)_{50}$  is equal to

$$(t_2)_{50} = (.50) (10) (t_1)_{\max} = 125 \times 10^{-6} \text{ in.} \quad (6.7)$$

The energy flux across the band into the workpiece is equal to  $R_1$  times the average cutting energy per chip divided by the average chip cross sectional area. The details of this calculation are presented in Appendix B.

In a similar way, the temperature rise  $T_s$  due to sliding is calculated as a band source of strength  $R_2$  times the sliding energy  $q_f$  ( $q_f$  is given in Table 14) moving at the velocity  $V$ . From observations of the face of the grinding wheels, the wear flats at this wear flat area ( $A = 3.5\%$ ) are typically about .004 inch, and this value is used for the band width. These calculations are presented in Appendix C.

Both of these temperature distributions and their superposition are shown in Figure 33. Curve (a) is the temperature rise due to cutting and curve (b) is due to sliding. Zero on the abscissa represents the cutting edge, with the chip to its left and the wear flat to its right. Note that this scale is distorted with the chip magnified 20 times compared to the wear flat.

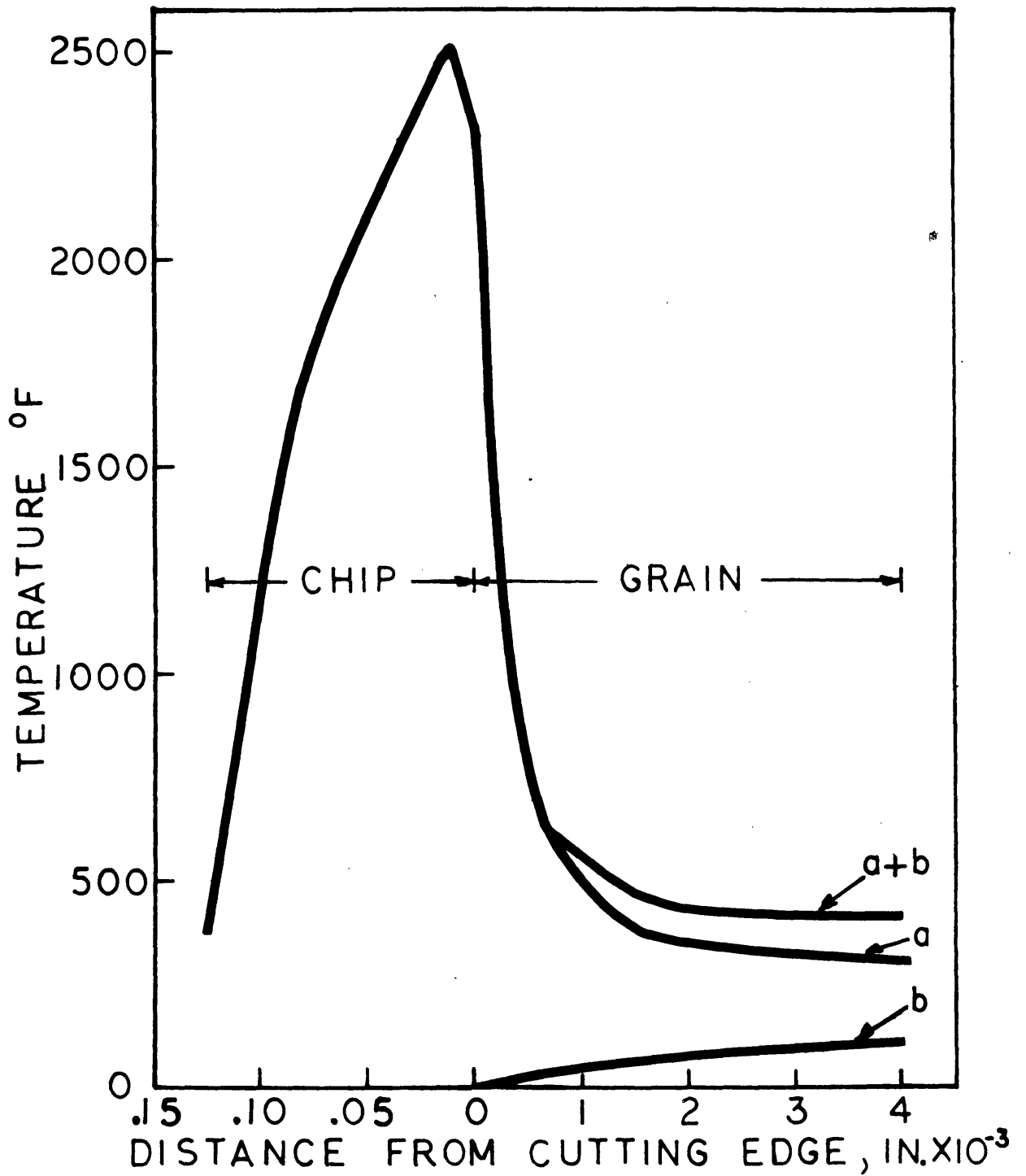


Figure 33. Distribution of calculated grinding temperatures along work-piece surface. Curve (a) is for temperature rise due to cutting, curve (b) is for temperature rise due to sliding.

The peak temperature rise occurs at the shear plane and can approach the melting point (2798°F.) of the steel. The temperature rise over most of the grain is smaller, with the major contribution still due to the cutting.

There is an additional temperature  $T_A$  due to the cutting and sliding of other grains in the grinding area. This is approximated by a band source moving at the workpiece velocity  $v$ , having a width equal to the undeformed chip length  $l_c$ , and the strength equal to  $R$  times the total grinding energy. This calculation presented in Appendix D gives a maximum value

$$(T_A)_{\max} = 721^{\circ}\text{F}$$

and an average value

$$(T_A)_{\text{ave}} = 538^{\circ}\text{F}$$

The average value,  $(T_A)_{\text{ave}}$ , can be interpreted as the average initial temperature which a grit "sees". The actual grinding temperatures would then be about 500 degrees above those given in Figure 33.

## VII. SURFACE FINISH

### 7.1 Introduction

Grinding is often employed as a finishing process where accurate surfaces of good finish are required. Consequently it is important to understand the factors which affect the quality of the surface produced.

### 7.2 Results and Discussion

The surface finish generated during grinding was measured every twenty passes for the 1018 steel workpiece using both the "course" and "fine" dressing techniques. These measurements were obtained simultaneously with the data previously presented in Tables 5 and 6.

The test results are presented in Table 16 and plotted in Figure 34 for the different wheel grades. It is interesting to compare these results with those in Figures 10 and 12. With the fine dress a good surface finish in the range of 10 to 15 microinches is obtained below the transition, with very slight improvement noted with harder wheels. Beyond the transition, where burning occurs, the finish deteriorates rapidly to about 30 or 40 microinches.

The coarse dressed wheels give a much poorer surface finish than the fine dressed wheels below the transition. Here again, the harder wheels give a slightly improved finish.

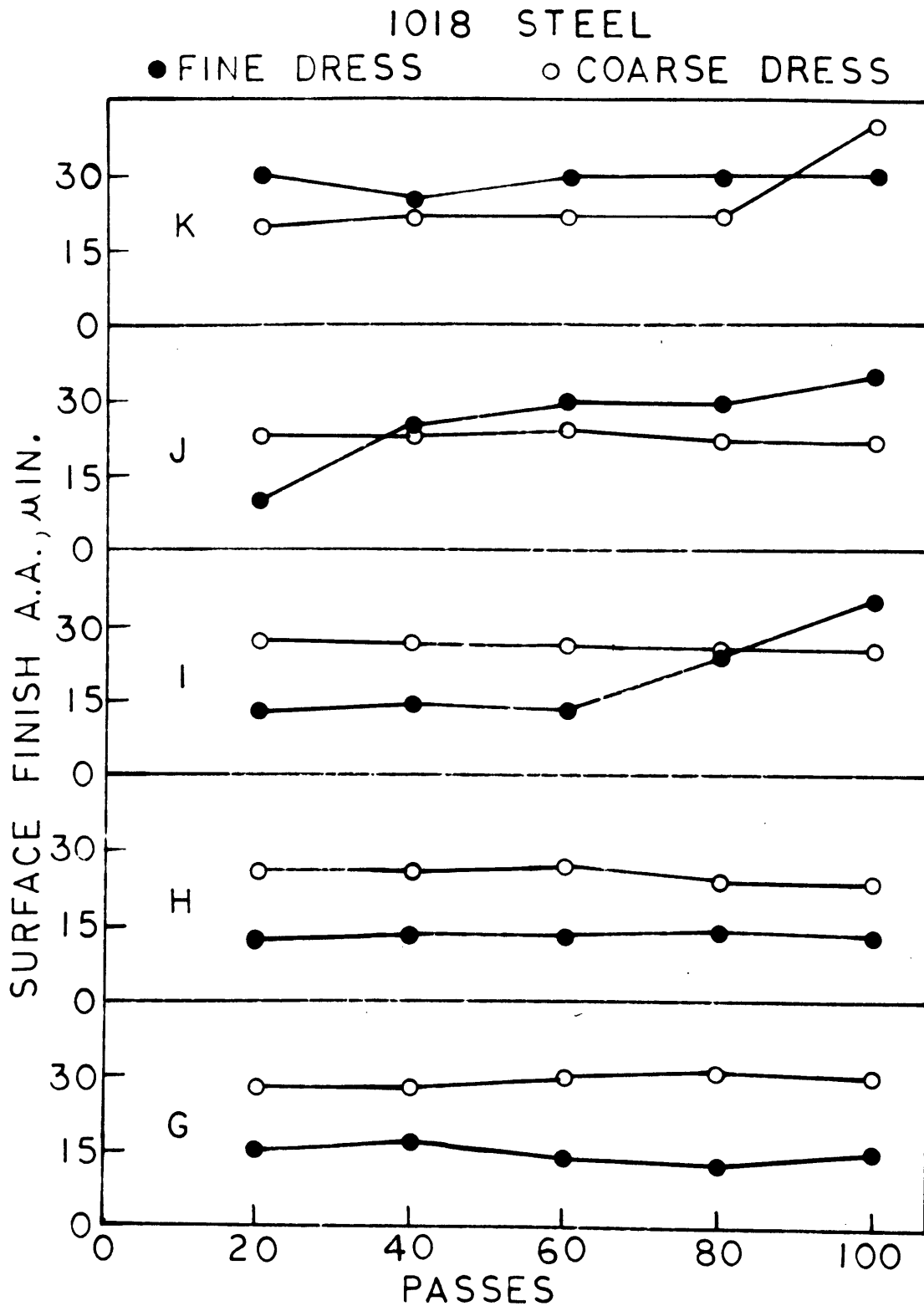


Figure 34. Surface finish versus the number of passes for fine and coarse dressing for 1018 steel,  $V = 6250$  ft./min.,  $v = 8$  ft./min.,  $d = .001$  in. (The letters denote wheel grades.)



Theoretical considerations of the finish produced in surface grinding have often been based only on the geometry of the undeformed chips. Orioka<sup>(45)</sup> and Nakayama and Shaw<sup>(46)</sup> considered this problem both theoretically and experimentally and determined that the height differences between the tips of the active grits is usually a more significant factor. This is consistent with the present findings where, in the absence of workpiece burn, the "fine" dressing produces a significantly better significantly better surface finish. The two additional spark out passes for fine dress apparently reduce the height difference among the active grains.

## VIII. FRACTURE WEAR

### 8.1 Introduction

Grinding wheel wear is usually determined as the decrease in the radius of the grinding wheel. As previously mentioned, the wheel wear before redressing usually amounts to a small fraction of a grain dimension, yet it will be shown that a significant portion of the wear consists of particles almost as big as whole grains. Determination of wheel wear from the weight of the abrasive particles removed, and a study of their size distribution, therefore provides a more fundamental approach to the study of grinding wheel wear.

In this section, the results of the grinding wheel wear studies are presented for the 1018 steel using both the "fine" and "coarse" wheel dressing and for the 52100 steel using the "fine" dressing. A sieve analysis of the wear particles was performed to determine the amount of bond fracture. A quantitative relation was obtained between the grinding wheel wear and the grinding forces.

### 8.2 Results

The test results are presented in Tables 17-19 for the 1018 steel with the fine dress, 1018 steel with the coarse dress, and 52100 with the fine dress respectively. The accumulated wear is plotted against the number of passes in Figures 35-37.

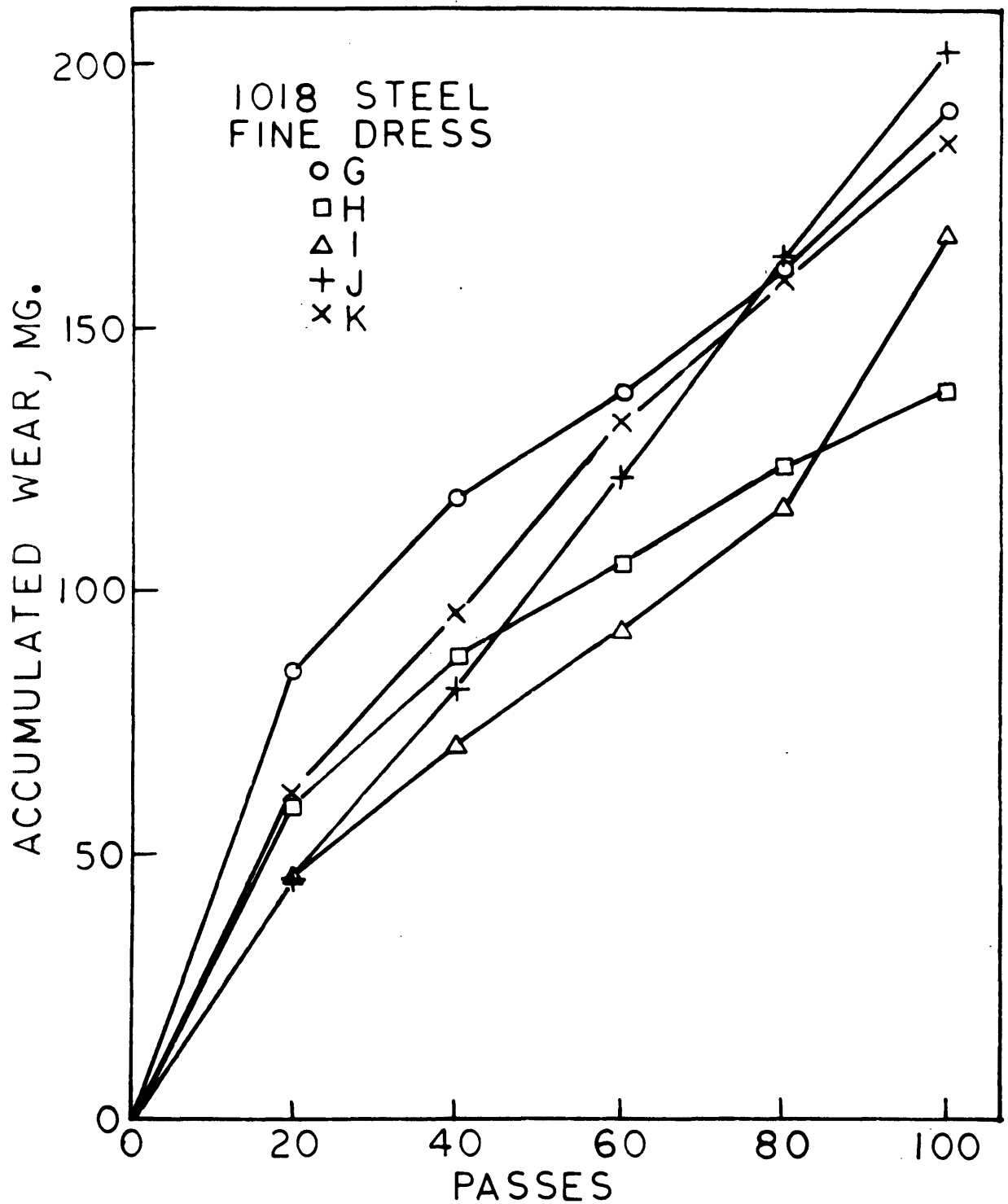


Figure 35. Accumulated wear versus the number of passes for 1018 steel, fine dress,  $V = 6250$  ft./min.,  $v = 8$  ft./min.,  $d = .001$  in. (The letters denote wheel grades.)

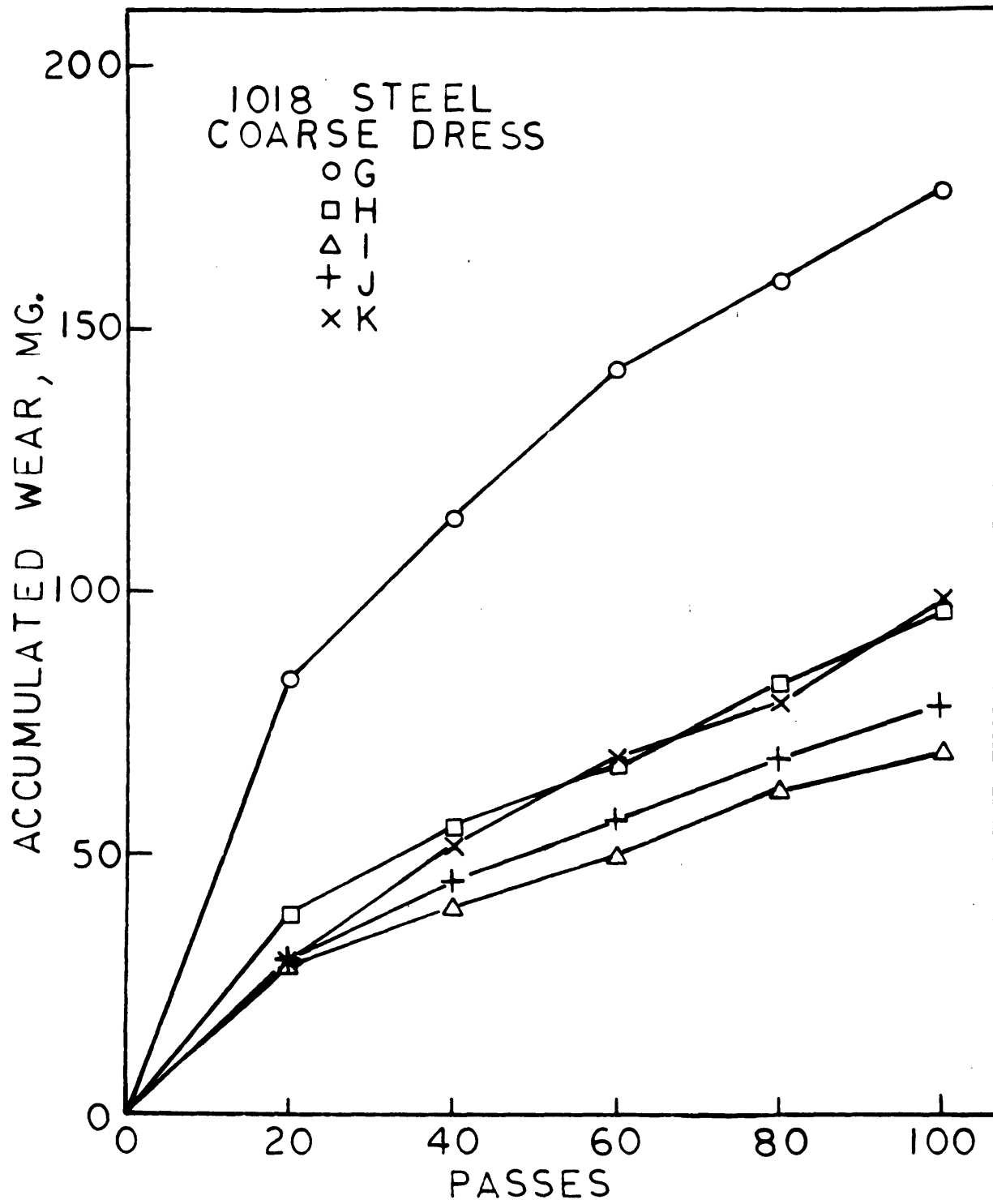


Figure 36. Accumulated wear versus the number of passes for 1018 steel, coarse dress,  $V = 6250$  ft./min.,  $v = 8$  ft./min.,  $d = .001$  in. (The letters denote wheel grades.)

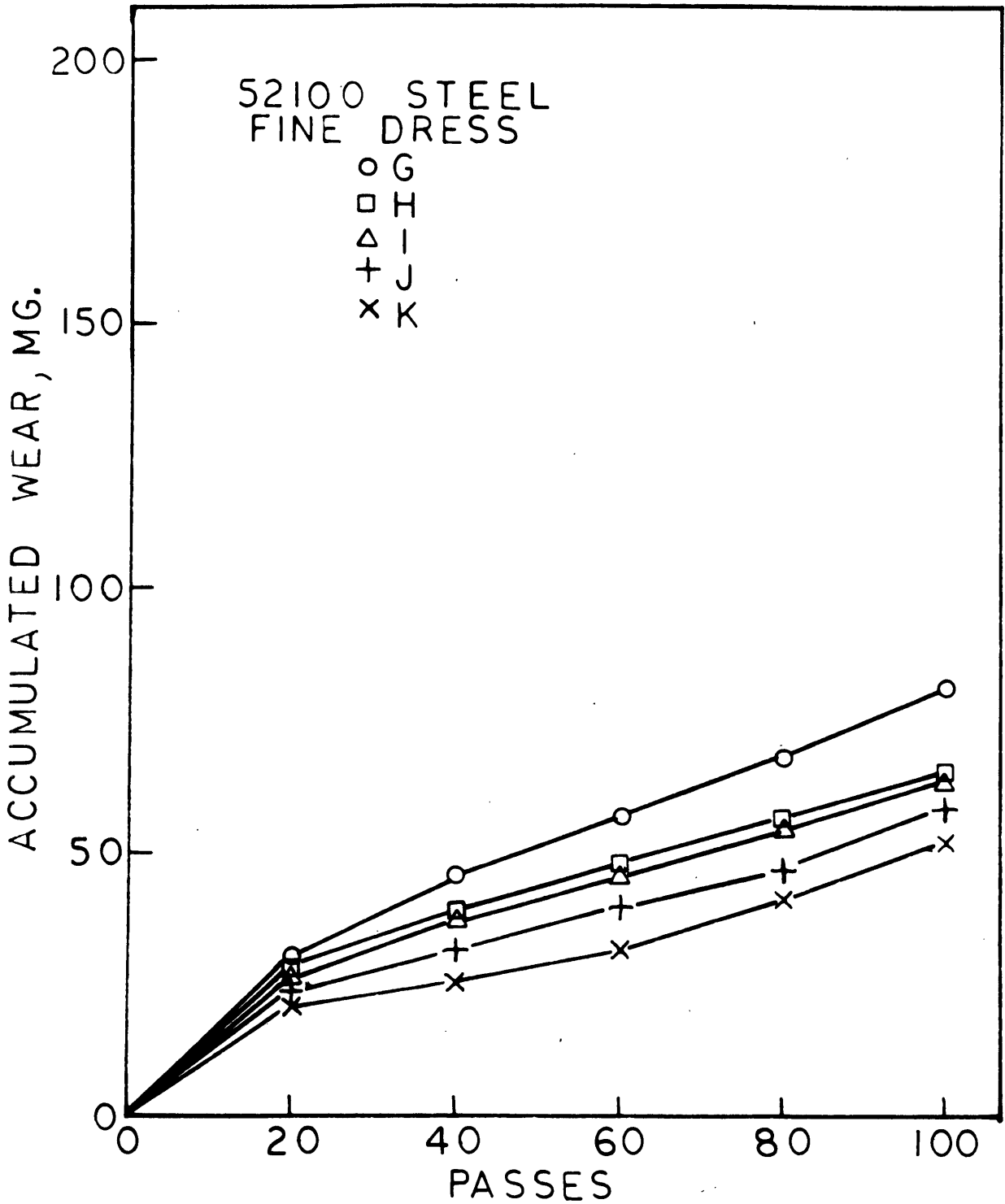


Figure 37. Accumulated wear versus the number of passes for 52100 steel, fine dress,  $V = 6250$  ft./min.,  $v = 8$  ft./min.,  $d = .001$  in. (The letters denote wheel grades.)

It appears that the wear rate curve is characterized by three distinct regimes, all of which are evident in the results for the I-grade wheel in Figure 35. The first regime shows a high initial run in wear. This is followed in the second regime by a more or less constant but smaller wear rate. In the third regime, the wear rate rises again. This increasing wear rate corresponds to the transition or grinding burn previously mentioned. For both J- and the K- grade wheels (Figure 35), the grinding force transition occurs near the beginning of the test. In this case, only the third wear regime can be clearly observed.

With the coarse dressed wheels and the 1018 steel workpiece (Figure 36), only the first and second regimes are clearly visible except after 80 passes with the K-grade wheel where burning occurred. The maximum wear was obtained with the intermediate I-grade wheel.

The results for the 52100 steel (Figure 37) clearly show only the run-in a steady state wear, and the harder wheels experienced less wear than the softer ones. Workpiece burn did occur after about 60 passes with the K wheel and 80 passes with the J wheel, but the third wear regime did not appear.

The size distributions of abrasive wear particles are presented in Figures 38-40 for the different wheel grades. The distribution for the wheel abrasive particles is also given for comparison. As grinding proceeded the particle size distribution remained relatively unchanged and the curves are for the total wear in 100 passes for each wheel. The per cent bond fracture corresponding to each of these distributions is presented in Figure 41.

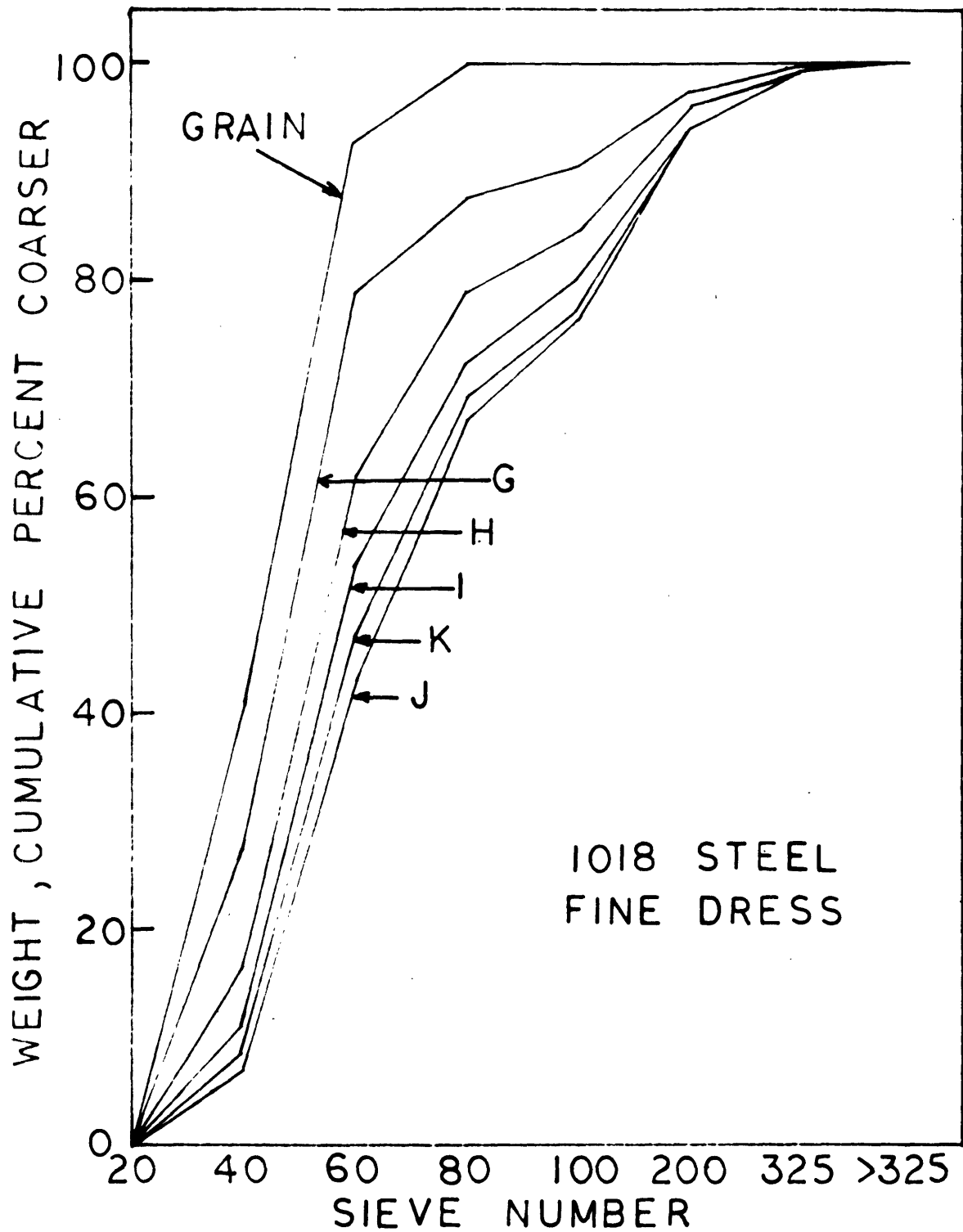


Figure 38. Particle size distribution of wear particles and abrasive grain for 1018 steel, fine dress,  $V = 6250$  ft./min.,  $v = 8$  ft./min.,  $d = .001$  in. (The letters denote wheel grades.)

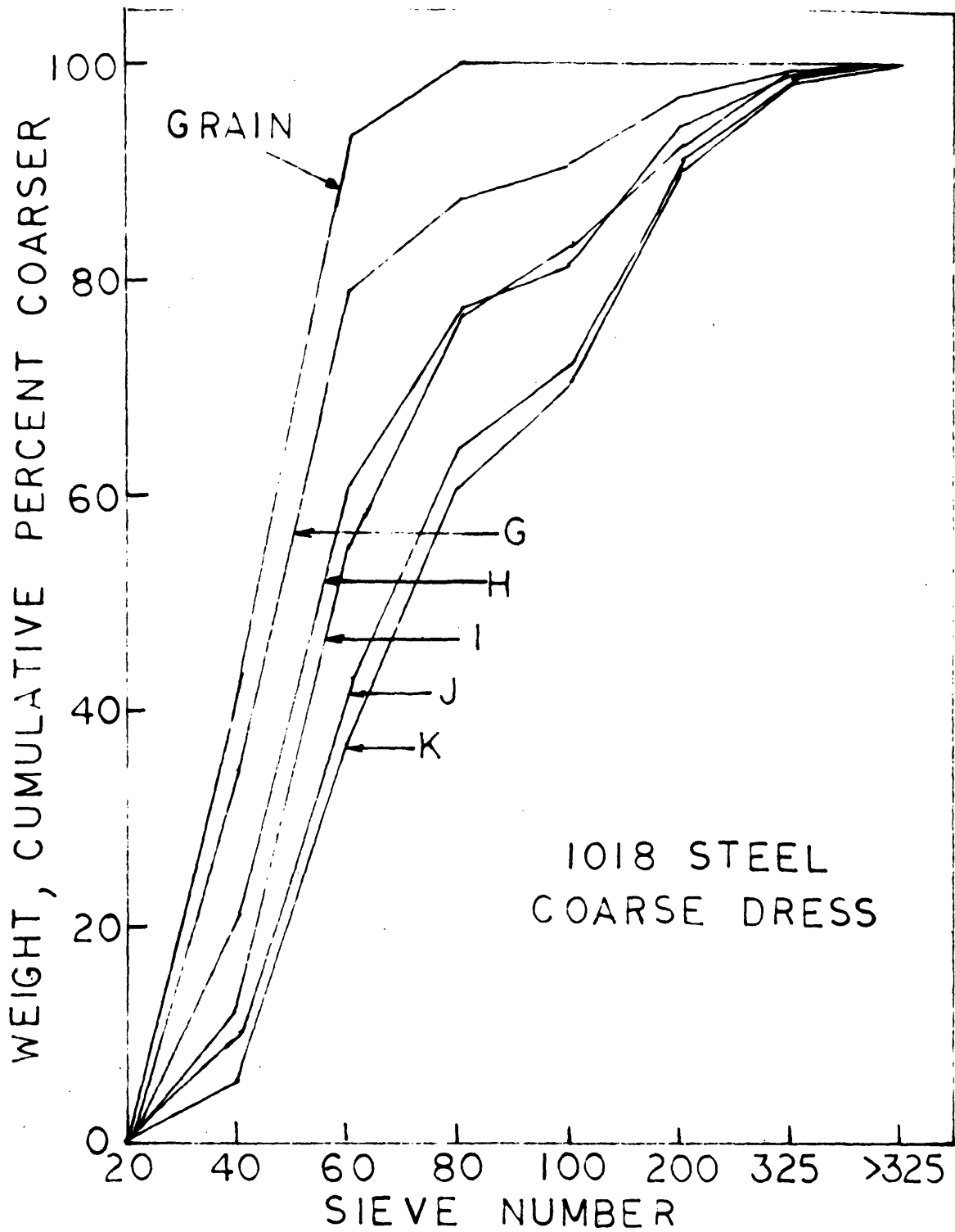


Figure 39. Particle size distribution of wear particles and abrasive grain for 1018 steel, coarse dress,  $V = 6250$  ft./min.,  $v = 8$  ft./min.,  $d = .001$  in. (The letters denote wheel grades.)



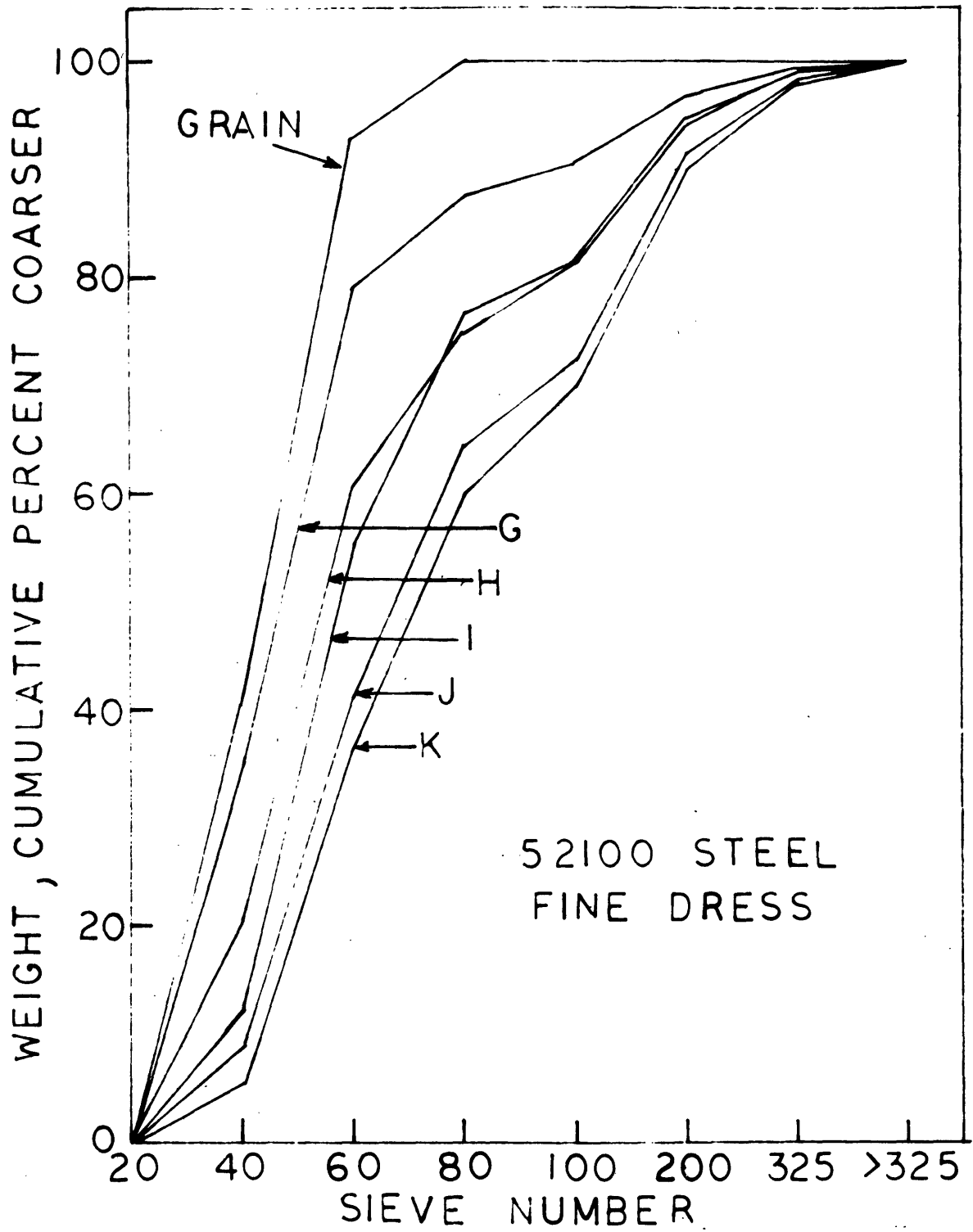


Figure 40. Particle size distribution of wear particles and abrasive grain for 52100 steel, fine dress,  $V = 6250$  ft./min.,  $v = 8$  ft./min.,  $d = .001$  in. (The letters denote wheel grades.)

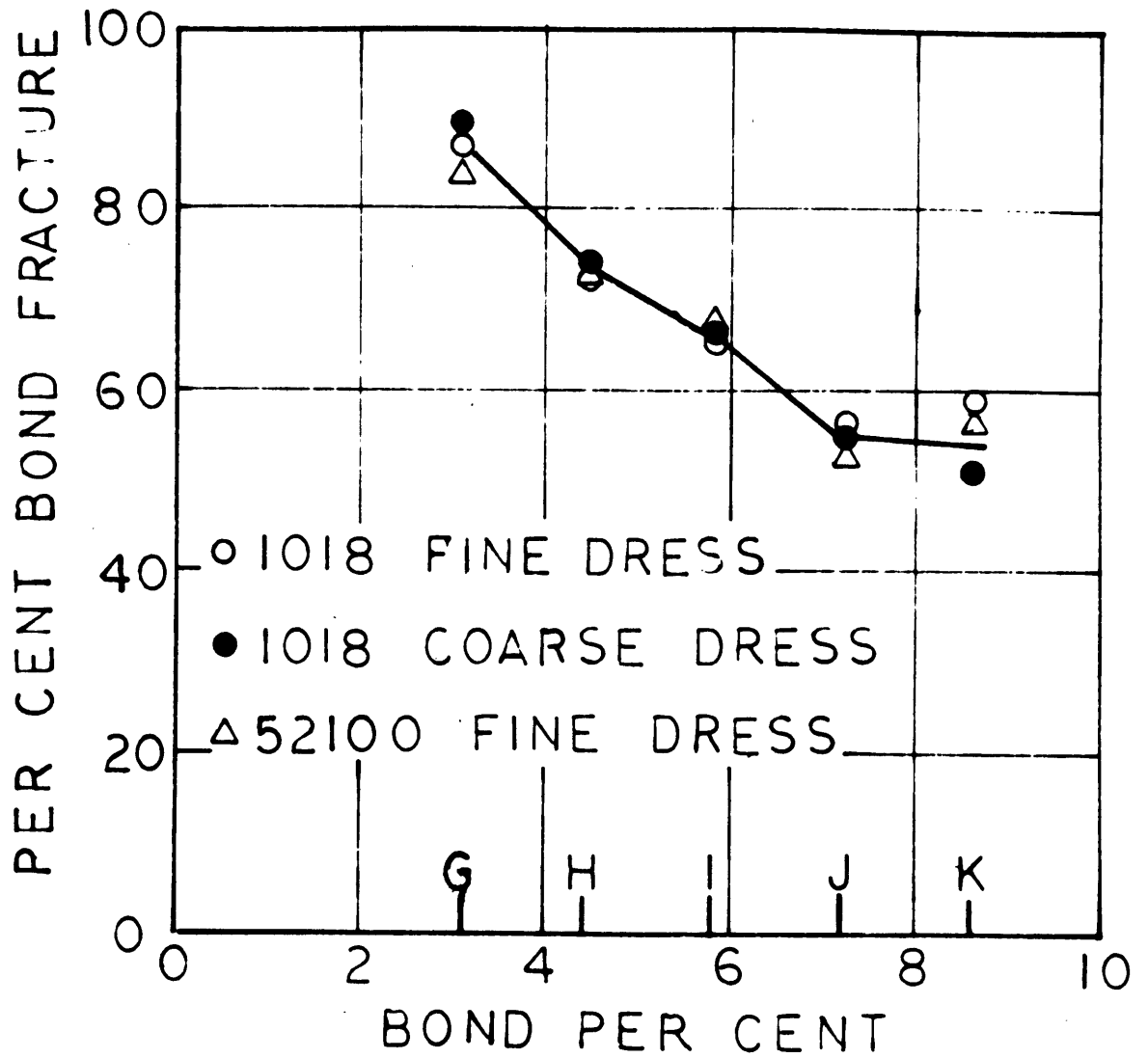


Figure 41. Per cent bond fracture versus bond per cent for wear particles. Corresponds to particle size distributions given in Figures 38 - 40. (The letters denote wheel grades.)

As in the case of dressing particles (Figures 7 and 8), the harder wheels generally have larger wear particles. Presumably, this is again due to the fact that with harder wheels with more bonding agent, a fracture within the grain is more likely to occur before dislodgement at the bond. The wear particles are slightly bigger than the dressing particles, Figure 7.

### 8.3 Discussion

Most of the grinding wheel wear consists of particles which are almost as big as the initial grains. This observation has formed the basis of the statistical analysis of the particles where it has been assumed that the overall wear rate is proportional to the rate at which bond fractures occur. Since the bond material is a brittle substance, the rate at which the bonds are fractured should depend in some way upon the maximum tensile stresses in the bond bridge.

Consider an active grain in the wheel surface (Figure 42) which is subjected to a horizontal force  $f_H$  and a vertical force  $f_V$ . Due to  $f_H$ , a positive bending stress which is proportional to  $f_H$  is induced in the bond at the plane AB. Likewise, the vertical force  $f_V$  induces compressive stresses at AB. The maximum tensile stress in the bond is then given by

$$\sigma_t = c_1 f_H - c_2 f_V \quad (8.1)$$

where  $c_1$  and  $c_2$  are constants.

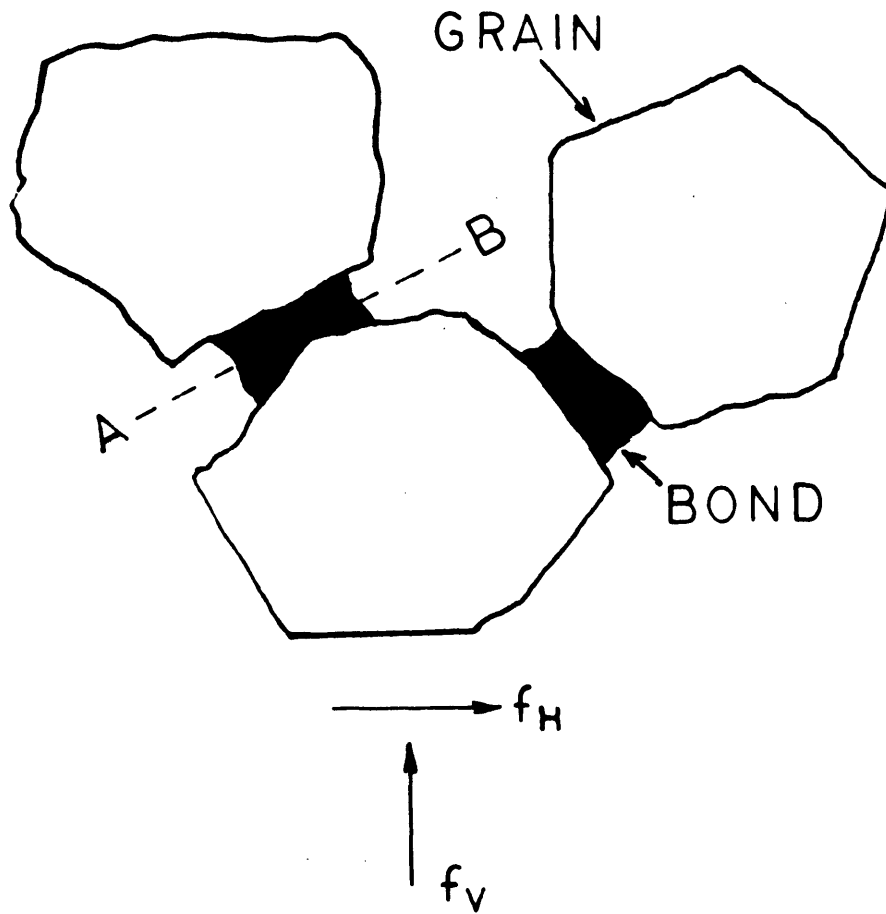


Figure 42. Illustration of the force on an active grain.

For harder wheels with more bonding agent, the forces at the bond bridges are distributed over a larger area and therefore the stresses are lower. With the bond bridges between the grains approximated as penny-shaped slugs of constant thickness, the stresses would vary inversely with the fraction of bonding agent in the wheel,  $V_b$ . The tensile stress in equation 8.1 can thus be written as

$$\sigma_t = K \left( \frac{f_H - \beta f_V}{V_b} \right) \quad (8.2)$$

where  $K$  and  $\beta$  are constants. The expression within the parenthesis is called the "bond stress factor".

For each contact between an active grain and the workpiece, there is a probability  $p_B$  that a bond fracture will occur. The total wear  $W$  is proportional to the product of the probability of bond fracture  $p_B$  and the number of contacts  $N$  between the active grains and the workpiece.  $N$  is proportional to the number of grains  $n$  that are "instantaneously" in contact with the workpiece. Therefore the wear per active grain  $w$  is given as

$$w = \frac{W}{n} \propto p_B \quad (8.4)$$

Experimentally, the value of  $n$  is obtained by multiplying the number of active grains per square inch (Tables 5, 6, and 7) by the apparent area of contact  $a_A$  between the wheel and the workpiece. The values of  $f_H$  and  $f_V$  can then be obtained by dividing  $F_H$  and  $F_V$  by  $n$ .

In view of the above, the wear rate per active grain  $w$  should depend in some yet undetermined way on the bond stress factor. Indeed

when  $w$  is plotted against the bond stress factor (with  $\beta = .20$ ) a single straight line (Figure 43) is obtained on a semilogarithmic plot. ( $w$  in equation 8.4 is taken as the wear in 20 passes.) The corresponding probabilities are also given. The data points in this figure are only for the steady state wear. The wear rate per active grain is given by the formula

$$w = .27 \exp \left[ .51 \left( \frac{F_H - .20 f_v}{V_b} \right) \right] \quad (8.5)$$

and the probability of bond fracture is given by

$$P_B = 3.32 \times 10^{-6} \exp \left[ .51 \left( \frac{f_H - .20 f_v}{V_b} \right) \right] \quad (8.6)$$

The constants .27 and .51 in equation 8.5 were determined by the methods of least squares with the bond stress factor taken as the error free variable.

According to equations 8.2, 8.5, and 8.6, the probability of bond fracture and hence the wear rate is found to depend exponentially on the tensile stress in the bond bridge. This same type of dependence was suggested by Yoshikawa<sup>(23, 24)</sup> who considered the bond fracture from the standpoint of static fatigue where the rate of fracture is expressed by the Arrhenius equation. Although it is questionable whether the fracture occurs in this way, the analysis does give an equation which is consistent with the experimental observations.

The total wear observed after 100 passes (Figures 35-37) requires that only about one in twenty of the active grains experience a bond fracture. It would therefore be expected that most of the grains initially

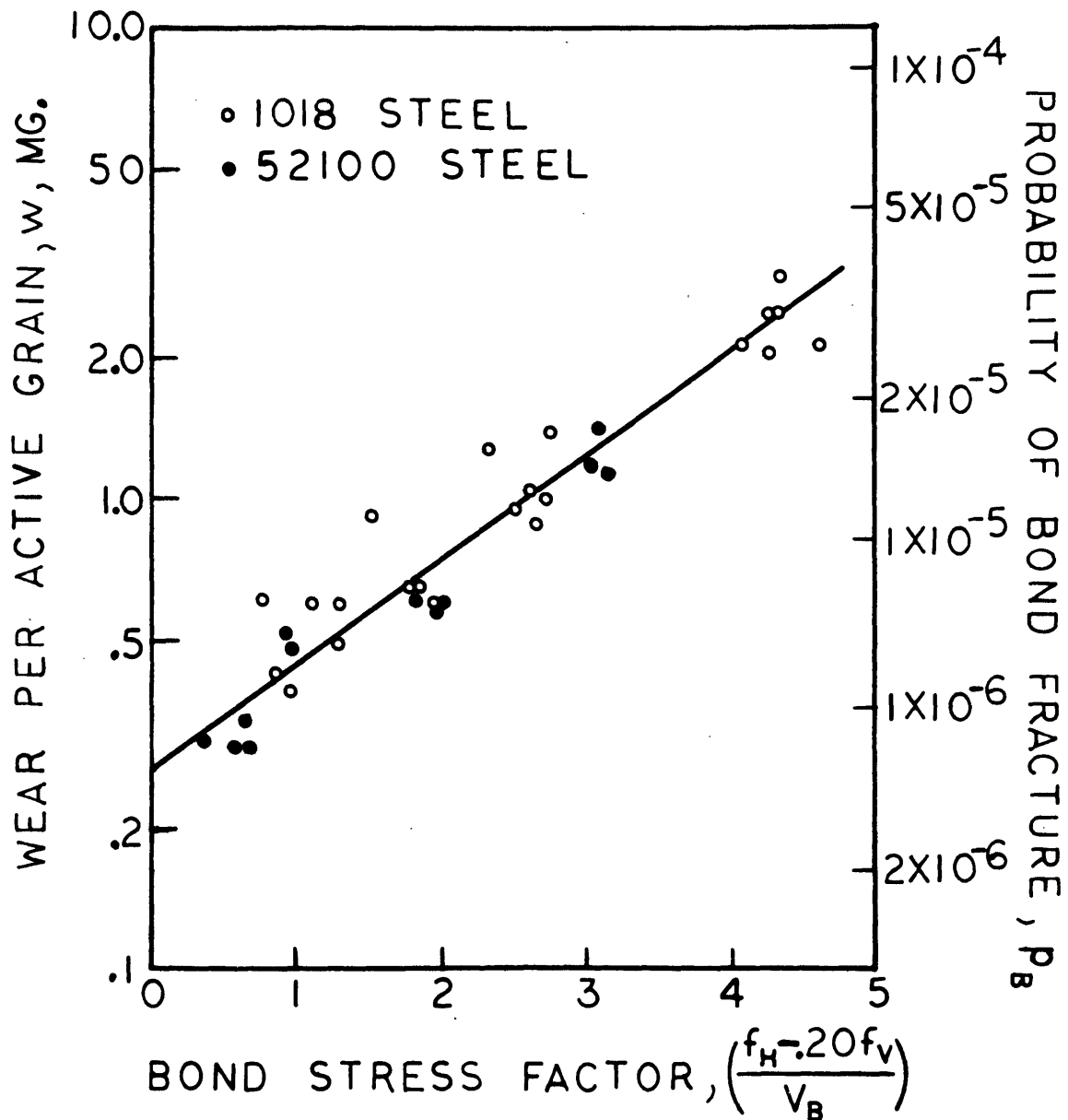


Figure 42. Correlation between the wear per active grain and the bond stress factor.

active would persist for the duration of the test. Furthermore, since the radial wear is only a small fraction of a grain dimension very few "new" active grains would appear. Therefore, it is to be expected that the number of active grains in the wheel surface remain relatively unchanged as grinding proceeds. This was found to be true (Figure 15).

The particle size distributions (Figures 38-40) indicate that a small percentage of the total wear consists of attritious wear particles. A rough estimate of this percentage can be made as follows. For this example, the results for the I-grade wheel with the fine dress and the 1018 steel workpiece are used.

The average wear flat area over 100 passes (Figure 11) is about 3.5%. The total area of the wheel which grinds is equal to the wheel circumference ( $\pi D = 25.12$  in.) times the width of the workpiece ( $b = .25$ ) or  $6.28$  in.<sup>2</sup>, and the total area of the wear flats is 3.5% of this or  $.22$  in.<sup>2</sup>. The radial wheel wear after 100 passes has been measured to be  $.0006$  in. and therefore, the total volume of attritious wear is  $(.0006) \times (.22)$  or  $1.22 \times 10^{-4}$  in.<sup>3</sup>. Multiplying by the density of aluminum oxide ( $\rho = .56 \times 10^5$  mg./in.<sup>3</sup>) the attritious wear in 100 passes is about 6.8 milligrams. Comparing this to the accumulated wear (Figure 35), the attritious wear constitutes about 10 per cent of total wear.

This is more than would be expected from the particle size distributions (Figure 38) where attritious wear particles would be expected to be smaller than 325 mesh. Undoubtedly some of the attritious wear debris is not recovered. However, this does not change the previous conclusion that most of the wear is due to grain and bond fracture.



## IX. CONCLUSIONS

In this section the important conclusions of this investigation are presented.

1. The wear flat area on the face of the wheel uniquely determines the grinding force components for a particular workpiece material and for given grinding conditions. Both the horizontal and vertical force components increase linearly with the wear flat area. (For steels this is true only up to a critical wear flat area where burning occurs.)

This linear variation between grinding force and wear flat area is explained by considering the force as the sum of a cutting force due to chip formation and a sliding force due to rubbing between the wear flats and the workpiece.

2. The specific cutting energy required in grinding increases linearly with the melting temperature of the workpiece. In most cases, the average wear flat pressure is also higher for materials which require a larger specific cutting energy.

3. Grinding burn with steel occurs at a critical wear flat area which depends on the particular steel being ground. For all the steels, burning occurs at the same total grinding energy.

4. Finer dressing results in a larger initial wear flat area on the wheel and a greater tendency toward workpiece burn. On the other hand, with finer dressing a better surface finish is obtained. For a particular grinding operation, these two opposing factors must be carefully considered.

5. Most of the grinding wheel wear is due to grain and bond fracture. The rate at which the fracture wear occurs is directly related to the grinding forces.

6. With harder wheels, smaller particles are produced since with their stronger bonds, there is a greater probability of fracturing within the grain than at the bond. This is also related to the fact that harder wheels have more active grains, larger wear flat areas, and hence require larger grinding forces.

7. Attritious wear particles constitute an almost insignificant portion of the total grinding wheel wear. However, in finish grinding, the attritious wear is the most important type of wear as it is directly related to the size of the wear flats, grinding forces, and workpiece burn. The abrasive best-suited for a particular workpiece should have both a low attritious wear rate and a low rubbing friction coefficient.

8. Virtually all the sliding energy and about 60 per cent of the cutting energy are conducted to the workpiece as heat. Grinding errors due to thermal expansion of the workpiece can be minimized by reducing the wear flat area. This is accomplished using either a softer wheel or a coarser dressing technique. For instance, at 3.5% wear flat area with 1018 steel (Figure 16), the thermal expansion for ten grinding passes is about .0007 inch. At 1.0% wear flat area, the thermal expansion is reduced by about 50%. A proportionally greater decrease in thermal expansion is obtained for material which have a higher ratio of sliding energy flux,  $q_F$ , to specific cutting

energy,  $u_c$ .

9. Peak grinding temperatures, which occur at the shear plane of the chip, approach (or even exceed) the melting temperature of the workpiece. Over the whole wear flat, surface temperatures on the order of 1100°F are obtained for mild steel.

## X. SUGGESTIONS FOR FUTURE WORK

1. The study of the relationship between the wear flat area and grinding force should be extended to other conditions of speed and feed. For such an investigation it would be desirable to use a grinding machine and wheels which have high speed capabilities of up to 10,000 R.P.M. This should shed light on the dynamic effects in the contact between the grain and the workpiece. It will also be interesting to observe if and in what manner the specific cutting energy varies with the geometry and rate of chip formation.
2. In finish grinding, the abrasive best suited for a particular workpiece should have a low attritious wear rate and low rubbing friction coefficient. Therefore, it would be desirable to study the sliding friction and wear of abrasive materials against workpiece materials under simulated grinding conditions of load, speed, and temperature. This should provide a rational basis of abrasive selection for finish grinding.
3. The grinding forces can be considered as the sum of cutting and sliding components. It would be desirable to study the action of grinding fluids in this light. The possible lubrication effects of these fluids could be clearly observed.
4. Fracture wear studies should be continued for other grinding conditions. In the long run, it might be possible to obtain a generalized expression (analogous to equation 8.5) which will predict the wheel wear as a function of grinding forces, wheelspeed, grain size, bond material,

etc. This should be particularly applicable to abrasive machining (bulk metal removal) where abrasive costs constitute a large portion of the total expense.

## REFERENCES

1. G.I. Alden, "Operation of Grinding Wheels in Machine Grinding", Trans. A.S.M.E., 1914, pp. 451-460
2. R. Wóxen, "Wheel-Wear in Cylindrical Grinding", Ingeniors Vetenskaps Akademien Handlingar, Nr. 124, 1933
3. E. Rabinowicz, Friction and Wear of Materials, John Wiley and Sons, Inc., 1965
4. L.P. Tarasov, "Grindability of Tool Steels, Trans A.S.M., 1951, pp. 1144-1174
5. W.R. Backer, M.E. Merchant, "On the Basic Mechanics of the Grinding Process, Trans. A.S.M.E., Vol, 80 (1958), pp. 141-148
6. J. Peklenik, "Beitrag zu Grundlagen des Scheifens", Doctoral Dissertation, Aachen Technische Hockschule, 1957
7. J. Peklenik, "Untersuchen Uber Das Verschleisskriterium Beim Schleifen", Industrie-Anzeiger, Vol. 80 (1958), No. 19, pp. 280-284
8. H. Yoshikawa, "Criterion of Grinding Wheel Tool Life", Bull. Japan Society of Grinding Engineers, Vol. 3 (1963), pp. 29-32
9. H. Yoshikawa, "Theory of Tool Life for Grinding Wheel", Paper Presented at 15th Annual Meeting, C.I.R.P., Liege, Belgium, August 1965
10. H.H. Tsuwa, "On the Behaviors of Abrasive Grains in Grinding Process", Bull. Japan Society of Grinding Engineers, Vol. 1 (1961), pp.7-8
11. H. Tsuwa, "An Investigation of Grinding Wheel Cutting Edges", Trans. A.S.M.E., Series B., Vol. 86, Nov. 1964, p. 371
12. H. Tsuwa and S. Kawamura, "On the Wear by Attrition of Abrasive". Bull. Society of Precision Engineering, Vol. 2, No. 1, 1966
13. Y. Tanaka, H. Tsuwa, S. Kawamura, "Effect of Grinding Conditions on the Performance of Grinding Wheels", Journal of Japan Soc. of Precision Engineering, Vol. 31 (1965), No. 3 (Translated by K. Nakayama)
14. R.S. Hahn, "Technical Factors in the Operation of Grinding Machines", A.S.T.M.E., Paper No. MR 67-592, (1967)

**PAGES (S) MISSING FROM ORIGINAL**

PAGE 102 MISSING

29. G.S. Reichenbach, J.E. Mayer, S. Kalpakcioglu, and M.C. Shaw, "The Role of Chip Thickness in Grinding", Trans. A.S.M.E., Vol. 78 (1956), p. 847
30. R.W. Story, "Forces and Force Ratios in Grinding with Coated Abrasives", A.S.M.E. Paper No. 67—WA/Prod -13
31. K. Okushima, K. Hitomi, "Progress of Flank Wear and Variation of Tool Forces", Bull. Japan Society of Precision Engineering, Vol. 1.,No. 2. 1965, p.69
32. E.G. Thomsen, A.G. Mac Donald, S. Kobayashi, "Flank Friction Studies with Carbide Tools Reveal Sublayer Plastic Flow", Trans. A.S.M.E., Vol. 84 B, 1963, p.53
33. G.F. Micheletti, A. De Fillippi, R. Ippolito, "Tool Wear and Cutting Forces in Steel Turning, CIRP International Conference on Manufacturing Technology, 1967, p. 513
34. N.N. Zorev, "Mechanics of Contact on the Clearance Surface", Chapter 3, pp. 129-180, in Metal Cutting Mechanics, Translated from Russian, Published by Pergamon Press, 1966
35. L.A. Galin, Contact Problems in the Theory of Elasticity, Translated from Russian, Published by North Carolina State College, School of Sciences and Applied Mathematics, Oct. 1961
36. H. Opitz, W. Ernst, K.F. Meyer, "Grinding at High Cutting Speeds", Proc. of 6th International M.T.D.R. Conference, September 13-15, 1965, pp. 581-595
37. W.E. Littman, The Influence of the Grinding Process on the Structure of Hardened Steel, Sc. D. Thesis, M.I.T, November 1953. Most of this is also published under the same title by W.E. Littman and J. Wulff, Trans. A.S.M., Vol. 47, 1955, pp. 692-714
38. L.P. Tarasov, "Some Metallurgical Aspects of Grinding", Machining-Theory and Practice, A.S.M., 1950, pp. 409-464
39. J.O. Outwater, M.C. Shaw, "Surface Temperatures in Grinding", Trans. A.S.M.E., Jan. 1952, pp. 73-86
40. J.C. Jaeger, "Moving Sources of Heat and the Temperature at Sliding Contacts", Proc. Royal Society of New South Wales, Vol. 76, (1942), pp. 203-224



41. K. Sato, "Grinding Temperature", Bull. Japan Society of Grinding Engineers, Vol. 1 (1961), pp. 31-33
42. R.H. Brown, "Forces in Single Grit Grinding", M.S. Thesis, M.I.T., August 1957
43. See K. Sato, "Progress of Researches on Grinding Mechanics in Japan", Bull. Japan Society of Grinding Engineers, Vol. 5 (1965), pp. 1-25
44. C.J. Smithells, Metals Reference Book, Vol. II, 3rd Edition, 1962
45. T. Orioka, "Probabilistic Treatment on the Grinding Geometry", Bull. Japan Society of Grinding Engineers, Vol. 1 (1961), pp.27-29
46. K. Nakayama, M.C. Shaw, "An Analytical Study of the Finish Produced in Surface Grinding", Unpublished

## APPENDIX A

### CALCULATION OF THE MAXIMUM NUMBER OF ACTIVE GRAINS

The maximum number of active grains per square inch in the wheel surface is assumed to be identical to the number of grains which intersect one square inch of a plane which passes through the grinding wheel. For simplicity, the packing of grains is assumed to be cubic, with the center of each grain located at a point where four cubes meet. The plane in question is assumed to contain a square array of grains.

For a wheel with the densest possible packing, the grain spacing is equal to the mean grain diameter. For such a wheel, the per cent of grain has been experimentally determined to be 58 per cent for the 32 A46 abrasive. This was accomplished by tightly packing abrasive grains into a known volume and comparing their weight to the weight which would result if the volume were 100% aluminum oxide. The wheels used here are 48 per cent abrasive. Their mean grain spacing is therefore equal to the cube root of 58/48 times the mean grain diameter or .018 inches. The maximum number of active grains per square inch is then  $1/(\text{.018})^2$  or 3240 grains/inch<sup>2</sup>.

## APPENDIX B

### CALCULATION OF TEMPERATURE DUE TO CUTTING

The cutting temperature is calculated as moving band source of width equal to  $(t_2)_{50}$  as given by equation 6.7. More precisely this is a rectangular source of dimensions  $(t_2)_{50}$  by  $1/2 r (t_1)_{\max}$  but the band source solution provides a good approximation<sup>(40)</sup>.

The total cutting energy is

$$F_{HC} V = (1.333)(6250) \frac{12}{60} = 1666 \frac{\text{in. lb.}}{\text{sec.}} \quad (\text{B.1})$$

of which the fraction  $R_1$  is conducted to the workpiece. Since the cross sectional area of the chip at 50 per cent of the cut is also the average chip cross sectional area, the source strength  $q_c$  which is the energy flux into the workpiece is given by

$$q_c = \frac{R_1 F_{HC} V}{A_a C [(t_2)_{50} \times \frac{r}{2} \times (t_1)_{\max}]} = \frac{(.61)(1666)}{(.09)(6000)(2.34)10^{-8}} = 3.22 \times 10^8 \frac{\text{in. lb.}}{\text{in.}^2 \text{ sec.}} \quad (\text{B.2})$$

For moving heat source calculations, it is necessary to calculate the value of the nondimensional variable  $L$  which is defined as

$$L = \frac{\sqrt{1}}{2\alpha} \quad (\text{B.3})$$

where

$l$  = half width of band

$\sqrt{v}$  = velocity of the source

$\alpha$  = thermal diffusivity

In this case

$$\begin{aligned} \alpha &= 9.4 \times 10^{-3} \text{ in.}^2/\text{sec} \\ l &= \frac{(t_1)_{\text{max}}}{4} = 62.5 \times 10^{-6} \text{ in.} \\ V &= v = 6250 \text{ ft./min} = 1250 \frac{\text{in}}{\text{sec.}} \end{aligned}$$

and therefore

$$L = \frac{(1250)(62.5 \times 10^{-6})}{(2)(9.4 \times 10^{-3})} = 4.15 \quad (\text{B.4})$$

The temperature distribution on the surface is obtained as a function of the non-dimensional variable X,

$$X = \frac{\sqrt{x}}{2\alpha} \quad (\text{B.5})$$

where x is the local variable in the plane of the source measured from the center of the band in the direction of the velocity V.

The temperature distribution is given by the function

$$T_c = \frac{2q_c \alpha}{\pi k V} [ I(X + L) - I(X - L) ] \quad (\text{B.6})$$

where k is the thermal conductivity ( $k = 4.10 \text{ lb./sec.}^\circ\text{F}$ ) and  $I(X+L)$  and  $I(X-L)$  are integrals which cannot be explicitly evaluated and are given in tabular form in reference (40).

Equation B.6 then becomes

$$T_c = \frac{(2)(3.22 \times 10^{-8})(9.4 \times 10^{-3})}{(\pi)(4.10)(1250)} [ I(4.15 + X) - I(4.15 - X) ] \quad (\text{B.7})$$

Table B.1 gives the values of  $T_c$  as a function of X. With the appropriate shift in the variable x, this result is plotted in Figure 33 as curve (a).

## APPENDIX C

### CALCULATION OF TEMPERATURES DUE TO SLIDING

Essentially the same procedure as in Appendix B is used to calculate the temperature  $T_s$  due to sliding between the wear flat and the workpiece. The source strength or energy flux to the surface is given by  $R_2$  times  $q_f$  where  $q_f$  is given in Table 14. In this case  $R_2$  is approximately unity and  $q_f$  is  $2.28 \times 10^6$  in.lb./(in.<sup>2</sup> sec.).

The other parameters of interest are

$$\alpha V = v = 1250 \text{ in./sec.}$$

$$l = (.004)/2 = .002 \text{ in.}$$

$$\alpha = 9.4 \times 10^{-6} \text{ in.}^2/\text{sec.}$$

and  $k = 4.10 \text{ lb./}(\text{sec. } ^\circ\text{F}).$

The nondimensional parameter  $L$  is then given by

$$L = \frac{v l}{2 \alpha} = \frac{(1250)(2 \times 10^{-3})}{(2)(9.4)(10^{-3})} = 133 \quad (\text{C.1})$$

For such a large value of  $L$ , the temperature distribution under the band ( $-L \times L$ ) is approximated by

$$T_s = \frac{2q_f \alpha}{\pi k v} \sqrt{2\pi(L-X)} \quad (\text{C.2})$$

The maximum temperature rise  $(T_s)_{\max}$  occurs at the trailing edge of the band and is equal to

$$(T_s)_{\max} = \frac{2q_f \alpha}{\pi k v} \sqrt{2\pi} = \frac{(2)(2.28 \times 10^6)(9.4 \times 10^{-3})(2\pi)}{(\pi)(4.10)(1250)} = 110^\circ\text{F}$$

(C.3)

and the average temperature rise within the band  $(T_s)_{ave}$  is two-thirds of the maximum or

$$(T_s)_{ave} = \frac{2}{3} (T_s)_{max} = 74^\circ\text{F}. \quad (\text{C.4})$$

With the appropriate shift of the coordinate  $x$ , the temperature distribution in equation C.2 is presented as curve (b) in Figure 33.

## APPENDIX D

### CALCULATION OF THE AVERAGE TEMPERATURE IN THE GRINDING AREA

The heat source is taken as a band of width  $l_c$ , the undeformed chip length, with a velocity equal to the table speed  $v$ . The grinding energy input rate  $Q$  is given by

$$Q = F_H V \quad (D.1)$$

where  $F_H$  is taken at  $A = 3.5\%$  from Figure 16, and the total energy flux  $q$  is equal to  $Q$  divided the apparent area of contact  $A_a$ .

$$q = \frac{Q}{A_a} = \frac{3.42 \times 10^3}{.0225} = 1.52 \times 10^5 \quad \frac{\text{in.lb.}}{\text{in.}^2 \text{ sec.}} \quad (D.2)$$

The fraction of this energy conducted to the workpiece is obtained from Figure 31 where  $R$  at  $A = 3.5\%$  is approximately .80.

The value of the nondimensional variable  $L$  is then

$$L = \frac{1}{2} = \frac{(8 \times \frac{12}{60}) (.009 \times \frac{1}{2})}{2(9.4 \times 10^{-3})} = 3.8 \quad (D.3)$$

For this value of  $L$ , from reference (40), the maximum value of the temperature in the band is equal to

$$(T_A)_{\max} = \frac{(6.3)(2)Rq\alpha}{\pi kv} = \frac{(6.3)(2)(.80)(1.52 \times 10^5)(9.4 \times 10^{-3})}{(\pi)(4.10)(8 \times \frac{12}{60})} = 721^\circ\text{F} \quad (D.4)$$

and the average value over the band is

$$(T_A)_{\text{ave}} = \frac{(4.7)(2)Rq\alpha}{\pi kv} = 538^\circ\text{F.}$$

Table 1. Description of Wheels

Wheel	Grain	Grain	Bond Weight	Grain Volume
<u>Designation</u>	<u>Type</u>	<u>Size</u>	<u>Per Cent</u>	<u>Per Cent</u>
32A461G8VG	32 A	46	3.1	48
32A461H8VG	32 A	46	4.4	48
32A461I8VG	32 A	46	5.8	48
32A461J8VG	32 A	46	7.2	48
32A461K8VG	32 A	46	8.6	48



Table 2. Workpiece Materials

<u>Material</u>	<u>Nominal Composition, %</u>	<u>Rockwell Hardness</u>
SAE 1018 Steel	.18C, .25 Mn, Bal Fe	89 B
AlS1 52100 Steel	1.00C, .35 Mn, .30 Si, 1.40 Cr, Bal Fe	62 C
T1 High Speed Steel	0.7C, 18W, 4Cr, 1V, Bal Fe	64 C
Molybdenum	100 Mo	95 B
130 A Titanium	92 Ti, 8 Mn	33 C
Niobium	100 Nb	95 B
Stellite No. 6B	3.00* ni, 2.00* Si, 3.00* Fe 2.00* Mn, 30 Cr, 1.50 Mo, 4.25 W, 1.25 C, Bal. Co	38 C

\* Maximum

Table 3. Wheel Dressing - Experimental Results

<u>Wheel Designation</u>	<u>Dress</u>	<u>Active Grains/in.<sup>2</sup></u>	<u>Wear Flat Area, A, %</u>	<u>Per Cent Bond Fracture</u>
32A461G8VBE	coarse	424	.50	70.4
	fine	476	.55	
32A461H8VBE	coarse	567	.97	59.2
	fine	592	1.06	
32A461I8VBE	coarse	669	1.20	50.2
	fine	849	1.48	
32A461J8VBE	coarse	939	1.67	43.8
	fine	1132	1.85	
32A461K8VBE	coarse	1145	2.04	39.6
	fine	1235	2.32	

Table 4. Sieve Number - Screen Opening

<u>Sieve Number</u>	<u>Screen Opening, in.</u>
20	.0331
40	.0165
60	.0098
80	.0070
100	.0059
200	.0029
325	.0017

Table 5. Forces and Wear Flats - 1018 Steel, Fine Dress

( V = 6250 ft./min., v = 8 ft./min., d = .001 in.)

Wheel	Passes	Active Grains per in <sup>2</sup>	Wear Flat Area A, %	Wear Flat Area/Grain in. <sup>2</sup> x 10 <sup>-6</sup>	Horizontal Force F <sub>H</sub> , lbs.	Vertical Force F <sub>V</sub> , lbs.	F <sub>H</sub> /F <sub>V</sub>
32A461G8VG	20	270	.57	21.1	1.64	2.02	.81
	40	424	.73	17.3	1.56	2.03	.77
	60	437	1.13	25.8	1.56	1.85	.84
	80	514	1.23	23.9	1.63	1.91	.85
	100	<u>514</u>	1.50	29.2	1.66	1.96	.85
	Ave.	432					
32A461H8VG	20	578	1.37	23.7	1.89	2.39	.79
	40	566	1.19	21.0	1.81	2.21	.82
	60	643	1.99	30.9	1.84	2.30	.80
	80	566	1.41	24.8	2.04	2.43	.84
	100	<u>643</u>	1.71	26.6	1.96	2.70	.73
	Ave.	600					
32A461I8VG	20	1119	2.80	25.2	2.49	3.12	.80
	40	1132	3.43	30.2	2.69	3.43	.79
	60	1119	3.84	34.2	3.07	4.49	.68
	* 80	1132	4.77	42.1	4.07	9.42	.43
	* 100	<u>1106</u>	5.30	47.9	6.35	22.85	.28
	Ave.	1122					
32A461J8VG	20	926	3.31	35.7	3.12	4.83	.64
	* 40	1350	5.32	39.4	4.66	8.88	.52
	* 60	1106	5.60	50.7	7.30	29.25	.25
	* 80	1222	6.80	55.4	7.25	31.45	.23
	* 100	<u>1363</u>	6.02	44.2	7.97	34.95	.23
	Ave.	1193					
32A461K8VG	* 20	1350	5.97	44.3	6.50	18.78	.35
	* 40	1325	6.27	47.5	7.80	31.95	.24
	* 60	1273	6.62	51.8	8.04	34.20	.24
	* 80	1530	7.31	47.9	8.94	38.40	.23
	* 100	<u>1363</u>	7.55	55.4	8.25	36.75	.22
	Ave.	1368					

\* Workpiece Burned

Table 6. Forces and Wear Flats - 1018 Steel, Coarse Dress

(V = 6250 ft./min., v = 8 ft./min., d = .001 in. )

<u>Wheel</u>	<u>Passes</u>	<u>Active Grains per in.<sup>2</sup></u>	<u>Wear Flat Area A,%</u>	<u>Wear Flat Area/Grain in.<sup>2</sup> x 10<sup>-6</sup></u>	<u>Horizontal Force F<sub>H</sub>, lbs</u>	<u>Vertical Force F<sub>V</sub>, lbs.</u>	<u>F<sub>H</sub>/F<sub>V</sub></u>
32A4618VG	20	398	.44	11.2	1.33	1.55	.86
	40	360	.56	15.5	1.36	1.57	.87
	60	347	.49	14.0	1.38	1.60	.87
	80	386	.44	11.5	1.36	1.51	.86
	100	<u>334</u>	.66	19.8	1.45	1.56	.93
	Ave.	365					
32A461H8VG	20	604	1.04	17.3	2.00	2.45	.82
	40	630	1.48	23.4	2.04	2.49	.82
	60	668	1.81	27.0	2.12	2.74	.77
	80	630	1.81	28.8	2.20	2.87	.77
	100	<u>669</u>	2.00	29.9	2.31	3.11	.74
	Ave.	640					
32A461I8VG	20	682	1.20	17.6	1.96	2.06	.94
	40	669	1.57	23.4	2.00	2.30	.86
	60	720	1.53	21.2	2.09	2.43	.86
	80	707	1.94	27.4	2.19	2.75	.80
	100	<u>759</u>	1.90	25.2	2.40	3.26	.74
	Ave.	707					
32A461J8VG	20	952	1.67	17.6	2.02	2.25	.90
	40	862	1.85	21.6	2.06	2.23	.92
	60	862	2.41	28.1	2.06	2.34	.88
	80	862	2.63	30.6	2.49	3.04	.82
	100	<u>966</u>	2.59	27.0	2.40	3.00	.80
	Ave.	900					
32A461K8VG	20	1273	2.91	23.0	2.13	2.34	.91
	40	1183	2.96	24.8	2.21	2.64	.84
	60	1170	3.28	28.1	2.36	3.15	.75
	80	1170	4.12	35.3	2.72	4.02	.68
	* 100	<u>1157</u>	4.16	36.0	4.47	12.26	.36
	Ave.	1190					

\* Workpiece burned

Table 7. Forces and Wear Flats - 52100 Steel, Fine Dress

(V = 6250 ft./min., v = 8 ft./min., d = .001 in.)

<u>Wheel</u>	<u>Passes</u>	<u>Active Grains per in<sup>2</sup></u>	<u>Wear Flat Area A, %</u>	<u>Wear Flat Area/Grain in.<sup>2</sup> x 10<sup>-6</sup></u>	<u>Horizontal Force F<sub>H</sub>, lbs.</u>	<u>Vertical Force F<sub>V</sub>, lbs.</u>	<u>F<sub>H</sub>/F<sub>V</sub></u>
32A461G8VG	20	399	.49	12.3	1.51	3.25	.46
	40	424	.58	13.7	1.53	3.45	.44
	60	463	.81	17.5	1.62	3.77	.43
	80	399	.76	19.0	1.67	3.98	.42
	100	<u>437</u>	.88	20.1	1.70	4.09	.42
	Ave.	424					
32A461H8VG	20	579	.69	11.9	1.95	4.74	.41
	40	630	.97	15.4	2.04	4.91	.42
	60	669	1.11	16.6	2.56	5.21	.44
	80	656	1.48	22.6	2.31	5.92	.39
	100	<u>720</u>	1.67	23.2	2.51	6.72	.37
	Ave.	651					
32A461I8VG	20	836	1.34	16.0	2.11	4.72	.45
	40	836	1.71	20.5	2.34	5.06	.46
	60	797	1.90	23.8	2.13	5.47	.39
	80	784	1.76	22.4	2.23	5.96	.37
	100	<u>887</u>	1.71	19.3	2.36	6.79	.35
	Ave.	841					
32A461J8VG	20	1067	1.99	18.7	2.11	4.72	.45
	40	1080	2.04	18.9	2.17	5.13	.42
	60	1106	2.55	23.1	2.26	5.66	.40
	80	1042	2.78	26.7	2.57	7.66	.34
	*100	<u>1119</u>	3.05	27.3	3.34	12.75	.26
	Ave.	1095					
32A461K8VG	20	1106	1.44	13.0	2.43	4.19	.57
	40	1119	1.76	15.9	2.43	4.87	.50
	60	1080	2.69	25.9	2.70	6.34	.43
	* 80	1170	3.29	28.1	5.28	22.64	.23
	*100	<u>1106</u>	3.80	34.4	5.45	24.34	.22
	Ave.	1116					

\* Workpiece burned

Table 8. Forces and Wear Flats - T1 Steel, Fine Dress

(V = 6250 ft./min., v = 8 ft./min. d = .001 in. )

<u>Wheel Designation</u>	<u>Passes</u>	<u>Wear Flat Area, A, %</u>	<u>Horizontal Force, F<sub>H</sub>, lbs.</u>	<u>Vertical Force, F<sub>V</sub>, lbs.</u>
32A461G8VG	10	.72	1.83	6.54
	20	.90	2.00	6.92
	30	.95	2.04	8.08
	40	1.06	2.09	8.68
	50	1.20	2.09	8.68
32A461H8VG	10	1.44	2.35	8.85
	20	1.71	2.43	9.62
	30	1.91	2.70	11.92
	* 40	2.22	2.83	13.46
	* 50	2.08	3.04	15.38
32A461J8VG	* 10	1.99	2.83	10.38
	* 20	2.36	3.04	12.31
	* 30	2.36	3.48	18.46
	* 40	2.59	5.00	26.92
	* 50	2.78	5.43	34.61

\* Workpiece burned

Table 9. Forces and Wear Flats - 130 A Titanium, Fine Dress

(  $V = 6250$  ft./min,  $v = 8$  ft./min.,  $d = .001$  in. )

<u>Wheel Designation</u>	<u>Passes</u>	<u>Wear Flat Area, A, %</u>	<u>Horizontal Force, <math>F_H</math>, lbs.</u>	<u>Vertical Force, <math>F_V</math>, lbs.</u>
32A461G8VG	10	1.48	2.77	10.19
	20	1.48	2.77	8.68
	30	1.16	2.55	7.74
	40	.88	2.34	7.55
	50	.97	2.21	7.55
32A461H8VG	10	4.03	6.38	13.21
	20	3.52	5.53	12.45
	30	3.66	5.96	13.58
	40	3.80	5.98	12.45
	50	3.98	6.17	13.21
32A461J8VG	10	4.40	5.53	11.32
	20	4.31	5.74	12.83
	30	5.51	5.53	14.15
	40	4.54	5.50	13.58



Table 10. Forces and Wear Flats - Niobium, Fine Dress

(V = 6250 ft./min., v = 8 ft./min., d = .001 in.)

<u>Wheel Designation</u>	<u>Passes</u>	<u>Wear Flat Area, A, %</u>	<u>Horizontal Force, F<sub>H</sub>, lbs.</u>	<u>Vertical Force, F<sub>V</sub>, lbs.</u>
32A461G8VG	10	1.02	3.62	4.91
	20	1.27	4.47	5.85
	40	1.20	3.91	5.47
32A461H8VG	10	3.24	7.87	12.07
	20	3.61	8.72	13.96
	30	3.33	8.09	12.83
32A461I8VG	10	4.86	9.36	17.36
	20	5.19	9.79	19.62
	30	5.05	10.21	20.38
32A461K8VG	10	5.42	11.49	14.62
	20	6.53	12.77	23.40

Table 11. Forces and Wear Flats - Molybdenum, Fine Dress

(V = 6250 ft./min., v = 8 ft./min., d = .001 in.)

<u>Wheel Designation</u>	<u>Passes</u>	<u>Wear Flat Area, A, %</u>	<u>Horizontal Force, F<sub>H</sub>, lbs.</u>	<u>Vertical Force, F<sub>V</sub>, lbs.</u>
32A461G8VG	10	.86	3.83	6.04
	20	.46	3.83	5.28
	30	.65	2.98	4.53
	40	.31	2.77	3.77
32A461H8VG	10	3.28	11.49	20.38
	20	3.82	12.77	22.64
	30	4.07	13.19	22.64
	40	3.84	13.62	22.64
32A461K8VG	10	4.35	15.32	24.15
	20	5.79	16.17	27.36
	30	6.29	18.72	32.08
	40	6.29	18.72	32.08

Table 12. Forces and Wear Flats - Stellite No. 6B, Fine Dress

(V = 6250 ft./min., v = 8 ft./min., d = .001 in. )

<u>Wheel Designation</u>	<u>Passes</u>	<u>Wear Flat Area, A, %</u>	<u>Horizontal Force, F<sub>H</sub>, lbs.</u>	<u>Vertical Force, F<sub>V</sub>, lbs.</u>
32A461G8VG	10	1.57	2.68	9.43
	20	1.57	3.19	11.32
	30	1.67	3.62	14.34
	40	1.20	3.70	15.47
	50	1.39	3.53	15.09
32A461H8VG	10	1.57	3.83	13.58
	20	2.04	4.26	17.36
	30	2.31	4.89	20.38
	40	2.64	5.53	27.34
	50	2.54	5.74	28.30
32A461J8VG	10	2.64	5.32	25.47
	20	3.10	5.96	30.19
	30	3.01	6.38	32.08
	40	3.19	6.81	33.96
	50	3.29	7.23	36.79
32A461K8VG	10	3.06	6.38	32.08
	20	3.52	6.60	33.96
	30	3.56	7.66	39.62
	40	3.56	7.66	42.45
	50	4.07	7.87	43.40

Table 13. Forces and Wear Flats - 1018 Steel, Fine Dress

(V = 3125 ft./min., v = 4 ft./min., d = .001 in.)

<u>Wheel Designation</u>	<u>Passes</u>	<u>Wear Flat Area, A, %</u>	<u>Horizontal Force, <math>F_H</math>, lbs.</u>	<u>Vertical Force, <math>F_V</math>, lbs.</u>
32A461G8VG	20	.42	1.87	2.57
	40	.63	1.74	2.34
	60	.46	1.70	2.26
	80	.44	1.83	2.38
	100	.44	1.79	2.42
32A461H8VG	20	1.20	2.55	3.02
	40	1.57	2.47	2.83
	60	1.39	2.55	2.94
	80	1.85	2.64	3.21
	100	1.76	2.94	3.28
32A461I8VG	20	2.64	3.83	5.09
	40	2.87	4.68	6.04
	* 60	3.43	4.89	8.30
	* 80	3.80	5.74	11.32
	* 100	4.21	7.02	15.85
32A461K8VG	20	2.92	4.26	5.28
	40	4.21	6.80	10.56
	* 60	4.77	8.09	18.11
	* 80	4.63	8.94	23.40
	* 100	5.37	8.30	23.58

\* Workpiece burn

Table 14. Summary of Results From Least Square Analysis

Workpiece	V ft./min.	v ft./min.	d inch	c	F <sub>VC</sub> lbs.	F <sub>VC</sub> lbs.	F <sub>HC/FC</sub>	$\bar{p}$ lbs./in. <sup>2</sup>	$\mu$	u <sub>c</sub> in. lbs./in. <sup>3</sup> x 10 <sup>6</sup>	q <sub>f</sub> in. lbs./in. <sup>2</sup> x 10 <sup>6</sup>
1018 Steel	6250	8	.001	.86	1.30	1.33 + .22	.97	2980 +470	.61	4.05	2.28
*1018 Steel Burn	6250	8	.001	.85				40860 +3300	.15		7.82
52100 Steel	6250	8	.001	.77	1.55 + .26	3.17 + .46	.49	5800 +1250	.31	4.83	2.23
*52100 Steel Burn	6250	8	.001	.83				60630 +18350	.18		13.56
T1 Steel	6250	8	.001	.94	1.34 + .27	4.52 + .82	.30	14580 +2630	.21	4.18	3.89
*T1 Steel Burn	6250	8	.001	.89				147,000 +17290	.13		22.96
130 A Titanium	6250	8	.001	.93	1.60 + .49	6.72 + .59	.24	6590 +750	.66	4.99	5.45
Niobium	6250	8	.001	.99	2.34 + .51	1.43 + .48	1.64	15,410 +630	.46	7.31	8.91
Molybdenum	6250	8	.001	.99	2.13 + .49	2.90 + .65	.74	21,020 +730	.57	6.66	14.96
Stellite No. 6 B	6250	8	.001	.97				54,132 +1990	.15		10.29
1018 Steel	3125	4	.001	.93	1.22 + .27	1.58 + .36	.77	5590 +940	.82	3.80	2.86
*1018 Steel Burn	3125	4	.001	.89				38,050 +4990	.24		5.61

\* Corresponds to Force vs. Wear flat relationship beyond transition

Table 15. Energy Partition - 1018 Steel, Fine Dress

(V = 6250 ft./min., v = 8 ft./min., d = .001 in.)

<u>Wheel Designation</u>	<u>Wear Flat Area, A,%</u>	<u>Energy to Workpiece,R</u>
32A461G8VG	.74	.64
32A461H8VG	1.34	.69
	2.82	.75
32A461K8VG	3.06	.76
	3.98	.81

Table 16. Surface Finish, 1018 Steel

(V = 6250 ft./min., v = 8 ft./min., d = .001 in.)

<u>Wheel Designation</u>	<u>Passes</u>	<u>Fine Dress</u>	<u>Coarse Dress</u>
32A461G8VG	20	15 microinches	28 microinches
	40	17	28
	60	14	30
	80	12	31
	100	15	30
32A461H8VG	20	12	26
	40	13	26
	60	13	27
	80	14	24
	100	13	24
32A461I8VG	20	12	27
	40	14	26
	60	13	25
	80	25	25
	100	35	25
32A461J8VG	20	10	23
	40	25	23
	60	30	24
	80	30	22
	100	35	22
32A461K8VG	20	20	20
	40	25	22
	60	30	22
	80	30	22
	100	30	40

Table 17. Wheel Wear - 1018 Steel, Fine Dress

( V = 6250 ft./min., v = 8 ft./min., d = .001 in.)

<u>Wheel Designation</u>	<u>Passes</u>	<u>Wear, Mg.</u>	<u>Accumulated Wear, Mg.</u>
32A461G8VG	20	85.0	85.0
	40	33.0	118.0
	60	20.1	138.1
	80	23.5	161.6
	100	29.0	190.6
32A461H8VG	20	59.6	59.6
	40	28.6	88.2
	60	17.4	105.6
	80	18.4	124.0
	100	12.7	136.7
32A461I8VG	20	46.3	46.3
	40	23.9	70.2
	60	22.5	92.7
	80	23.0	115.7
	100	52.0	167.7
32A461J8VG	20	46.0	46.0
	40	35.0	81.0
	60	39.8	120.8
	80	41.2	162.0
	100	40.3	202.3
32A461K8VG	20	61.6	61.6
	40	33.6	95.2
	60	35.2	130.4
	80	28.4	158.8
	100	26.0	184.8



Table 18. Wheel Wear - 1018 Steel, Coarse Dress

( V= 6250 ft./min., v = 8 ft./min., d = .001 in.)

<u>Wheel Designation</u>	<u>Passes</u>	<u>Wear, Mg.</u>	<u>Accumulated Wear, Mg.</u>
32A461G8VG	20	83.3	83.3
	40	30.6	113.9
	60	28.0	158.6
	80	16.7	158.6
	100	17.4	176.0
32A461H8VG	20	39.0	39.0
	40	16.6	55.6
	60	12.0	67.6
	80	14.8	82.4
	100	13.9	96.3
32A461I8VG	20	29.0	29.0
	40	11.1	40.1
	60	10.4	50.5
	80	11.3	61.8
	100	8.4	70.2
32A461J8VG	20	30.1	30.1
	40	14.4	44.5
	60	11.6	56.1
	80	11.8	67.9
	100	10.0	77.9
32A461K8VG	20	29.5	29.5
	40	21.9	51.4
	60	16.5	67.9
	80	11.2	78.9
	100	19.1	98.0

Table 19. Wheel Wear - 52100 Steel, Fine Dress

( V= 6250 ft./min., v = 8 ft./min., d = .001 in.)

<u>Wheel Designation</u>	<u>Passes</u>	<u>Wear, Mg.</u>	<u>Accumulated Wear, Mg.</u>
32A461G8VG	20	30.0	30.0
	40	15.6	45.6
	60	11.3	56.9
	80	10.9	67.8
	100	13.4	81.2
32A461H8VG	20	29.2	29.2
	40	10.1	39.3
	60	8.6	47.9
	80	8.7	56.6
	100	8.8	65.4
32A461I8VG	20	25.7	25.7
	40	12.6	38.3
	60	9.8	48.1
	80	9.1	57.2
	100	7.2	64.4
32A461J8VG	20	23.4	23.4
	40	31.1	31.1
	60	39.4	39.4
	80	46.6	46.6
	100	58.5	58.5
32A461K8VG	20	20.7	20.7
	40	4.7	25.4
	60	5.8	31.2
	80	9.5	40.7
	100	12.1	52.8

Table B.1 Calculated Values of T<sub>c</sub>

<u><math>X = \frac{Vx}{2\alpha}</math></u>	<u>T<sub>c</sub>, °F</u>
L	376
.5L	1410
0	1940
-.5L	2350
-L	2327
-2L	1367
-3L	1053
-3.5L	989
-5L	865
-10L	639
-20L	414
-30L	357
-50L	320
-80L	263

### BIOGRAPHICAL NOTE

The author was born June 20, 1941 in Boston, Massachusetts. He lived in Malden, Massachusetts until his graduation from the Malden public schools in 1959.

In 1959, the author entered M.I.T. where he was awarded the degrees of Bachelor of Science in Mechanical Engineering in 1963, and Master of Science in 1965. His master's thesis entitled "Behavior of Liquid Lubricants in Vacuum" was supervised by Dr. G. S. Reichenbach.

The author was elected to Pi Tau Sigma and Sigma Xi while attending M.I.T.

The author was married to the former Judith Greenberg of Valley Stream, New York on August 30, 1964.